Greenland and North Atlantic climatic conditions during the Holocene

- as seen in high resolution stable isotope data from Greenland ice cores.

Bo Møllesøe Vinther

Ph.D. Dissertation

Supervisors:
Katrine Krogh Andersen
Sigfús Jóhann Johnsen

Ice and Climate
Niels Bohr Institute
Faculty of Science

University of Copenhagen

Submitted

1st of August 2006

Acknowledgements

Contents

List of Tables

Chapter 1

Motivation and outline

It has become increasingly evident, that the short time period spanned by instrumental observations of atmospheric conditions does not provide the information needed to understand the anthropogenic influence on climate. Hence there is an urgent need to use natural proxies of climate variability to expand our knowledge of past climatic conditions beyond the instrumental era.

Ideally the field of climate dynamics should be provided with millennial scale seasonally resolved information on climate variability for all regions of the world, in order to facilitate the separation of the background of natural climate variability from a possible human anthropogenic effect on climate [Jones et al., 2001a].

Gathering thousands of years of seasonally resolved proxy data is a very demanding task indeed. For most regions of the world, natural proxies spanning multiple millennia do exist, but not in seasonal or even annual resolution. A notable exception from the general picture is the Greenland area, as ice core records from the Greenland ice sheet can provide both high resolution and millennias worth of climate data. The isotopic record can be related to Greenland temperature conditions, as first proposed by Dansgaard [1954]. During the past 50 years enormous efforts have been put into the retrieval and analysis of Greenland ice core records, resulting in huge advances in our understanding of the climatic system.

The aim of this Ph.D. project has been to collect existing Greenland Holocene high resolution δ^{18}O and δD records from the many years of ice core drilling, supplement the very high resolution Dye-3 ice core measurements and use these data to deliver high resolution proxies of climatic conditions in the Greenland area as well as the North Atlantic region.

The dissertation is structured as a steady movement toward this ambitious goal:

In **chapter 2** stable isotope records from 20 Greenland ice cores are used to investigate the relations between seasonally resolved Greenland stable isotopes and local as well as regional temperature conditions and atmospheric

circulation patterns. In this chapter highly resolved δ^{18}O from the Dye-3 area is found to be especially well suited for the creation of seasonal δ^{18}O time series.

This finding leads directly to the decision that the highly resolved Dye-3 δ^{18}O record should be expanded. The sampling and measuring of 12000 additional Dye-3 stable isotope samples is documented in **chapter 3**.

In **chapter 4** the new Dye-3 data is first of all used for dating purposes, as a prerequisite for the creation of seasonally and annually resolved proxies of Greenland climatic conditions is an accurate dating of the Greenland ice cores. Hence all available data from the Dye-3, GRIP and NGRIP ice cores is used to date the Holocene sections of these cores, forming a synchronized dating for the three cores. A dating that is transferred to the Renland core at the end of the chapter.

Having the ice cores on a common time scale, the climatic analysis can begin. In **chapter 5**, modeling of observed borehole temperature profiles is used both to determine the best possible δ^{18}O to temperature calibration and investigate likely scenarios of past elevation change of the Greenland ice sheet. Past elevation has to be estimated for the ice core drill sites, as changes in elevation affect the δ^{18}O and thereby mask the underlying climatic signals.

Chapter 6 is devoted to the creation and interpretation of 8 millennia of seasonally and annually resolved stable isotope data from the Dye-3 ice core. The knowledge gained on past Greenland ice sheet elevation changes in the previous chapter is used indirectly to correct the Dye-3 data both for past elevation change and complications stemming from the fact that the Dye-3 site is located down stream from the ice divide.

Discussions of the many results presented in the dissertation are generally placed within the above chapters, while **chapter 7** discusses some findings and assumptions put forward, that did not relate to one specific chapter in the dissertation. The main conclusions for the dissertation as a whole are drawn in **chapter 8**.

Finally it should be noted that an overview paper about Greenland ice core isotope records in general, which was made in cooperation with Sigfús J. Johnsen is reprinted in **Appendix A** and a few notes on gaussian smoothing of time series are given in **Appendix B** at the end of the dissertation.

Chapter 2

Climatic signals in multiple highly resolved Greenland stable isotope records

Twenty ice cores drilled in medium to high accumulation areas of the Greenland ice sheet have been used to extract seasonally resolved stable isotope records.

Relations between the seasonal stable isotope data and atmospheric flow as well as Greenland and Icelandic temperatures are investigated both for the winter and summer seasons.

The winter season stable isotope data are influenced by the North Atlantic Oscillation (NAO) and very closely related to Greenland west coast winter temperatures during the past 200 years.

The summer season data are related to Stykkisholmur summer temperatures and the North Atlantic SST conditions in Icelandic waters.

The results strongly suggest that the temperature and circulation signals in the seasonal data can be used in high-resolution reconstructions of climatic conditions in the North Atlantic region. This is encouraging as several highly resolved Greenland ice core records cover most of the last two millennia.

2.1 Introduction

During the past 10 years studies of seasonal ice core δ^{18}O records from the Greenland ice sheet have indicated, that in order to gain a firm understanding of the relations between Greenland δ^{18}O and climatic conditions in the North Atlantic region, it is important to have not only annually, but seasonally resolved ice core δ^{18}O data [Barlow et al., 1997; Rogers et al., 1998; Vinther et al., 2003a]. In Vinther et al. [2003a] it was in fact documented that taking the step to seasonally resolved Greenland δ^{18}O data paved the way for resolving crucial information about the North Atlantic Oscillation (NAO), which has been determined to be the dominant mode of atmospheric
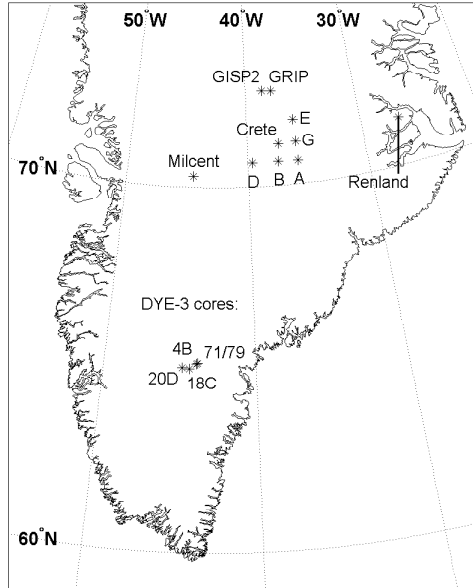
Figure 2.1: Locations of Greenland ice cores used for this study.

variability in the northern Hemisphere [Hurrell, 1995; 1996; Hurrell and van Loon 1997; Hurrell et al., 2003].

The aim of this chapter is to use an array of seasonally resolved Greenland ice core δ^{18}O data in combination with long series of temperature and pressure data, both station based and gridded in order to map out and document the relations between seasonal Greenland δ^{18}O data and both atmospheric flow and temperature. Furthermore it will be investigated how the definition of summer and winter seasons in the ice core δ^{18}O data affects the relations with temperature including how temperature relations with seasonal δ^{18}O data differs from relations with annually resolved δ^{18}O data.

Exploiting that the 20 ice core records available to this study are located in different areas of the Greenland ice sheet (see figure 2.1 and table 2.1), the investigation will be carried out as to document both local as well as regional scale relations between the seasonal δ^{18}O data and atmospheric flow and temperature. Furthermore, following the approach of both Fisher et al. [1996] and Vinther et al. [2003a] noise reduction and simplification of the Greenland δ^{18}O data will be pursued both through stacking and principal component analysis of the ice core data set.

2.2 Meteorological data

In order to obtain as solid relations as possible between the ice core δ^{18}O data and the meteorological evidence, it has been decided to restrict the investigation to meteorological data sets with the longest possible time span.

4

Table 2.1: Ice core drill site locations and core details.[a]

Drill site	Lat. °N	Long. °W	Elevation m a.s.l.	Acc. rate m ice eq./yr	Drill year	Core length m
Crete	71.12	37.32	3172	0.289	1974	404.0
Dye-3 71	65.18	43.83	2480	0.56	1971	372
Dye-3 79	65.18	43.83	2480	0.56	1979[b]	2037
Dye-3 4B	65.17	43.93	2491	0.535[c]	1983	173.8
Dye-3 18C	65.03	44.39	2620	0.44[c]	1984	113.0
Dye-3 20D	65.06	44.87	2620	0.44	1984	115.8
GRIP 89-1	72.58	37.64	3238	0.23	1989	260.1
GRIP 89-2	72.58	37.64	3238	0.23	1989	70.2
GRIP 89-3	72.58	37.64	3238	0.23	1989[b]	3028.8
GRIP 91	72.58	37.64	3238	0.23	1991	82.3
GRIP 92	72.58	37.64	3238	0.23	1992	107.3
GRIP 93	72.58	37.64	3238	0.23	1993	229.5
GISP2-D	72.60	38.50	3200	0.245	1989	199.0
Milcent	70.30	44.50	2410	0.54	1973	398
Renland	71.57	26.73	2350	0.50	1988	324.4
Site A	70.63	35.82	3092	0.292[c]	1985	128.6
Site B	70.65	37.48	3138	0.306[c]	1984	105.6
Site D	70.64	39.62	3018	0.354[c]	1984	100.1
Site E	71.76	35.85	3087	0.215[c]	1985	77.8
Site G	71.15	35.84	3098	0.249[c]	1985	70.8

[a]Data sources are: [Langway et al., 1985; Clausen et al., 1988; Clausen and Hammer, 1988; Dansgaard et al., 1993; Barlow et al., 1993].
[b]Cores were drilled to bedrock during a few years of fieldwork.
[c]Accumulation rates calculated using measured density profiles and depths of the Laki volcanic erruption (1783 A.D.) from [Clausen and Hammer, 1988].

Based on experience from prior investigations [Barlow et al., 1997; Rogers et al., 1998; Vinther et al., 2003a] special emphasis has been given to local temperature data and the North Atlantic Oscillation data.

2.2.1 SW Greenland temperatures

The Vinther et al. [2006a] monthly resolved temperature data series for south-west Greenland spans the period 1784 to 2005. The temperature data are based on observations from 13 different locations along the southern and westerns coasts of Greenland. Even though the Vinther et al. [2006a] data are incomplete (data are missing from 15 winters and 37 summers between 1784 and 1852) they represent a significant improvement over prior Greenland temperature data sets, that contained no information on temperatures before 1873 [e.g. Box, 2002].

2.2.2 Stykkisholmur temperatures

As the Vinther et al. [2006a] temperature data set does not include data from the east coast (observations from the Greenland east coast commenced as late as 1894 and only at one location, Ammasalik), it was decided to use the long temperature data set from Stykkisholmur (Iceland) [Jonsson, 1989] for comparisons with the ice core data, in order to have some data indicative of climate east of the Greenland ice sheet. The Stykkisholmur temperature data spans the period back to 1830.

2.2.3 Index for the North Atlantic Oscillation

The North Atlantic Oscillation (NAO) is best described through a principal component analysis of sea level pressure in the North Atlantic Region. A most useful approximation to this approach is, however, to base an index of the NAO on pressure observations near or at the centers of action of the NAO (the Azores/Iberian Peninsula and Iceland). Using pressure observations from Stykkisholmur and Gibraltar, Jones et al., [1997] presented a NAO index reaching back to 1821. The Jones et al. [1997] NAO index (now with a few modifications by Vinther et al. [2003b]) is still the only NAO index based on instrumental pressure observation, that reaches this far back in time. Hence it was decided to use this measure of the NAO for the investigation of the Greenland ice core data.

2.2.4 Northern hemisphere sea level pressure and temperature data

In order to obtain relations between the ice core data and northern hemisphere patterns of atmospheric flow and temperature, two gridded data sets (HadSLP2 and HadCRUT2v) were included in the investigation. The HadSLP2 sea level pressure (SLP) data set is the latest and most comprehensive

edition of the Hadley Centres global 5 by 5 degree gridded SLP data set [Allen and Ansell, 2006]. The gridded SLP-data reaches back to 1850. Had-CRUT2v is a 5 by 5 degree temperature anomaly dataset that combines land air temperature anomalies and sea surface temperature anomalies [Jones et al., 1999; 2001b]. HadCRUT2v spans the period from 1870 to present.

2.3 The ice core data

20 individual ice core records from 14 different locations on the Greenland ice sheet (see figure 2.1 and table 2.1) have been selected for this survey. The selected records all comply with the following two criteria: (1) The ice cores should at least span the period covered by Greenland temperature data (i.e. back to 1784) and (2) the annual accumulation at the drill sites should be sufficient (larger than 20 cm of ice equivalent per year) that the seasonal oscillations in the δ^{18}O data are not obliterated by firn diffusion (see appendix A.3).
All ice core records are series of δ^{18}O except for the GISP2 δD record. As δD has a variability which is 8 times larger than δ^{18}O, the GISP2 δD record has been divided by 8, as to conform with the 19 δ^{18}O records.

2.3.1 The diffusion problem

As described in details in appendix A.3, Greenland ice core δ^{18}O (and δD - both will be referred to only by δ^{18}O in the following) data is smoothed by diffusional processes in the top 60 meter of the ice sheet [Johnsen 1977a, Johnsen et al., 2000]. As the diffusion dampens the annual oscillations in the δ^{18}O data, creating artificial trends in summer and winter season time series of δ^{18}O, it is crucial that the δ^{18}O data are corrected for diffusion before any interpretation is pursued. Two different approaches have been used in order to avoid diffusion related trends in the ice core δ^{18}O data. For ice cores drilled in areas that never or very rarely experience significant summer melting (Crete, GRIP, GISP2, Milcent, Sites A, B, D, E and G) traditional diffusion correction has been carried out [Johnsen et al., 2000]. For drill sites that experience modest summer melting somewhat more often, the traditional method fails, as even a few melt layers can create large gradients in the δ^{18}O data, which in turn results in spurious high-frequency oscillations (ringing) in the diffusion corrected data. Hence an approach quite opposite to diffusion correction is pursued: Instead of correcting the data for diffusion, data are artificially diffused as to have experienced the same level of diffusion, thus assuring that the annual oscillations in the δ^{18}O data are damped equally throughout each record. The drawback of this approach is that the resulting δ^{18}O record somewhat mixes the summer and winter season, a problem which luckily is of minor concern for the ice cores in question (the Renland core and the Dye-3 cores), due to the high accumulation rates at these drill sites (see table 2.1).

2.3.2 The dating of the ice cores

After diffusion correcting the δ^{18}O data, the existing time scales for the 20 ice cores has been slightly modified as the winter minima and summer maxima (used to define mid-winter and mid-summer) in the diffusion corrected data can be shifted slightly in depth as compared to the raw δ^{18}O data. Furthermore through intercomparison with nearby records and scrutiny of volcanic markers in conductivity records, a few inconsistencies have been corrected in the Dye-3 20D, GISP2, Site E and Site G time scales. Generally speaking, the fact that the 1783 eruption of Laki is one of the most prominent conductivity signals in ice cores all around Greenland [Clausen and Hammer, 1988] is a great help for the dating effort concerned with the past ∼220 years in all the Greenland ice cores.

2.3.3 The definition of seasons

The question of how to best define seasons in the Greenland δ^{18}O data has long been neglected. The only markers in the δ^{18}O data, which can be used for this purpose are the summer maxima and winter minima in the records. Both 19th and 20th century temperature data from Stykkisholmur and SW Greenland unanimously suggest that the summer temperature maximum in the region occurs in July/August and the winter minimum occurs in January/February, hence it seems prudent to assume that this also is the case for the minima and maxima in the δ^{18}O data. As there are no such indicators of spring and autumn in the δ^{18}O records it is very hard to pinpoint these seasons in the records. The following will therefore focus on the summers and winters only.

Using the assumption that δ^{18}O and temperature extrema in the Greenland region occur simultaneously it is investigated how to best define the summer and winter seasons in the δ^{18}O data. In order to obtain ice core δ^{18}O information with a minimum amount of noise, records from the same locations are stacked and a principal component analysis is carried out on the resulting 14 ice core δ^{18}O series (hence Dye-3 71 and Dye-3 79 are stacked, as are all GRIP cores). Thereafter correlations between the time series for the first principal component (PC1) and the SW Greenland and Stykkisholmur temperature data has been calculated for different choices of season length, both for the summer and winter data. The resulting correlations for the winter and summer seasons can be seen in figure 2.2 and figure 2.3 respectively.

From figure 2.2 (left) it can be seen that the most significant correlation (r=0.7) between SW Greenland winter temperatures and the PC1 of winter season Greenland δ^{18}O is obtained if the winter season is defined as 50% of the annual accumulation in the ice cores and Nov-Apr is used to define winter in the temperature data. When comparing to Stykkisholmur temperatures (figure 2.2 - right) the same peak around 50% of the annual accummulation can be discerned. It can, however, be seen that the most
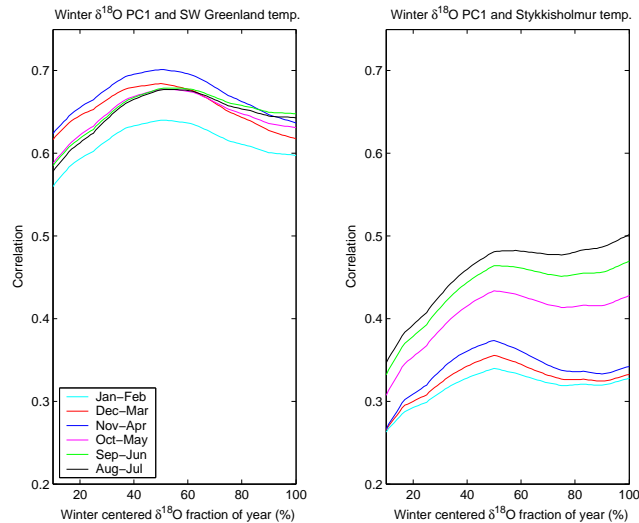
Figure 2.2: Correlations between the first principal component of winter season $\delta^{18}O$ and various selections of SW Greenland/Stykkisholmur temperatures for different choices of winter centered fraction of year in the ice core data. Correlations are calculated for the period 1784 to 1970.

significant correlation is obtained if annual Stykkisholmur temperatures are compared to annually resolved (100% of the annual accumulation) $\delta^{18}O$ data. Hence it is only if the winter season temperatures are to be resolved that it is advantagous to use seasonal $\delta^{18}O$ data. This is in contrast to the comparsion with the SW Greenland temperaures, there it was found that even when looking at annual temperatures (Aug-Jul) correlations are highest when winter season and not annual $\delta^{18}O$ is used. In figure 2.3 the same analysis is performed for the summer season. Quite surprisingly it can be seen that Greenland summer $\delta^{18}O$ relates poorly to SW Greenland temperatures. In fact annual $\delta^{18}O$ data and annual SW Greenland temperatures relate much better than the summer data and a distinct minimum in correlation between SW Greenland temperatures and the PC1 of Greenland summer $\delta^{18}O$ is obtained for a choice of season about 50% of the annual accummulation in the ice cores. The relations between Stykkisholmur temperatures and Greenland $\delta^{18}O$ are, however, much stronger for the summer season with the correlation exceding r=0.6 for a choice of summer season totaling about 80% of the annual accumulation.

It is interesting to observe that the annual Greenland $\delta^{18}O$ data (corresponding to 100% of the annual accumulation) seems to be a combination of a winter (Nov-Apr) temperature signal related to the SW coast of Greenland (r=0.64) and a summer (May-Oct) temperature signal related to Iceland and thereby the Greenland east coast (r=0.59). As the SW Greenland winter temperatures and Stykkisholmur summer temperatures only have 11% vari-

9
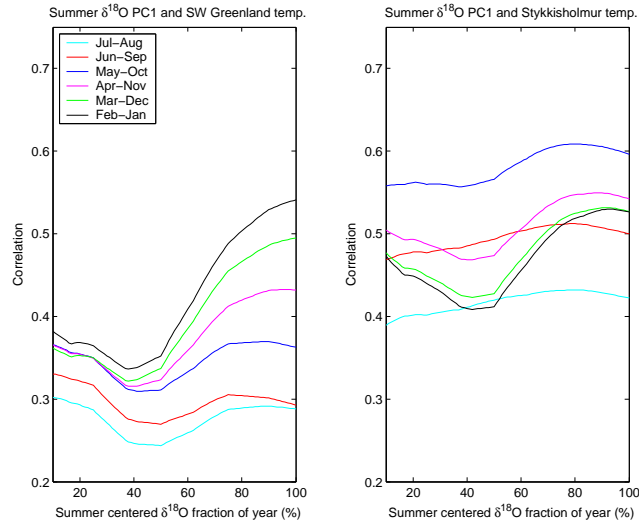
Figure 2.3: Correlations between the first principal component of summer season δ^{18}O and various selections of SW Greenland/Stykkisholmur temperatures for different choices of summer centered fraction of year in the ice core data. Correlations are calculated for the period 1831 to 1970.
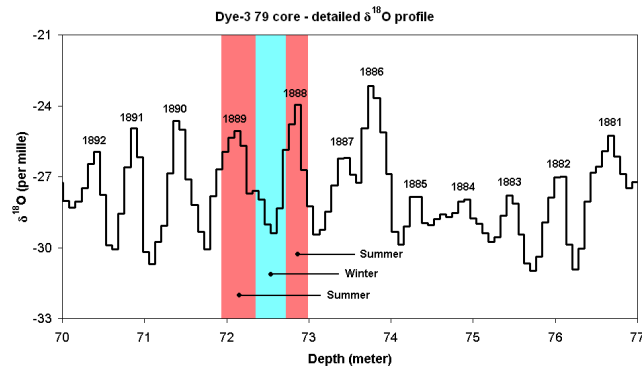
Figure 2.4: Example of the dating and the definition of summer and winter seasons in the Dye-3 79 ice core.

ance in common, they do explain approximately 2/3 of the variance observed in the PC1 of the Greenland annual δ^{18}O data.

The advantage of having seasonally resolved δ^{18}O data is therefore the ability to disentangle these two dominant signals in the δ^{18}O records. With this in mind, it was decided to define both the summer and winter season as 50% of the annual accumulation in the ice cores. This definition has several advantagous: First of all the summer and winter time series stay independent, as there is no overlap in data use. Secondly the correlation between winter δ^{18}O and SW Greenland temperatures are most significant for this choice of season. Thirdly the summer δ^{18}O is almost unrelated to SW Greenland summer (May-Oct) temperatures (r<0.25) for this choice of summer season, while Stykkisholmur summer temperatures still correlates quite strongly (r>0.55). Hence defining the δ^{18}O seasons as 50% of the annual accumulation yields both a high degree of independance between summer and winter δ^{18}O data and a high degree of disentanglement of the east and west coast temperature signals which are mixed into the annual δ^{18}O data. An example of the chosen definition of seasons can be seen in figure 2.4, while time series of winter and summer δ^{18}O for 14 different locations on the Greenland ice sheet can be seen in figure 2.5 and 2.6 respectively.

2.4 The seasonal δ^{18}O data

Looking at the 14 winter season δ^{18}O series presented in figures 2.5 and 2.6 it can be seen that the time series from Renland and Dye-3 show least variability in the high frequency domain. It should immediately be noted that this lack of variability is a consequence of special diffusion correction applied to these series, not a climatic feature. The artificial extra diffusion imposed on the Renland and Dye-3 series simply dampens the amplitude of the annual cycle, thereby influencing the seasonal variability.

A more interesting feature in the data is the substantial agreement on the larger climatic features between the different Dye-3 cores, indicative of a quite good signal to noise ratio (SNR) in the high accumulation data from southern Greenland. The same general agreement is not seen in between the Crete and Site A to G cores, probably due to the lower accumulation rate in central Greenland resulting in a lower SNR. Calculating SNR for the period shown in figures 2.5 and 2.6 (1778-1970) both for the GRIP (6 cores) and Dye-3 (2 cores) sites confirms this assertion: GRIP SNR is 0.57 (winter) and 0.89 (summer) while Dye-3 SNR is 1.43 (winter) and 2.12 (summer). This large difference in SNR between the two sites is in agreement with previous studies of SNR in annual δ^{18}O data: Johnsen et al. [1997] reported an SNR of ∼0.9 for GRIP cores, while Fisher et al. [1985] found an SNR of ∼2.4 for the Dye-3 cores. Hence the SNR is generally higher in the both the summer and annual δ^{18}O data than in the winter season data, but the ratio between the SNRs at the two sites is almost conserved. It is speculated
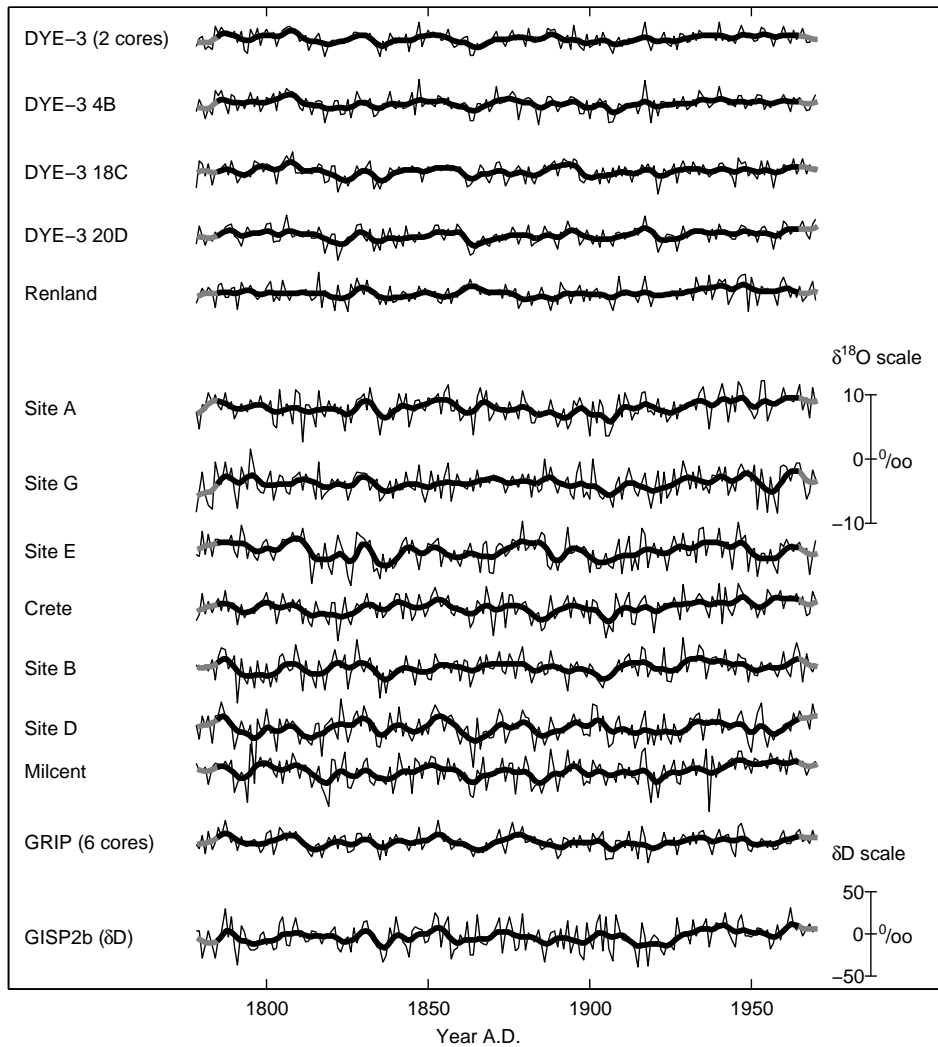
Figure 2.5: Winter season δ^{18}O (and δD) data from 14 different locations on the Greenland ice sheet. Notice that the top 5 series have been diffusion corrected differently from the bottom 9 series, see text for details. Thick lines are decadally filtered data (lines are grey if the filtered values are based on incomplete data) For note on filtering see appendix B.
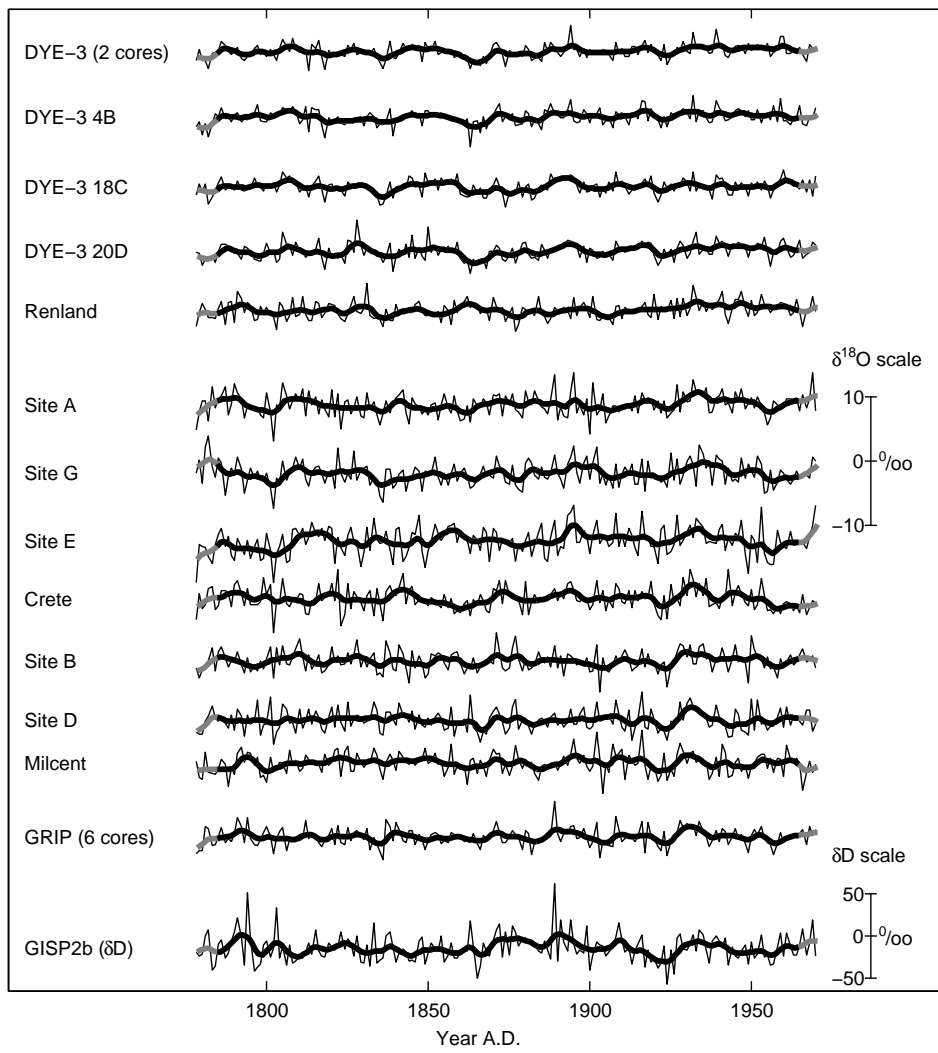
Figure 2.6: As Fig. 2.5 but for summer season δ^{18}O and δD.

13
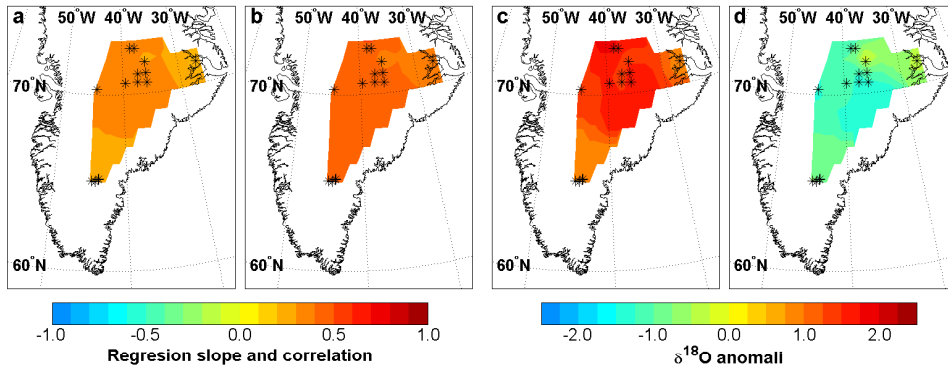
Figure 2.7: Spatial maps of relationships between SW Greenland Nov-Apr temperatures and winter season δ^{18}O (and δD/8) data for the period 1785-1970. Panel (a) shows the slopes of linear regressions between δ^{18}O and the Nov-Apr temperature. Panel (b) shows the correlation between winter δ^{18}O and the Nov-Apr temperature. Panels (c) and (d) shows the average anomalies in winter δ^{18}O corresponding to the 5% of the Nov-Apr periods which registered the highest and lowest temperatures respectively.

that the relatively low winter SNR is a consequence of the winters having more severe (windy) conditions than the summers, resulting in a winter stratigraphy which is more disturbed by sastrugi formation.

2.5 Winter season δ^{18}O and regional meteorological conditions

2.5.1 Relation to SW Greenland temperatures

In figures 2.7a and 2.7b the spatial distributions of the linear regression slopes and linear correlations between the 14 winter season δ^{18}O series and Nov-Apr SW Greenland temperatures are presented. It can be seen (figure 2.7b) that correlations are almost equal for all sites except for the sites in the eastern part of Greenland were correlations are slightly weaker. A result which isn't surprising given the fact that the eastern sites are farthest away from the SW Greenland temperature observation sites. The tendency to a lower than average regression slope in southern Greenland (see figure 2.7a) is probably a consequence of the lower variability forced upon the southern Greenland series. The variability issue is also seen in the two extreme-plots (figures 2.7c and 2.7d), which are in broad agreement with the slopes shown in figure 2.7a.
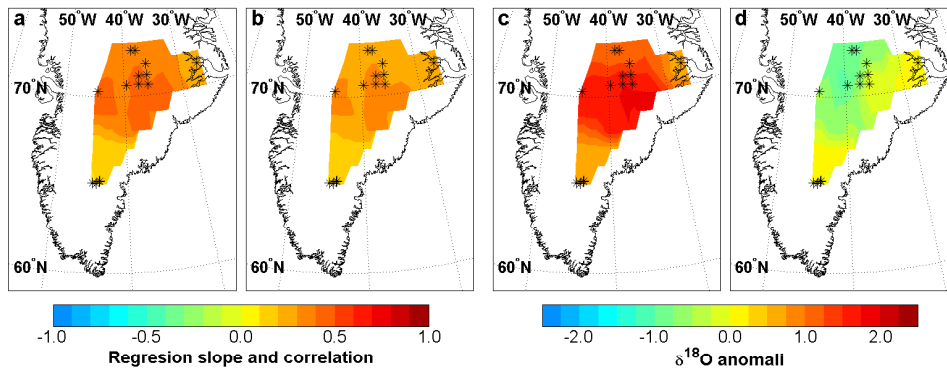
Figure 2.8: As Fig. 2.7, but relationships with Stykkisholmur Nov-Apr temperatures for the period 1831-1970.

2.5.2 Relation to Stykkisholmur temperatures

Figures 2.8a and 2.8b present spatial distributions of the linear regression slopes and linear correlations between the 14 winter season δ^{18}O series and Nov-Apr Stykkisholmur temperatures. The figures suggest that the central Greenland winter season δ^{18}O series have the strongest relation to Stykkisholmur winter temperatures, while the southern Greenland winter season δ^{18}O series are very weakly related to Stykkisholmur winter temperatures. This assertion is in agreement with observations from extreme years shown in figures 2.8c and 2.8d. Again δ^{18}O from the cores which are nearest (Site A to G and Crete) the temperature observation site (Stykkisholmur) have the strongest relations to the temperature record.

2.5.3 Relation to the NAO

In figures 2.9a and 2.9b the spatial distributions of the linear regression slopes and linear correlations between the 14 winter season δ^{18}O series and the Nov-Apr average NAO index are presented. The correlation plot (figure 2.9b) gives a strong indication that winter δ^{18}O from the southern Dye-3 cores and the central Greenland cores drilled on or west of the central Greenland ice divide (Crete, GRIP, GISP2, Site B, Site D and Milcent) are most significantly influenced by the NAO. A fact that is in conformity with coastal temperature observations, that shows the strongest influence of the NAO on SW Greenland temperatures, while east coast temperatures are much more weakly associated with the NAO [Box, 2002]. Again the extreme-plots are in broad agreement with the correlation plot, given the artificial low variability in the Dye-3 and Renland winter δ^{18}O records.
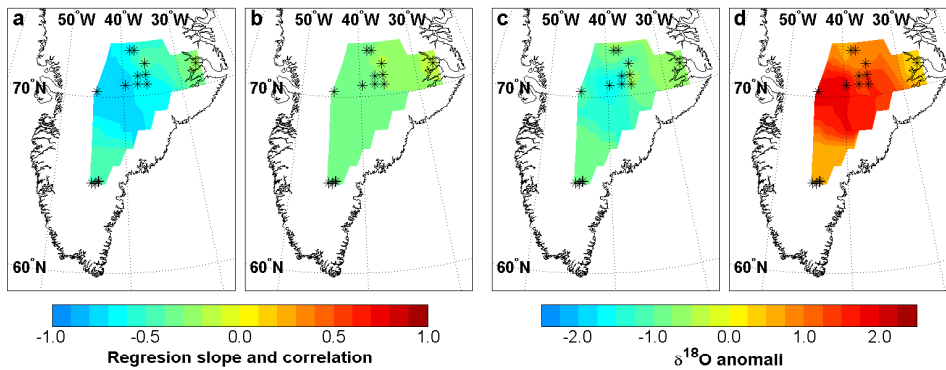
Figure 2.9: As Fig. 2.7, but relationships with the Iberian/Icelandic Nov-Apr NAO-index for the period 1823-1970.

2.5.4 Derivation of regional scale patterns in the winter season data

To gain information on regional scale patterns of variability in the Greenland ice core winter $\delta^{18}O$ data, the 14 data series shown in figure 2.5 have been subjected to principal component analysis. The variance explained by the first 7 principal components is listed in table 2.2. For the winter data it is clear that the first principal component (PC1) explains the bulk of the variance, while the second and third components (PC2 and PC3) only explain slightly more variance than the following components, which variances are almost equal. The following investigation will therefore be restricted to the first three principal components as the explained variance indicate that the following components are most likely to be dominated by data noise. In fact a study of temperature related proxy data by Fisher [2002] did show that when the variance explained by the PC2 and PC3 (based on analysis of 14 series) fell below 10% and 9% respectively, those components could consist of pure noise. Hence even the winter season PC2 and PC3 could be noise generated.

The loading patterns of the first three principal components on the 14 winter $\delta^{18}O$ records can be seen in figure 2.10. As found in the Vinther et al.

Table 2.2: Explained variance (in % of total) by each of the 7 first winter and summer $\delta^{18}O$ principal components

Season	PC1	PC2	PC3	PC4	PC5	PC6	PC7
Winter	39.8	9.4	7.9	5.6	5.3	4.9	4.8
Summer	35.0	13.7	9.9	6.3	5.4	4.8	4.7
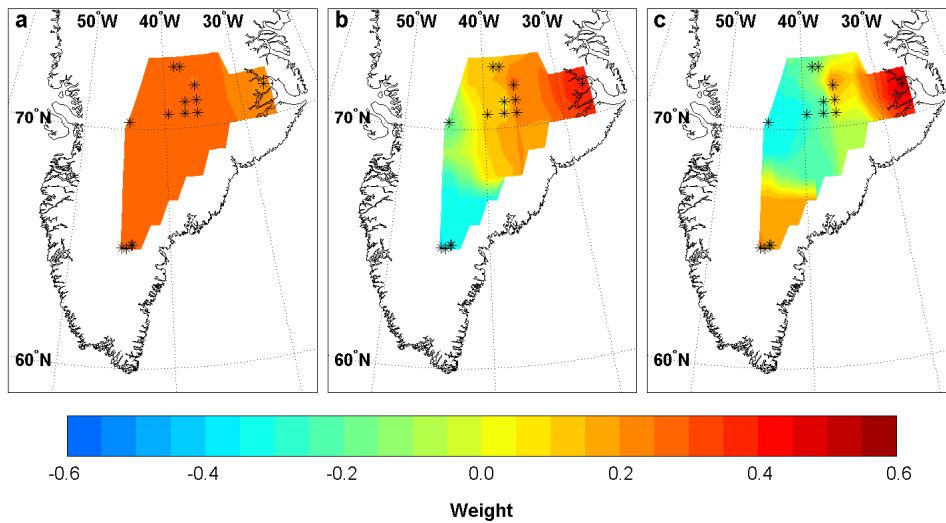
Figure 2.10: Spatial maps of the three first principal components of the winter season δ^{18}O data. Panel (a), (b) and (c) shows maps of the first, second and third component respectively.

[2003a] investigation the PC1 yields a regional scale pattern with positive loadings on all time series. The loadings on the easternmost cores are, however, somewhat smaller than for the majority of the 14 time series. The PC2 and PC3 loading patterns (figures 2.10b and 2.10c) are more complex with SW to NE and a NW-SE gradients respectively. It is especially interesting to see how both the PC2 and PC3 loadings change markedly going from west to east across the central Greenland ice divide (which passes in between Site A and Site B and through the Crete and GRIP drill sites). This enforces the perception that the ice divide exceeds significant influence on the air masses and precipitation patterns affecting Greenland δ^{18}O. The time series of the first three winter season principal components as well as SW Greenland Nov-Apr temperatures are depicted in figure 2.11. The correspondence between the SW Greenland temperatures and the PC1 time series is very convincing both on interannual and decadal time scales. The correlation between the two time series is r=0.71 (r=0.83 for the decadally filtered data) for the 1829 to 1970 period (the period where the SW Greenland winter temperature series has no gaps). The PC2 and PC3 time series are almost unrelated to the SW Greenland temperatures ($|r| < 0.1$).

2.5.5 The winter season principal components and Northern Hemisphere atmospheric flow and temperatures

Correlations between the first three Greenland winter season δ^{18}O principal component time series and gridded temperature and SLP data have been

17
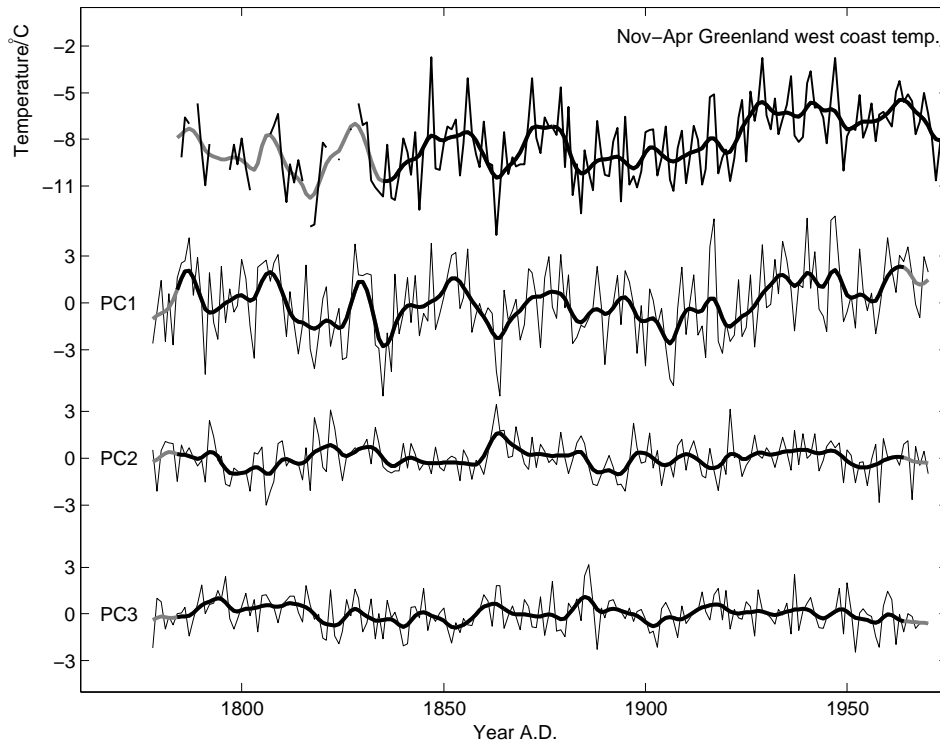
Figure 2.11: SW Greenland Nov-Apr temperatures and the time series for the first, second and third winter season $\delta^{18}O$ principal components. Thick lines are decadally filtered data (lines are grey if the filtered values are based on incomplete data).

calculated to better understand the relation between the principal components and hemispheric scale circulation as well as temperature patters. The maximum period covered both by the HadCRUT2v, HadSLP2 and the ice core data (1871-1970) has been divided into two subintervals (1871-1920 and 1921-1970) and correlations have been calculated for both periods between the gridded data and the PC1, PC2 and PC3 time series (see figure 2.12). In this manner both the correlation patterns themselves and the stability of the correlation patterns can be examined.

The spatial temperature and SLP correlation patterns associated with the PC1 time series are displayed in figures 2.12a and 2.12d. Both figures show clear NAO patterns with an Iceland/Azores pressure see-saw and SW Greenland/Scandinavia temperature see-saw. The NAO pattern is very stable indeed and the correlation between the long instrumental NAO-index and the winter $\delta^{18}O$ PC1 is r=-0.49 for the 1823-1970 period, much in agreement with the findings presented in Vinther et al. [2003a].

The PC2 and PC3 correlation patterns (see 2.12b, 2.12c, 2.12e and 2.12f) are less straight forward. In fact, no patterns seems to be stable during both
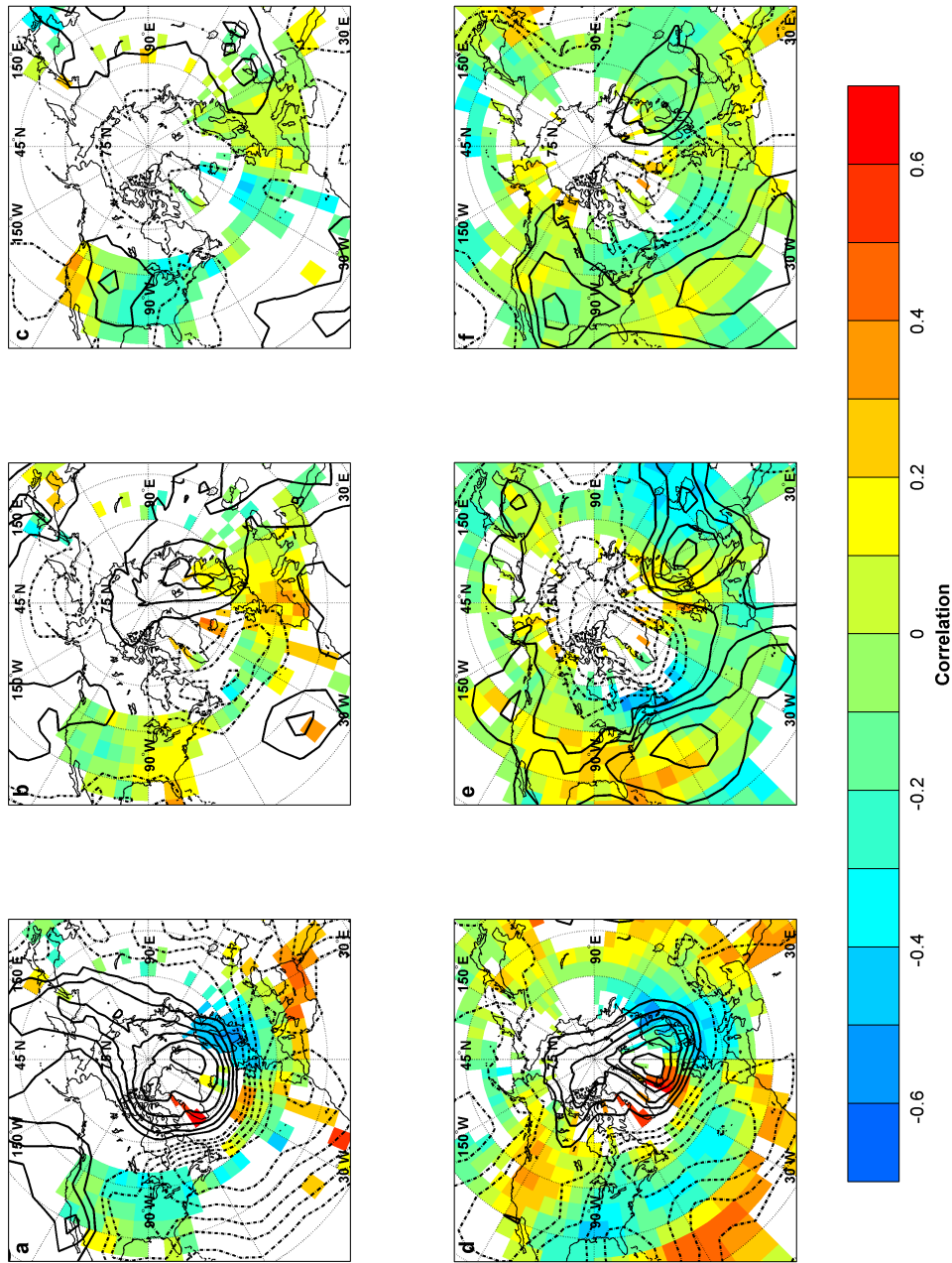
Figure 2.12: Spatial correlation maps of Nov-Apr sea level pressure (contours with 0.1 interval, solid lines indicate positive correlations, dashed lines negative) and temperature (colour coded) with respect to time series of the first (a,d), second (b,e) and third (c,f) winter season $\delta^{18}O$ principal components. Panel (a), (b) and (c) are calculated using the period 1871-1920 while panel (d), (e) and (f) are calculated using the period 1921-1970. Temperature grid-points with more than 20% missing values are left blank.

19
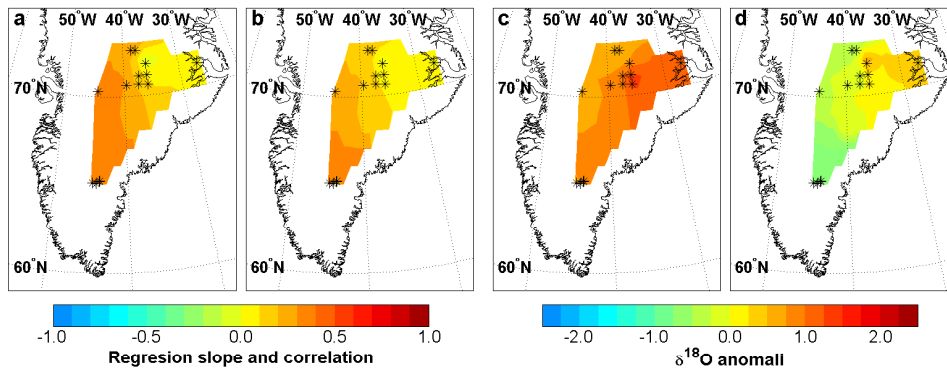
Figure 2.13: Spatial maps of relationships between SW Greenland May-Oct temperatures and summer season δ^{18}O (and D/8) data for the period 1785-1970. Panel (a) shows the slopes of linear regressions between δ^{18}O and the May-Oct temperature. Panel (b) shows the correlation between summer δ^{18}O and the May-Oct temperature. Panels (c) and (d) shows the average anomalies in summer δ^{18}O corresponding to the 5% of the May-Oct periods which registered the highest and lowest temperatures respectively.

50-year periods. This is an indication that most of the climatically relevant information in the Greenland winter δ^{18}O data is contained in the PC1 time series, whereas the PC2 and PC3 time series could very well be dominated by the high degree of noise in the winter season data, as indicated by the Fisher [2002] study.

2.6 Summer season δ^{18}O and regional meteorological conditions

2.6.1 Relation to SW Greenland temperatures

Figures 2.13a and 2.13b present the spatial distributions of the linear regression slopes and linear correlations between the 14 summer season δ^{18}O series and May-Oct SW Greenland temperatures. A clear SW to NE drop off in significance of correlations can be seen in figure 2.13b. This suggest that only summer season δ^{18}O records from cores very near the SW Greenland temperature observation sites enjoy strong relations with SW Greenland summer temperatures. The two extreme-plots (figures 2.13c and 2.13d) do give some support to this assertion, but it is interesting that both the southern and the eastern cores experience high δ^{18}O values when temperatures in SW Greenland are high (see figure 2.13c).
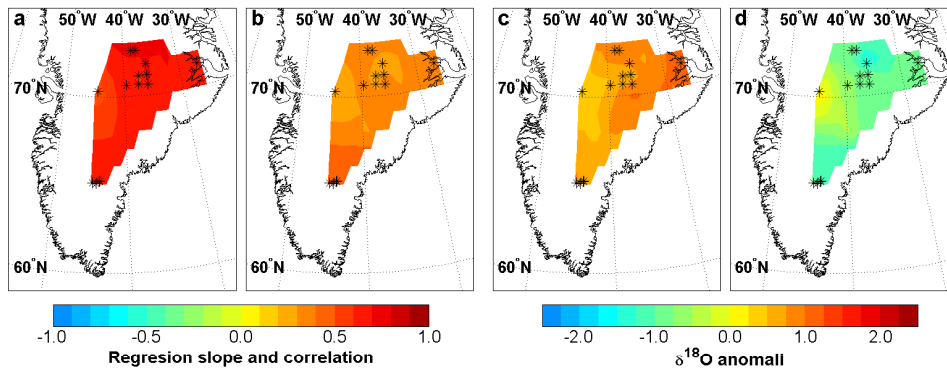
Figure 2.14: As Fig. 2.13, but relationships with Stykkisholmur May-Oct temperatures for the period 1831-1970.

2.6.2 Relation to Stykkisholmur temperatures

Figures 2.14a and 2.14b present the spatial distributions of the linear regression slopes and linear correlations between the 14 summer season δ^{18}O series and May-Oct Stykkisholmur temperatures. The combined information from the regression, correlation and extreme-value plots (figures 2.14c and 2.14d) suggest that only the Milcent core from west Greenland is weakly related to the Stykkisholmur summer temperatures. Furthermore the southern Greenland Dye-3 cores enjoys a particular strong relation with the Stykkisholmur temperature series.

2.6.3 Relation to the NAO

In figures 2.15a and 2.15b the spatial distributions of the linear regression slopes and linear correlations between the 14 summer season δ^{18}O series and the May-Oct average NAO index are presented. Generally speaking the relationship between Greenland summer δ^{18}O and the summer NAO seems to be very weak and insignificant. A slight E-W gradient in the relations can maybe be discerned in the regression plot (figure 2.15a), but this pattern is somewhat more vague in the two extreme-value plots (figures 2.15c and 2.15d). The lack of NAO influence on the Greenland summer season δ^{18}O data is in accordance with the findings of Box [2002] that Greenland summer temperatures correlates weakly and very erratically with the summer NAO index.

2.6.4 Derivation of regional scale patterns in the summer season data

As for the winter season data, principal component analysis is employed to gain information on regional scale patterns of variability in the Greenland
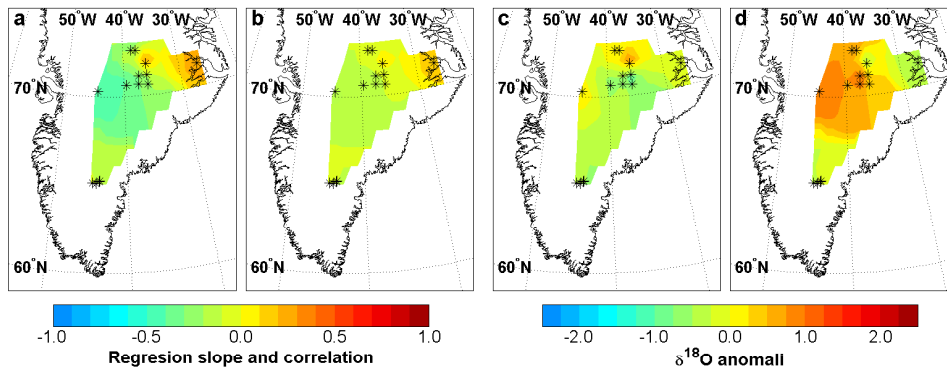
Figure 2.15: As Fig. 2.13, but relationships with the Iberian/Icelandic May-Oct NAO-index for the period 1823-1970.

ice core summer δ^{18}O data. The variance explained by the first 7 summer season principal components are listed in table 2.2. For the summer data it can be seen that the explained variance of the first principal component is less than for the winter data, while the second and third components (PC2 and PC3) explain somewhat more of the total variance as compared to the winter data. This indicates that the Greenland summer δ^{18}O data are a bit less coherent than the winter data and gives hope (also according to the Fisher [2002] study) that the summer PC2 and PC3 time series do contain more valuable climatic information, than was the case for the winter PC2 and PC3 series. Again the following components (PC4, PC5 and so on) have almost equal variance, which indicates that they are most likely to be dominated by data noise. The loading patterns of the first three principal components on the 14 summer δ^{18}O records can be seen in figure 2.16. The PC1 yields a regional scale pattern with positive loadings on all time series. The loadings on the easternmost and westernmost cores are, however, somewhat smaller than for the majority of the 14 time series. The PC2 and PC3 loading patterns (figures 2.16b and 2.16c) are more complex with S to N and E to W gradients respectively. Again it seems that the Greenland ice divide plays a role in the shape of the PC3 loading pattern. The time series of the first three summer season principal components as well as Stykkisholmur May-Oct temperatures are depicted in figure 2.17. The correspondence between the Stykkisholmur temperatures and the PC1 time series is quite convincing both on interannual and decadal time scales. The correlation between the two time series is r=0.58 (r=0.66 for the decadally filtered data) for the 1831 to 1970 period. It should be noted that the correlations between the PC1 of summer season δ^{18}O and Stykkisholmur May-Oct temperature are impressively high given the low summer temperature variability at Stykkisholmur. In fact the Stykkisholmur summer temperature variability is almost 3 times lower than the SW Greenland winter temper-

22
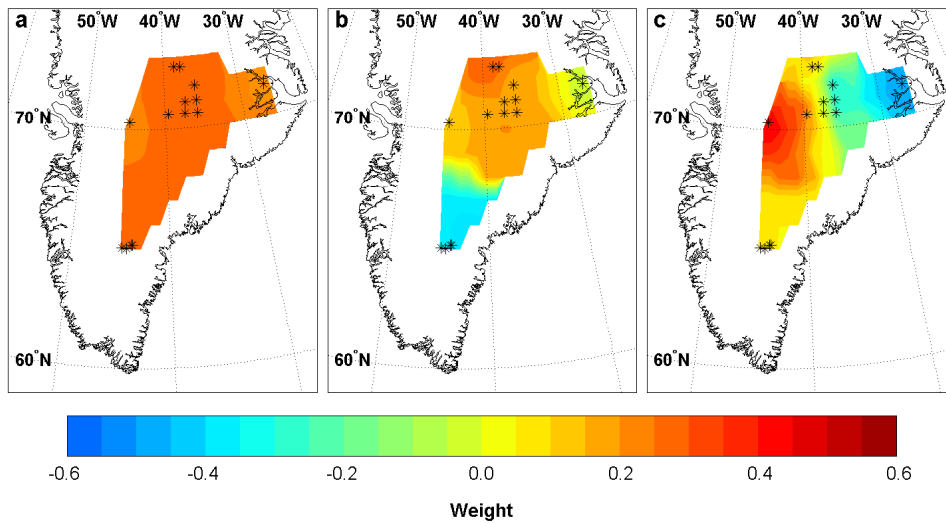
Figure 2.16: Spatial map of the three first principal components of the summer season δ^{18}O data. Panel (a), (b) and (c) shows maps of the first, second and third component respectively.

ature variability that was shown to be strongly associated with the PC1 of winter season δ^{18}O (see figure 2.11). The good correlation between the PC1 of summer season δ^{18}O and the modestly varying Stykkisholmur May-Oct temperatures are therefore indicative of the low level of noise in the summer δ^{18}O data.

2.6.5 The summer season principal components and Northern Hemisphere atmospheric flow and temperatures

Correlations between the first three Greenland summer season δ^{18}O principal component time series and gridded northern hemisphere temperature and SLP data s presented in figure 2.18. The maximum period covered both by the HadCRUT2v, HadSLP2 and the ice core data (1871-1970) has been divided into two subintervals (1871-1920 ans 1921-1970) and correlations has been calculated for both periods between the gridded data and the PC1, PC2 and PC3 time series. In this manner both the correlation patterns themselves and the stability of the correlation patterns can be examined.

The spatial temperature and SLP patterns associated with the summer PC1 time series are displayed in figures 2.18a and 2.18d. Both figures show that the PC1 is related to sea surface temperatures (SSTs) around Iceland and south of Greenland, whereas no persistent relation to atmospheric flow can be ascertained. The PC2 correlation patterns (see 2.18b and 2.18e) are difficult to interpret, as no patterns seems to be stable during both 50-year periods. This is in stark contrast to the very persistent combined
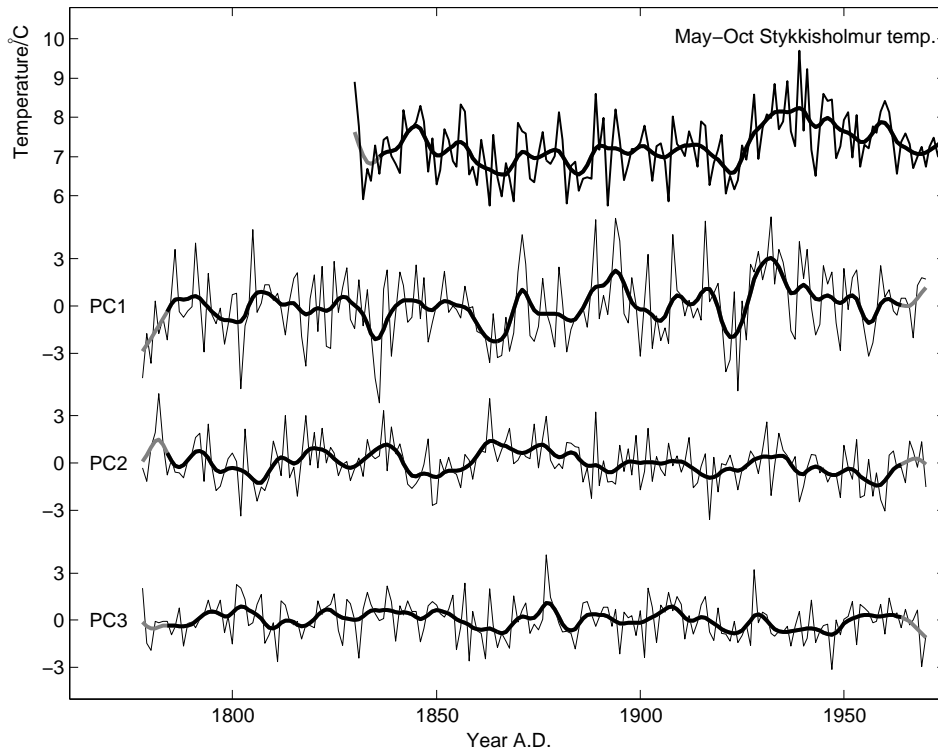
Figure 2.17: Stykkisholmur May-Oct temperatures and the time series for the first, second and third summer season $\delta^{18}O$ principal components. Thick lines are decadally filtered data (lines are grey if the filtered values are based on incomplete data).

pressure and temperature pattern associated with the summer PC3 time series (see 2.18c and 2.18f). Both 50-year periods show a combined Greenland/Scandinavia pressure and temperature see-saw. The E-W loading pattern associated with the summer time PC3 is therefore related to a high pressure over Greenland guiding cold air masses from the north along the Greenland east coast and warm southern air along the Greenland west coast, creating an E to W temperature gradient across the ice sheet.

2.7   Summary

Taking the step from annually to seasonally resolved Greenland records of ice core $\delta^{18}O$ is very important, as the seasonal resolution reveals the atmospheric and oceanic temperature and circulation patterns associated with the variability in the $\delta^{18}O$ records. Greenland winter season $\delta^{18}O$ is strongly related to SW Greenland winter temperatures and the wintertime NAO circulation pattern, while summer season $\delta^{18}O$ is associated with Stykkishol-
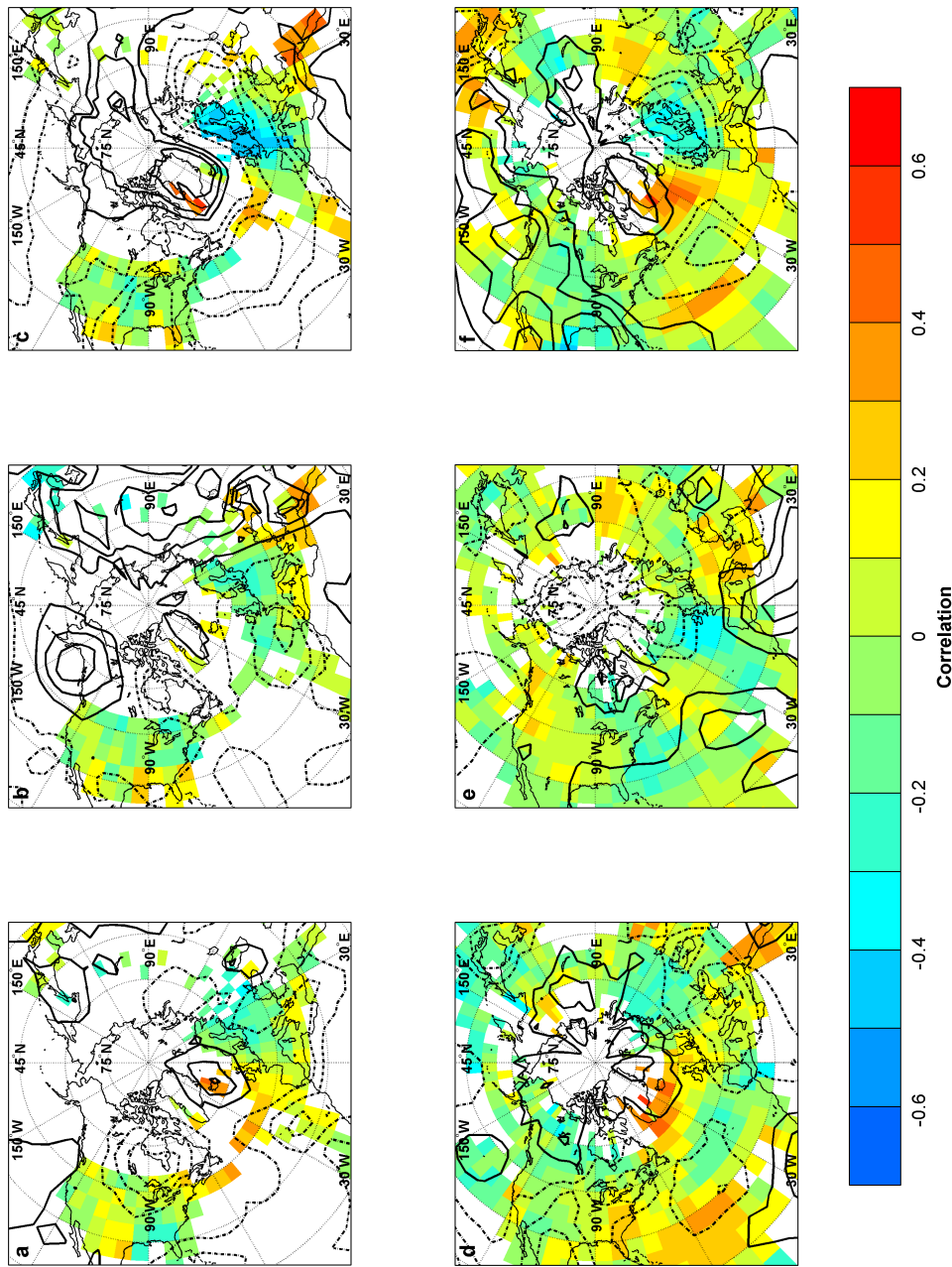
Figure 2.18: Spatial correlation maps of May-Oct sea level pressure (contours with 0.1 interval, solid lines indicate positive correlations, dashed lines negative) and temperature (colour coded) with respect to time series of the first (a,d), second (b,e) and third (c,f) summer season δ^{18}O principal components. Panel (a), (b) and (c) are calculated using the period 1871-1920 while panel (d), (e) and (f) are calculated using the period 1921-1970. Temperature grid-points with more than 20% missing values are left blank.

mur summer temperatures and summer SST conditions in Greenland and Icelandic waters. In annually resolved δ^{18}O these relations are not as easy to detect, as their fingerprints in the annual δ^{18}O are mutually obscured. Having signal to noise ratios (SNRs) markedly below the level observed of annual δ^{18}O, the Greenland winter season δ^{18}O data seems to be strongly influenced by noise processes such as sastrugi formation. An assertion which is underpinned by the fact that only the first principal component of the winter data could be shown to have stable relations with atmospheric flow and temperature patterns. SNRs also indicate that the summer δ^{18}O data are much less influenced by noise and stable atmospheric relations can be established even to the third summer δ^{18}O principal component. To obtain seasonal δ^{18}O data with reasonable SNRs it is probably necessary to stack multiple seasonal records for low accumulation areas, while records from areas with very high accumulation can much easier be used without stacking. Another interesting feature suggested by the multiple records of seasonal δ^{18}O data is that the central Greenland ice divide seems to have a significant influence on the air masses affecting the Greenland δ^{18}O. Therefore having ice core records from both east and west of the ice divide allows identification of regional scale atmospheric variability.

Despite the many difficulties associated with the creation of seasonally resolved time series of Greenland δ^{18}O (such as diffusion correction, high resolution sampling and accurate dating) it must be concluded that it is both possible and highly desirable to obtain seasonally resolved δ^{18}O data from Greenland ice cores, as such data can be used to identify past variability both of the NAO and North Atlantic SST conditions. Furthermore the information gained through analysis of seasonal δ^{18}O data improves the interpretation of annually or even less resolved Greenland δ^{18}O records.

Chapter 3

Expanding the detailed Dye-3 stable isotope series

In the previous chapter the importance of having seasonally resolved stable isotope data was documented. Furthermore it was found that seasonally resolved data from the high accumulation Dye-3 site had a very favorable signal to noise ratio. Hence it was decided to complete and extend the existing highly resolved stable isotope record from the Dye-3 deep core (see figure 3.1).

The existing Dye-3 record is composed of δ^{18}O data only, and it would therefore be natural to close the gaps in the record by carrying out more δ^{18}O measurements. However, as the remaining volume of ice from the Dye-3 core is very limited it was decided to make δD measurements instead. This choice is made because δD samples measured using a continues flow isotope ratio mass spectrometer (CF-IRMS) only requires 20% of the sample size normaly used for δ^{18}O measurements in Copenhagen. The CF-IRMS used for the δD measurements is situated at the AMS C14 Dating Centre at the University of Aarhus.

Two sections were chosen for δD sampling: The section from 1539.45m to 1625.25m and the section from 1676.95m to 1694.00m. The choice was based on a desire to extend the high resolution measurements through the 8.2kyr cold event (which have its minimum in δ^{18}O at $\sim$1691m) and a decision not to do more than 12.000 samples, in order to have a realistic chance of getting the job done in a timely manner.

3.1 Deriving the cutting scale

All existing highly resolved δ^{18}O data from the Dye-3 core have been sampled in accordance with a cutting-scale designed to yield 8 samples per year on average. This cutting-scale was based on an ice flow model that did not take into account the complicated flow in the Dye-3 area [Reeh, 1989]. As a result, a significant oversampling did occur, often yielding 10-11 samples
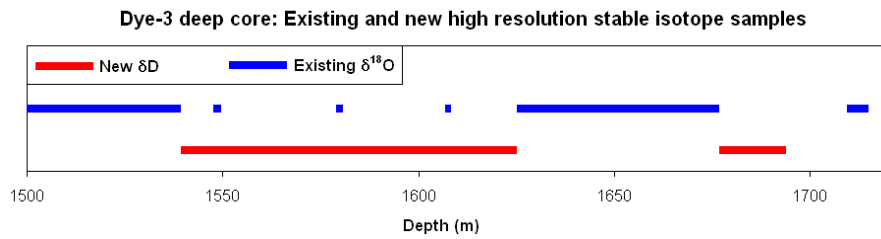
Figure 3.1: Schematic of the existing highly resolved δ^{18}O data (blue) from the 1500-1720m section of the Dye-3 deep ice core. The new highly resolved δD data sampled during this project (red) are also plotted.

per year.

In order to avoid doing labor-intensive oversampling, it was decided not to use the old cutting-scale for the new measuring effort. Instead a new cutting-scale was created based on annual layer counts in nearby sections of highly resolved δ^{18}O data. The new cutting-scale as well as the estimated annual layer thicknesses, which the scale is based on can be seen in figure 3.2.
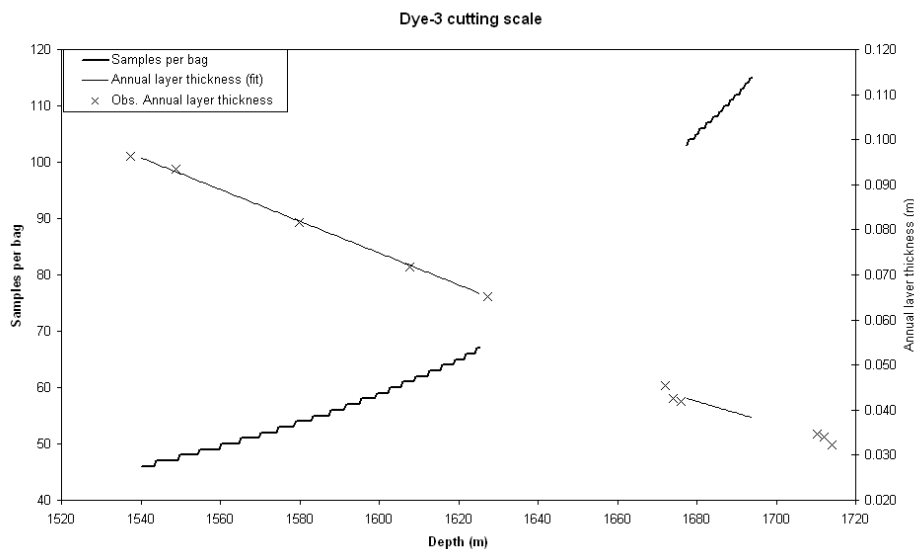
Figure 3.2: Cutting scale (heavy line) for the two sections selected for high resolution δD sampling (note that a bag has a length of 55cm). The cutting scale is formed from annual layer thickness estimates (thin line) that are based on annual layer counts in small sections of high resolution δ^{18}O (crosses).

28

3.2 Sampling procedure

For each bag of ice (a bag has a length of 55cm) a number of equally sized δD samples were cut on a band saw in accordance with the cutting-scale (figure 3.2). The samples were then put in sealed containers and melted slowly. The meltwater was immediately poured into airtight bottles and refrozen (a bottle can be seen in figure 3.3). The sample bottles were kept frozen during transport from Copenhagen to Aarhus (the location of the CF-IRMS) and then stored in a freezer at the University of Aarhus. Immediately before the samples were measured on the CF-IRMS, they were melted and transferred to small septum sealed glass vials (see figure 3.3). 110 vials at a time could then be fitted into the autosampler, that was connected to the CF-IRMS (see figure 3.4). The ice core sampling took almost 4 month to complete, including 2-3 weeks with extra assistance.

3.3 Mass spectrometry

A GV-Instruments Isoprime IRMS was used for the δD measurements. Samples were placed in a Euro Vector liquid autosampler that injected samples into a Euro Vector pyrolysis unit, were the samples were evaporated at $1070°C$ and reduced by chromium to gaseous hydrogen molecules. In a flow of helium the hydrogen was then carried to the mass spectrometer, which generate simultanous peaks of H_2 and HD at the collectors (Olsen et al. [2006] can be consulted for a more detailed description of the entire setup). For each sample a preliminary δD value is calculated with respect to a machine reference gas. These preliminary values have to be corrected for drift and calibrated to the VSMOW/SLAP scale using known standards. An example of a fully corrected batch of measurements can be seen in figure 3.5. Making an optimization of all facets in the system [Olsen et al.,2006], it was possible to do almost 400 measurements a day, not counting measurements of standards. Despite the short time spend measuring each sample, the noise in the data stayed below 0.5%₀₀, while the inter sample memory-effect (due to cross contamination of the samples) was held steady at 1-2% [Olsen et al.,2006].

The Kbh22 standard (δD=-168.4) and the Crete standard (δD=-262.2) were used for calibration of the δD data.

All 12.000 samples were measured using 14 weeks of machine time in 2004. It should be noted that the number of samples that could be measured per day was reduced to only 100 during the first five weeks, due to a software error.

Finally it should be mentioned that the CF-IRMS was situated in a room without air-conditioning. This is important because high temperatures do affect the stability of the machine reference gas (see figure 3.6). Great care was therefor taken to keep the room temperature below $25°C$, but a few

Figure 3.3: Samples were transfered from the airtight bottles to small septum-sealed vials, which could be penetrated by the syringe used by the autosampler.

Figure 3.4: The Euro Vector liquid autosampler which is connected to the CF-IRMS. There are room for 110 samples in the rotating tray.
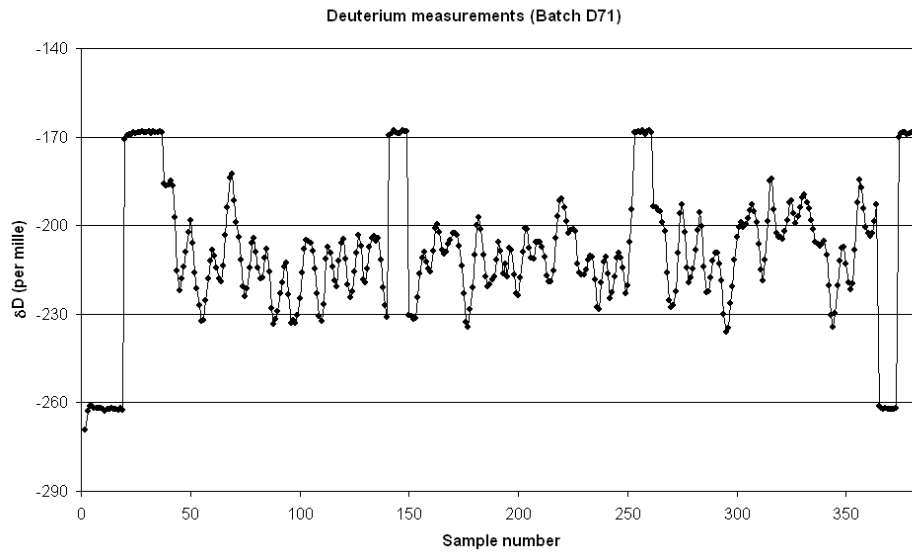
Figure 3.5: Example of a standard batch of measurements on the CF-IRMS, including 300 ice core samples plus standards. Note the standards used for calibration at the beginning and end of the batch, and the standards used for calibration control measured twice during the batch.
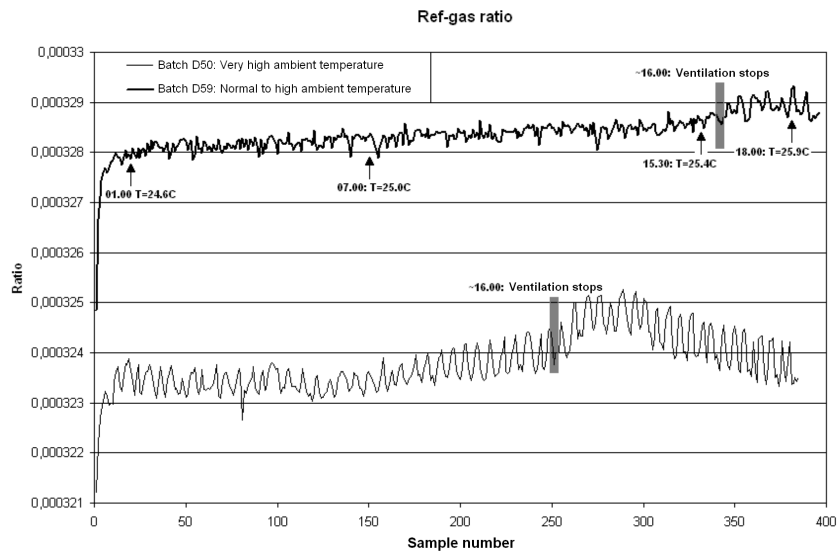
Figure 3.6: Temperature related disturbances in the reference gas during two batches of measurements.

batches had to be remeasured (including most of batch D50 shown in the figure).

3.4 Summary

From November 2003 to November 2004 12.000 samples were cut form the Dye-3 deep core and measured for δD as a part of this project. During the measuring process it was possible to optimize the CF-IRMS system to yield a throughput of 400 samples per day, without significantly increasing the data noise or the inter sample memory effect. The new measurements complete the Dye-3 high resolution stable isotope data down through the 8.2kyr event.

Chapter 4

Dating the Dye-3, GRIP, NGRIP and Renland ice cores throughout the Holocene

The following section presents the dating of the Holocene parts of the Dye-3, GRIP, NGRIP and Renland ice cores. Sections 4.1 to 4.8 are a copy of the paper:

Vinther, B. M., H. B. Clausen, S. J. Johnsen, S. O. Rasmussen, J. P. Steffensen, K. K. Andersen, S. L. Buchardt, D. Dahl-Jensen, I. K. Seierstad, M-L. Siggaard-Andersen, A. M. Svensson, J. Olsen and J. Heinemeier, A synchronized dating of three Greenland ice cores throughout the Holocene, *J. Geophys. Res.*, *111*, D13102, doi:10.1029/2005JD006921. 2006.

These sections describe and discusses the dating of the Dye-3, GRIP and NGRIP cores. Section 4.9 and section 4.10 are not part of the paper but later additions. Section 4.9 details the dating of the Renland ice core, while section 4.10 presents a general discussion of the dating of the four cores in relation to tree-ring based dating.

4.1 Abstract

As part of the effort to create the new Greenland Ice Core Chronology 2005 (GICC05) a synchronized stratigraphical timescale for the Holocene parts of the DYE-3, GRIP and NGRIP ice cores is made by using volcanic reference horizons in electrical conductivity measurements to match the cores.
The main annual layer counting is carried out on the most suited records only, exploiting that the three ice cores have been drilled at locations with different climatic conditions and differences in ice flow. However, supple-

mental counting on data from all cores has been performed between each set of reference horizons in order to verify the validity of the match. After the verification, the main dating is transferred to all records using the volcanic reference horizons as tie points. An assessment of the mean annual layer thickness in each core section confirms that the new synchronized dating is consistent for all three cores.

The data used for the main annual layer counting of the past 7900 years are the DYE-3, GRIP and NGRIP stable isotope records. As the high accumulation rate at the DYE-3 drill site makes the seasonal cycle in the DYE-3 stable isotopes very resistant to firn diffusion, an effort has been made to extend the DYE-3 Holocene record. The new synchronized dating relies heavily on this record of $\sim$75,000 stable isotope samples. The dating of the early Holocene consists of an already established part of GICC05 for GRIP and NGRIP which has now been transferred to the DYE-3 core.

GICC05 dates the Younger Dryas termination, as defined from deuterium excess, to 11,703 b2k; 130 years earlier than the previous GRIP dating.

4.2   Introduction

The vast Greenland ice sheet is an outstanding archive of past northern hemisphere atmospheric conditions. During the past decades, several ice coring efforts have been made in order to retrieve continuous records for the study of past climatic conditions [Dansgaard and Johnsen, 1969; Langway et al., 1985; Johnsen and Dansgaard 1992; Dansgaard et al., 1993; Meese et al., 1994; NGRIP Members, 2004].

To fully exploit the wealth of information provided by the ice cores, an accurate dating of the records is essential [e.g. Hammer et al. 1978]. Having ice cores from different parts of the ice sheet, cross dating of records is of great importance, because thoroughly cross dated records allow studies of local climate differences [Rogers et al., 1998]. Furthermore, it is possible to retrieve more accurate regional climatic signals by stacking the cross dated records [e.g. Vinther et al., 2003].

Here we present a new counted timescale for the DYE-3, GRIP and NGRIP ice cores, spanning the past 11.7 kyrs, the entire Holocene period. The timescale has been cross dated carefully using volcanic reference horizons, detectable in Electrical Conductivity Measurements (ECM) performed continuously on the cores. This new timescale that synchronizes the Holocene parts of the DYE-3, GRIP and NGRIP ice cores, is part of the ongoing effort to create the Greenland Ice Core Chronology 2005 (GICC05), a counted chronology reaching far beyond the last glacial maximum.

The ice flow properties at the DYE-3, GRIP and NGRIP drill sites are very diverse. At the DYE-3 site the high accumulation rate allows for extremely well preserved annual layers, detectable in all measured parameters. At the same time, however, the high accumulation rate leads to vigorous ice flow

Table 4.1: Ice core specifications and present drill site characteristics.

Ice Core	Elevation (m a.s.l.)	Latitude (°N)	Longitude (°W)	Mean air temp. (°C)
DYE-3	2480	65.18	43.83	-20
GRIP	3230	72.58	37.64	-32
NGRIP	2917	75.10	42.32	-32

Ice Core	Accumulation (m ice per year)	Ice Core length (m)	Years of drilling	
DYE-3	0.56	2037	1979-1981	
GRIP	0.23	3027	1989-1992	
NGRIP	0.19	3090	1996-2004	

which rapidly thins the annual layers with increasing depth. The GRIP and NGRIP drill sites, situated at the summit of the Greenland ice cap and on the northern ice divide respectively, are sites with more moderate accumulation and ice flow, which create conditions for slow but steady layer thinning. But because the NGRIP core has been drilled at a site of the ice cap subjected to bottom melting, the mean annual layer thickness never gets much smaller than the annual melt rate.

The differences between the glaciological conditions at the DYE-3, GRIP and NGRIP drill sites make these three ice cores an ideal combination for dating purposes. Through a large part of the Holocene, the high accumulation rate at DYE-3 allows robust identification of the annual cycles in stable oxygen and hydrogen isotope data. Hence some 12,000 new isotope samples have been cut and measured to complete and extend the DYE-3 stable isotope record. Below the 8.2 ka cold event, thinning of the annual layers makes identification of annual cycles in the DYE-3 stable isotopes difficult. Therefore GRIP Continuous Flow Analysis (CFA) measurements of chemical impurities in the ice have been used for annual layer counting below 7.9 ka b2k (before A.D. 2000).

The dating of the early Holocene using GRIP and NGRIP CFA data (GRIP data 7.9-11.7 ka b2k, NGRIP data 10.3-11.7 ka b2k) has been presented in Rasmussen et al. [2006]. Due to the relatively slow flow-induced thinning at NGRIP and the high resolution of the NGRIP CFA data, annual layers can be identified past the last glacial maximum. An extension of GICC05 down to 42 ka is discussed in K. K. Andersen et al. [submitted 2006] and A. Svensson et al. [submitted, 2006].

4.3   Ice Core Data

The locations of the DYE-3, GRIP and NGRIP drill sites are shown in Fig. 4.1, while further information on the cores and drill sites is given in Table 4.1. An overview of the temporal distribution of the ice core data used
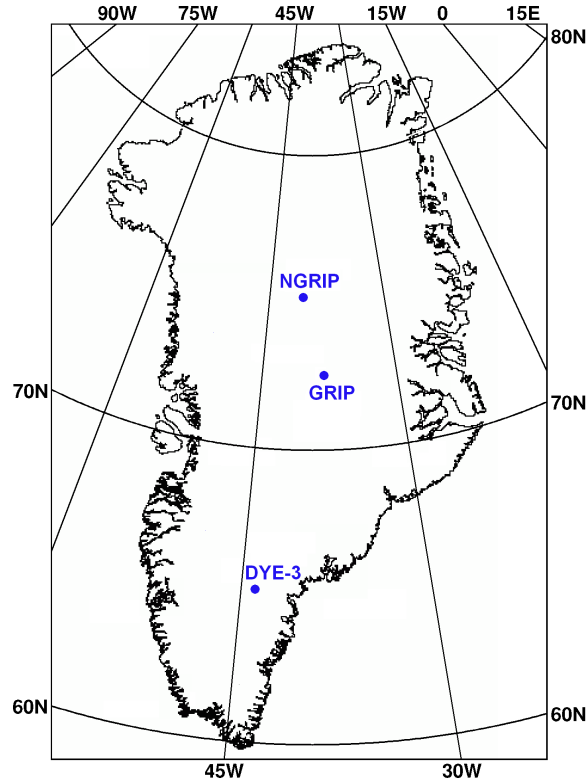
Figure 4.1: The three Greenland deep ice cores used in the construction of the Greenland Ice Core Chronology 2005. DYE-3, GRIP (Greenland Ice core Project) and NGRIP (North Greenland Ice core Project).

for the GICC05 dating can be seen in Fig. 4.2. Descriptions of data from each of the three ice cores are given in the following sections. To facilitate comparison of data availability between the ice cores, the common GICC05 ages of the sections will be used instead of referring to ice core depths.

4.3.1 DYE-3

An extensive amount of stable oxygen isotope measurements (δ^{18}O) has been carried out on the DYE-3 ice core during the early 1980s [Dansgaard et al., 1982]. 63,000 δ^{18}O samples at a resolution of 8 samples per year or higher cover the period back to the year 5815 b2k and the time interval from 6906 to 7898 b2k.

In this work an additional 12,000 ice samples from the periods 5816-6905 b2k and 7899-8313 b2k have been cut at a resolution of 8 samples per year in order to complete the DYE-3 stable isotope record and extend it through the 8.2 ka cold event. Stable hydrogen isotope measurements (δD) were carried out on these samples, exploiting the small sample size required for δD

36
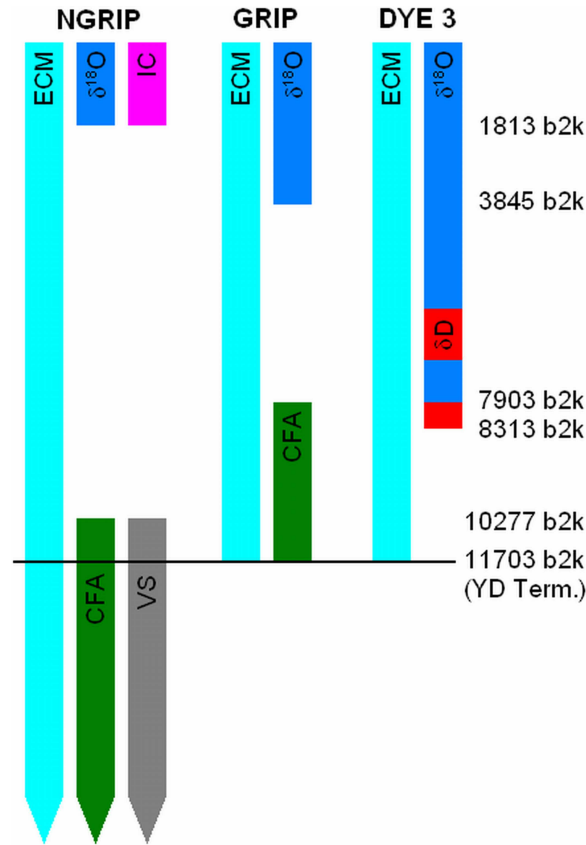
Figure 4.2: Overview of the ice core data used for constructing the Greenland Ice Core Chronology 2005. The termination of Younger Dryas (YD Term.) is indicated by the black line. ECM is Electrical Conductivity Measurement, IC is Ion Chromatography data, CFA is Continuous Flow Analysis data and VS is Visual Stratigraphy data.

measurements using a modern Continuous-Flow Isotope Ratio Mass Spectrometer (CF-IRMS). All 12,000 samples have been measured at the AMS 14C Dating Centre at the University of Aarhus on a GV Instruments CF-IRMS [Morrison et al., 2001].
ECM data are available down through the entire Holocene for the DYE-3 core [Hammer et al., 1980].

4.3.2 GRIP

Measurements of δ^{18}O at a resolution of 2.5 cm are available back to 3845 b2k [Johnsen et al, 1997]. This resolution corresponds to 7-10 samples per year (with fewest samples per year in the earliest part of the record due to flow-related thinning of the annual layers). Short sections of δ^{18}O measurements

are available through the rest of the Holocene, but they cover less than 10%
of the total time span and do not form a continuous record. ECM data are
available for the entire GRIP core [Clausen et al., 1997].

4.3.3 NGRIP

δ^{18}O measurements at a resolution of 2.5 cm are available back to 1813 b2k
[Dahl-Jensen et al., 2002]. This resolution corresponds to 7-9 samples per
year, again fewest in the earliest part of the record. Ion Chromatography
(IC) measurements of impurities have been made (at the Niels Bohr Insti-
tute, University of Copenhagen) back to 1813 b2k, at a resolution of 5 cm,
corresponding to ∼4 samples per year.
ECM data exist for the entire NGRIP core [Dahl-Jensen et al., 2002].

4.4 Methodology

The dating of the three ice cores is carried out in four steps. First the
ECM records of the three cores are used to match up volcanic reference
horizons. Secondly, between consecutive match points annual layers are
counted independently in each core. In the third step it is decided if possible
discrepancies in the annual counts between the cores can be resolved. If this
is not possible, a return to step 1 (the ECM match) is deemed necessary.
The fourth step is to find the number of years which is consistent with all
available data, and then impose the resulting dating on all three ice cores.
In this step the records showing the clearest annual cycles are given the
greatest weight.
The process of going through the four steps is carried out for all parts
of the DYE-3, GRIP and NGRIP Holocene records, thereby producing a
synchronized timescale valid for all three ice cores.
In the next sections we describe the dating procedure and the records used
in the different time periods of the Holocene, starting with the uppermost
year present in all three cores, 21 b2k (A.D. 1979).

4.4.1 21–1813 b2k

For this period, detailed δ^{18}O data from all three cores have been used. As
diffusion in the snow and firn layers (the upper 60-70 m of the ice sheet)
dampens the annual cycle in δ^{18}O significantly for areas of low accumula-
tion, it has been necessary to use deconvolution techniques [Johnsen 1977;
Johnsen et al. 2000] to re-establish the annual oscillations in the GRIP and
NGRIP records. Deconvolution is not necessary for the DYE-3 δ^{18}O data
due to the high accumulation rate at DYE-3 (see Table 1).
An example of the matching, deconvolution and layer count is given in Fig.
4.3. It is seen that the NGRIP δ^{18}O data set is on the limit of safe decon-
volution, whereas most annual layers are discernible in the measured GRIP
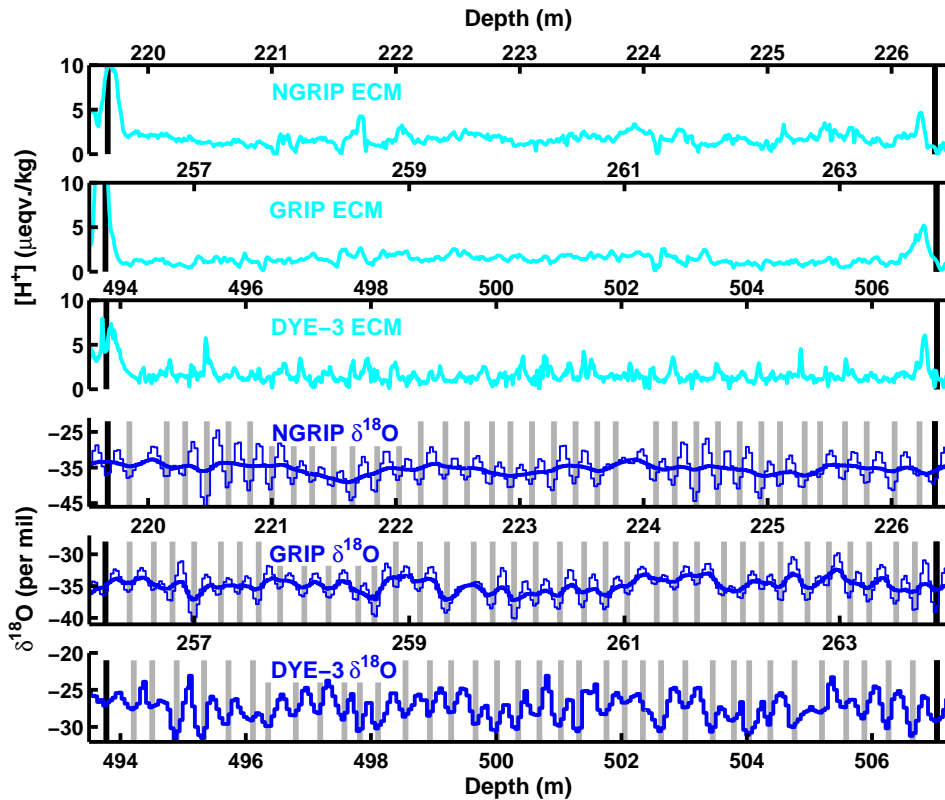
Figure 4.3: Top three graphs: Matching of the DYE-3, GRIP and NGRIP ECM records from A.D. 897 to A.D. 934. Reference horizons are indicated by black bars. Bottom three graphs: Detailed comparison of stable isotope records. Thick blue lines are measured data while thin lines are deconvoluted data, corrected for firn diffusion. Light grey bars indicate single years (winters) identified in the records.

δ^{18}O data before deconvolution. The measured DYE-3 δ^{18}O data is seen to exhibit clear annual cycles.

Multi parameter NGRIP IC impurity data are considered in the NGRIP annual layer count and the combined information of the NGRIP IC data and the deconvoluted δ^{18}O data proved sufficient for annual layer identification. However, during this period most weight is given to the DYE-3 δ^{18}O data and the deconvoluted GRIP δ^{18}O data, as the two δ^{18}O data sets are far better resolved than the NGRIP IC impurity data.

4.4.2   1814–3845 b2k

The NGRIP IC data and the 2.5 cm δ^{18}O data terminate at 1813 b2k leaving only the NGRIP ECM record with sufficient resolution for dating purposes.

As annual cycles are not always clearly represented in the ECM record, almost no weight is given to the NGRIP annual layer count in this section. NGRIP ECM is merely used to transfer the consensus annual layer count from DYE-3 δ^{18}O and GRIP deconvoluted δ^{18}O to the NGRIP core. ECM annual layer counting is typically associated with errors of 5-10%. If the discrepancy for a given matched section exceeds this expected error, the underlying match of volcanic reference horizons is reconsidered.

4.4.3 3846–7902 b2k

The GRIP 2.5 cm δ^{18}O data terminate at 3845 b2k leaving only the GRIP ECM record with sufficient resolution for dating purposes. Therefore almost no weight is given to the GRIP and NGRIP annual layer counts in this section. GRIP and NGRIP ECM data are merely used to transfer the annual layer count from DYE-3 δ^{18}O and δD data to the GRIP and NGRIP cores. Again, if the discrepancy in a section exceeds the expected error of 5-10%, the underlying match of volcanic reference horizons is reconsidered. Highly resolved GRIP δ^{18}O data are used in the dating procedure where available. An example of the transfer of the DYE-3 dating to the GRIP and NGRIP cores is given in Fig. 4.4.

4.4.4 7903–8313 b2k

The rapid thinning rate at the DYE-3 site allows progressing ice diffusion to dampen the annual cycle in the DYE-3 δ^{18}O and δD data (see Fig. 4.5). This dampening makes identification of annual layers increasingly difficult. Therefore, the dating of the GRIP core presented in Rasmussen et al. [2006] is transferred to the DYE-3 core in this section. There are no significant discrepancies between the (less certain) annual layer counts in the DYE-3 δD data and the counts based on GRIP CFA data for any part of the section.

4.4.5 8,314–11,703 b2k

Below 8313 b2k the DYE-3 annual layer counting is carried out on the DYE-3 ECM record. The DYE-3 ECM count is merely used to transfer the Rasmussen et al. [2006] dating of the GRIP (8,314–11,703 b2k) and NGRIP (10,277–11,703 b2k) cores to the DYE-3 core. Again, if the discrepancies in a section exceed the expected error of 5-10%, the underlying match of volcanic reference horizons has been reconsidered.

4.5 Dating Uncertainties

A range of issues may lead to uncertainties and errors in ice core time scales based on annual layer counting. The most important ones include: Imperfect core stratigraphy, core loss during drilling/handling of the core, data
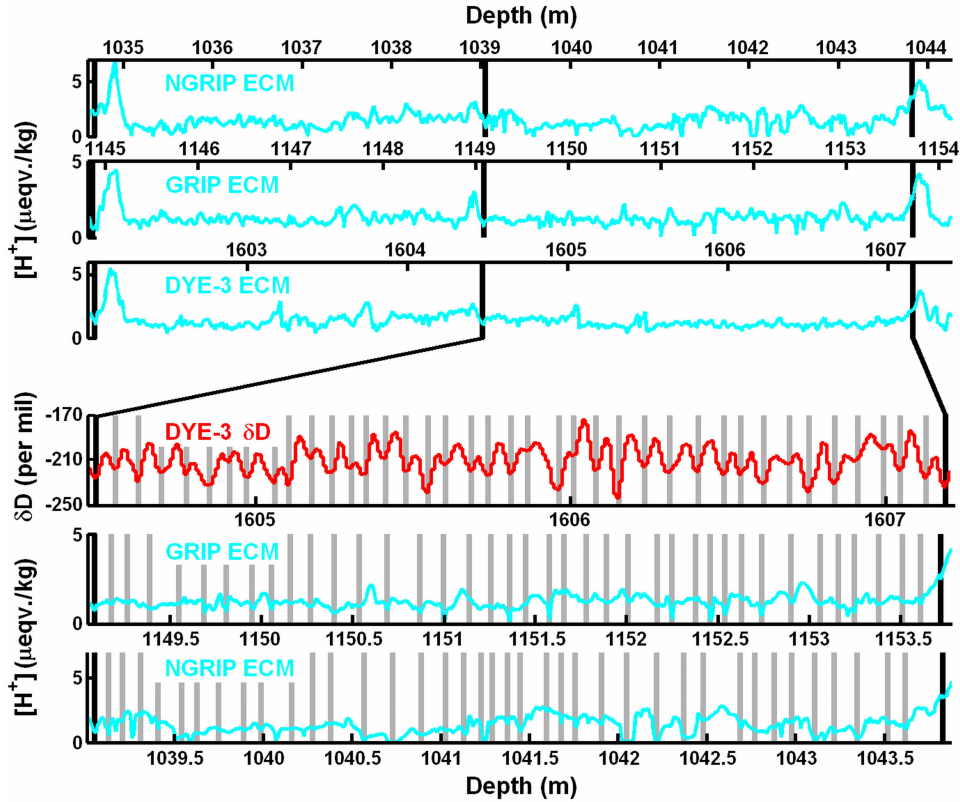
Figure 4.4: Top three graphs: Matching of the DYE-3, GRIP and NGRIP ECM records from 6559 b2k to 6632 b2k. Reference horizons are indicated by black lines. Bottom three graphs: Detailed matching of GRIP and NGRIP ECM based dating to the DYE-3 record from 6593 b2k to 6632 b2k. Light grey bars indicate single years (winters) identified in the records.

loss during sampling/measuring of the core, insufficient measuring resolution and misinterpretation of the records [Alley et al., 1997].

During the Holocene, the accumulation rate is known to have been relatively high. Hence the DYE-3, GRIP and NGRIP records should not suffer from any significant imperfections in stratigraphy. The existence of complete years without precipitation is extremely unlikely, especially for the DYE-3 high accumulation site.

Core loss and data loss have been minimal for the DYE-3, GRIP and NGRIP ice cores. Furthermore, having three ice cores available for the dating, any small section of missing data in one core can be studied in two unaffected ice cores. It shall be noted that due to differences in ice flow the time period spanned by DYE-3 brittle-zone does not overlap the periods covered by GRIP and NGRIP brittle-zones (the brittle-zone at a depth of approx. 800-1200 m, is a particularly fragile section of the ice core which is difficult
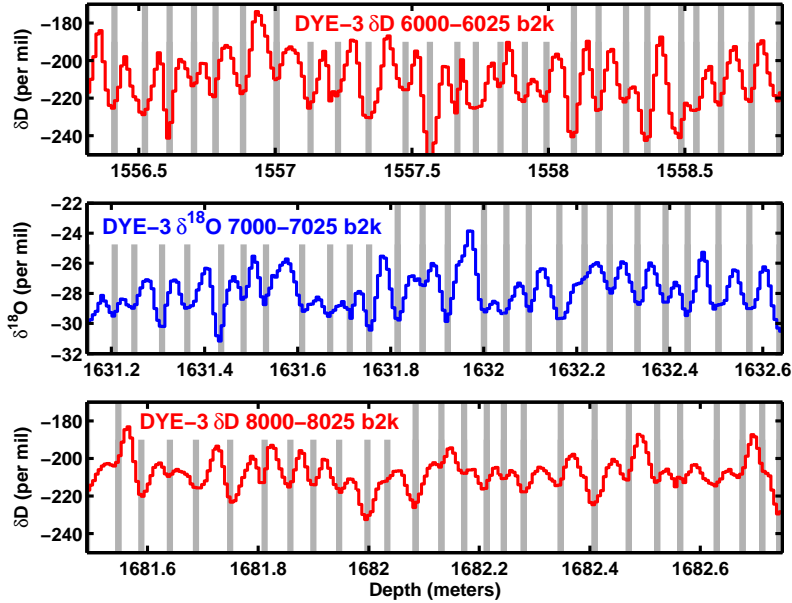
Figure 4.5: Three sections of the detailed DYE-3 stable isotope profile. The annual cycle is visible in all three sections despite progressive dampening induced by ice diffusion. Light grey bars indicate single years (winters) identified in the records.

to handle and sample [Shoji and Langway, 1982]). The DYE-3 ice is brittle from 1.9-3.6 ka b2k while GRIP and NGRIP brittle-zones span the periods 4.0-7.1 ka b2k and 4.7-8.0 ka b2k respectively. A non-brittle ice core is therefore available for all time periods covered by the GICC05 dating.

Having a stable isotope record based on 8 samples per year or better at the DYE-3 site, annual oscillations are resolved during the past 8300 years (see Fig. 4.3, 4.4 and 4.5). The sample resolution of the GRIP and NGRIP δ^{18}O data is also sufficient for safe layer counting to be carried out. However, the effective resolution of the GRIP and NGRIP records (and the DYE-3 record below $\sim$6.9 ka b2k) is influenced by diffusional smoothing of the δ^{18}O oscillations. Therefore deconvolution techniques [Johnsen, 1977; Johnsen et al., 2000] are applied to the stable isotope records in order to enhance their effective resolution (see Fig. 3). The sampling resolution of the NGRIP IC data ($\sim$4 samples per year) is some times marginal with respect to resolving annual layers.

The risk of misinterpreting the ice core records is probably the most significant contribution to uncertainties in the Holocene part of the GICC05 dating. Experience from the dating of multiple shallow ice cores (covering the most recent part of the Holocene) does however establish that δ^{18}O and δD data exhibit very reliable annual oscillations due to their close coupling to Greenland temperatures [Hammer et al., 1978]. Deconvolution of the stable

Table 4.2: Maximum counting errors for the Holocene part of the Greenland Ice Core Chronology 2005 (GICC05).

Top year Age (b2k)	Bottom year Age (b2k)	Max. counting error (%)
21	3845	0.25
3846	6905	0.50
6906	7902	2.00
7903	10276	2.00[a]
10277	11703	0.67[a]

[a]Max. counting errors from Rasmussen et al. [2006].

isotope data does pose the danger of introducing oscillations of non-annual origin, e.g. the small oscillation observed in the NGRIP deconvoluted $\delta^{18}O$ data at a depth of ∼224m in Fig. 4.3. The risk of misinterpreting such oscillations is mitigated by the availability of the DYE-3 stable isotope data, which do not need deconvolution.

Rasmussen et al. [2006] offers a discussion of the uncertainties concerning the dating based on the GRIP and NGRIP CFA data.

4.5.1 Uncertainties and bias evaluation for the annual layer counting

In the previous section it has been established that the uncertainties associated with core and measurement related issues are almost negligible. Therefore, possible misinterpretation of the ice core records is very likely to be the most significant contributor to uncertainties in the dating of the past 7.9 kyrs. Hence several strategies are used to asses this uncertainty. Following the methodology of Rasmussen et al. [2006], features in the ice core records which can neither be dismissed nor confirmed as annual layers using all data available, are recorded as uncertain years. Half of the number of uncertain years is subsequently included in the final timescale, while the other half is discarded. The maximum counting error is then defined as half of the number of uncertain years. This is to say, that uncertain years enter into the dating as 0.5±0.5 year. Maximum counting errors for different periods of the Holocene are given in Table 4.2. The error estimates are an expression of the difficulties encountered when interpreting the records, but does not take into account the possibility that the criteria used for identifying annual layers may be imperfect. Thus, the maximum counting errors does not reflect possible biases in the annual layer identification process [Rasmussen et al., 2006].

Direct estimation of the counting bias is possible for the past ∼1900 years where historically dated volcanic reference horizons are observed in the ice core records. The period between the A.D. 79 Vesuvius eruption and the A.D. 1362 Öraefajökull eruption has been chosen to evaluate possible

biases in the dating technique. Both the A.D. 79 Vesuvius eruption and the A.D. 1362 Öraefajökull eruption have recently been identified in tephra from the GRIP ice core (C. Barbante, personal communication, 2005; V. A. Hall and J. R. Pilcher, personal communication, 2006). Using the DYE-3 and GRIP δ^{18}O and ECM data a total of 1283 years are counted in between A.D. 79 and A.D. 1362. This is only one year (or $\sim$0.1%) more than the 1282 years known from historical records. It is therefore reasonable to conclude that the bias associated with counting annual cycles in DYE-3 and GRIP δ^{18}O data is very small, and certainly within the maximum counting error of 0.25% for the period back to 3845 b2k covered by both DYE-3 and GRIP δ^{18}O data.

From 3846 b2k to 6905 b2k, the DYE-3 stable isotope record is the only data set suited for annual layer counting. The maximum counting error doubles to 0.5% as doubtful features no longer can be investigated in a parallel δ^{18}O record. A bias estimate when using one record only can be obtained by looking at previous counted timescales for GRIP and DYE-3. According to Clausen et al. [1997] the period delimininated by the A.D. 79 Vesuvius eruption and the Minoan eruption of Thera has been independently dated in the DYE-3 and GRIP ice cores. In the GRIP core 1714 years were found, while 1723 years were found in the DYE-3 core. Compared to the new GICC05 dating, that uses both cores, discrepancies are -0.2% and 0.3% respectively. The counting bias introduced when using only one core is therefore within the 0.5% maximum counting error estimate.

The period from 6906 b2k to 7902 b2k is a problematic section in the Holocene part of the GICC05 dating. Progressing ice diffusion gradually smooths the DYE-3 stable isotope data, thereby weakening the annual cycle (see Fig. 4.5). Furthermore, deconvolution techniques are not entirely safe to use, as this part of the DYE-3 record contains some steep gradients in the δ^{18}O data. The gradients are due to more frequent surface melt during the climatic optimum. Therefore, the maximum counting error grows to 2.0% during the 6906-7902 b2k period. This estimate is an average for the entire 997 year long period, reflecting that the counting error increases throughout the period as diffusion effects progress.

An independent bias estimation for the 6906-7902 b2k period is difficult to obtain, because the combination of melt layers and progressing ice diffusion is unique to this part of the DYE-3 stable isotope data set. A comparison between annual layer counts in the overlapping period of DYE-3 δD and GRIP CFA data (7903-8314 b2k) indicates a slight bias (0.5-1.0%) towards an overstimation of the number of years in the DYE-3 record. The maximum counting error is, however, 2% for the GRIP CFA record from 7,903-10,276 b2k and $\sim$3% for the DYE-3 record from 7903-8314 b2k. A bias estimate of 0.5-1.0% is therefore below the threshold of safe detection.

As all bias estimates are well within the maximum counting errors given in Table 4.2, it is considered safe to use the maximum counting errors as an estimate of the total uncertainty associated with the GICC05 timescale
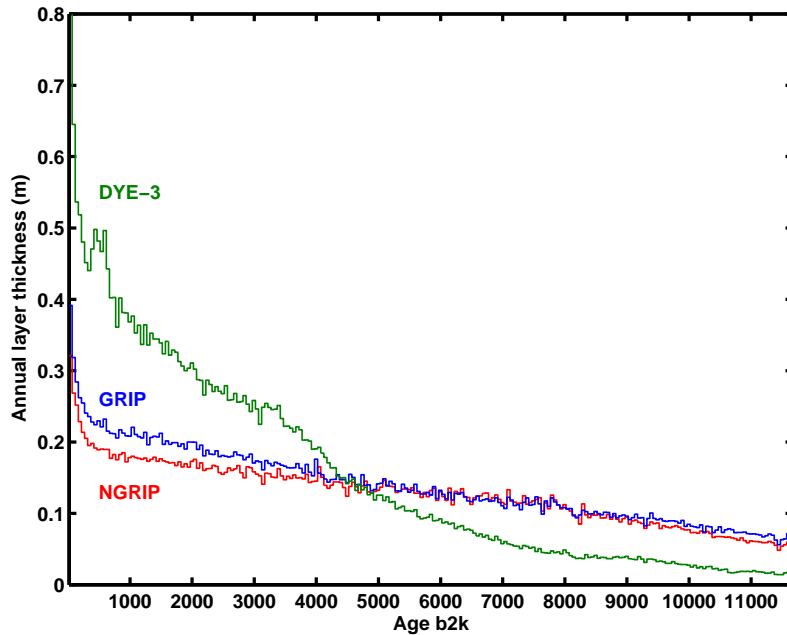
Figure 4.6: Holocene annual layer thickness profiles for the DYE-3, GRIP and NGRIP ice cores on the GICC05 timescale.

back to 6905 b2k. Before 6905 b2k biases are difficult to evaluate and the maximum counting errors are to be used more cautiously. A discussion of the maximum counting errors for the 7,903-11,703 b2k period can be found in Rasmussen et al [2006].

4.5.2 Uncertainties in the synchronization of the three ice cores

The three ice core records have been synchronized using volcanic reference horizons (see Fig. 4.3 and 4.4). The risk of mismatching the volcanic reference horizons is low as any such mismatch would create an easily detectable abrupt jump in the derived annual layer thickness record. It is reassuring that no such jumps can be detected in the GRIP and NGRIP annual layer thickness records (see Fig. 4.6). The DYE-3 annual layer thickness record exhibits a peculiar oscillation around 400-800 b2k which is caused by upstream depositional effects. These effects are due to the DYE-3 drill site being located in an area of vigorous ice flow over a mountainous bedrock leading to a rather uneven surface topography of the ice sheet [Reeh, 1989]. The uncertainty in the matching of ECM volcanic reference horizons is estimated to be one year at most, depending on the width and shape of the volcanically induced acidity peaks measured by ECM. Volcanic reference horizons are generally available for every ~50 years linking GRIP and NGRIP,

45

Table 4.3: Correlations between annually averaged ECM and their variances.

Top year Age (b2k)	Bottom year Age (b2k)	Correlation[a]			Variance $(\mu\mathrm{eqv./kg})^2$		
		D/G	D/N	G/N	DYE-3	GRIP	NGRIP
21	1813	0.24	0.27	0.46	0.25	0.35	0.38
1814	3845	0.23	0.07	0.24	0.15	0.22	0.17
3846	7902	0.27	0.30	0.48	0.23	0.21	0.36
7903	8313	0.19	0.24	0.37	0.08	0.12	0.29
8314	11703	0.40	0.39	0.49	0.21	0.41	0.55

D=DYE-3, G=GRIP and N=NGRIP.

and for every ∼100 years linking all three cores [Clausen et al. 1997]. The potential mismatch within matched sections is difficult to asses, but it is believed to be one year at most in the sections where stable isotope data are available for the annual layer counting. When the dating of a core relies only on ECM, the possible maximum mismatch within the matched sections is estimated to 2-3 years. For the part of the DYE-3 core from 8,314-11,703 b2k, which has been synchronized to the Rasmussen et al. [2006] GRIP and NGRIP dating, the maximum possible mismatch is estimated to be slightly higher, 4-5 years, as the mean annual layer thickness in this part of the DYE-3 record amounts to only a few centimetres (see Fig. 4.6).

In order to quantitatively evaluate the ECM match of the cores, correlation coefficients between DYE-3, GRIP and NGRIP annually averaged ECM records have been calculated (see Table 4.3). As common volcanic signals in the ECM records are expected to correlate (as seen in Fig. 4.3 and 4.4) the correlation coefficients between the ECM records can be regarded as a measure of the strength of the ECM match. Correlations are presented for the 5 periods of the Holocene outlined in sections 4.4.1-4.4.5 and for the three possible core combinations. Table 4.3 also provides the variances of the ECM records for each core in each section.

From Table 4.3 it can be seen that correlations vary significantly from section to section, but it is also seen that the variance of the ECM records differ between sections. In fact there is a considerable correspondence between ECM variances and correlations, i.e. the lowest correlations registered for the NGRIP core is found in the 1814-3845 b2k section, where NGRIP ECM has the lowest variance, whereas the highest correlations for NGRIP is found in the 8314-11703 b2k section where NGRIP ECM variance is at its highest.

The ECM variances provide a good estimate of the strength of the volcanic signals observed in the ECM records, as large ECM spikes (as shown in Fig. 4.3 and 4.4) will inevitably lead to an increase in the ECM variance. Hence the correspondence between correlations and variances strongly suggests that the differences in correlation between the different sections are predominantly an expression of the frequency and magnitude of volcanic

Table 4.4: GICC05 dates and depths for selected reference horizons observed in the DYE-3, GRIP and NGRIP cores.

Reference horizon	DYE-3	GRIP Depth (m)	NGRIP	Age (AD/-BC)	Age (b2k)	MCE[e] (yrs)
Öraefajökull[a]	326.70	165.10	142.75	1362	638	0
Hekla[a,b]	429.24	219.55	189.13	1104	896	0
Eldja	493.71	256.15	219.68	933	1066	1
Unknown	635.10	339.83	290.92	529	1471	2
Vesuvius[a]	779.99	429.08	367.80	79	1921	0
Unknown	876.39	493.04	423.15	-252	2251	1
Unknown	1093.53	641.73	555.35	-1077	3076	3
Thera (?)	1227.48	736.47	640.99	-1641[d]	3640[d]	5
Unknown	1443.33	931.78	824.15	-2933	4932	11
Unknown	1555.67	1074.60	964.10	-3993	5992	16
Unknown	1645.10	1225.05	1118.35	-5248	7247	27
8.2k peak	1691.06	1334.04	1228.67	-6237	8236	47
Tjorsà (?)	1708.92	1380.50	1273.45	-6699	8698	57
Unknown	1779.94	1598.91	1470.69	-9307	11306	96
Termination[c]	1786.20	1624.27	1492.45	-9704	11703	99

[a]The Öraefajökull, Hekla and Vesuvius eruptions have been used as historical tie points carrying no uncertainty.

[b]The Hekla eruption commenced in the autumn/winter of A.D. 1104, the signals in the ice cores corresponds to early A.D. 1105.

[c]The termination of Younger Dryas as determined by a shift in deuterium excess values.

[d]GRIP tephra shows that the Thera eruption commenced in 1642 B.C. The ECM signals peak in the annual layer 1641 B.C. (3640 b2k).

[e]Maximum Counting Error

ECM peaks in the sections; not an indication of problems with the ECM matching. That correlations between GRIP and NGRIP are generally higher than correlations with the DYE-3 record reflects the fact, that the GRIP and NGRIP drill sites are much closer to each other than to DYE-3, making it more likely that they contain common volcanic signals. Furthermore melt layers in the DYE-3 core tend to increase the non-volcanic variability of the DYE-3 ECM record.

4.6 Results

Table 4.4 gives depths and ages for selected reference horizons identified in the DYE-3, GRIP and NGRIP ice cores. Maximum counting errors in Table 4 are seen to cumulate before the A.D. 79 eruption of Mount Vesuvius, as this eruption is the oldest historically dated reference horizon in
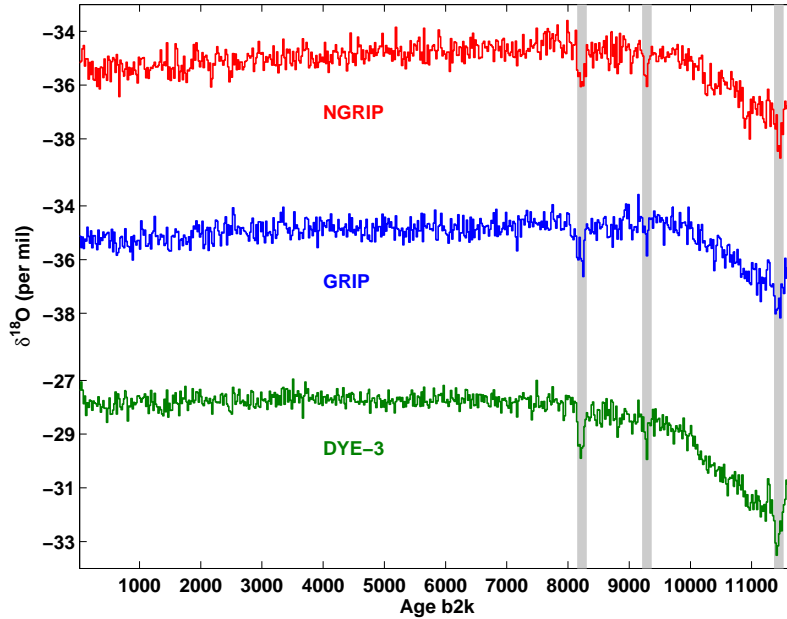
Figure 4.7: Holocene profiles of δ^{18}O for the DYE-3, GRIP and NGRIP ice cores on the GICC05 timescale. The 8.2 ka event, the 9.3 ka event and the 11.4 ka Preboreal Oscillation are indicated by grey shadings.

the ice cores. The Minoan Thera eruption [Hammer et al., 1987] is also found in all three ice cores. The GICC05 date for this eruption is 3641±5 b2k (1642±5 B.C.). It should be noted that it has been suggested that an Alaskan volcano, not Thera, was the source of the signals detected in the ice cores [Pearce et al., 2004]. This is, however, extremely unlikely as analysis of the GRIP ice core has established that the tephra from the eruption arrived in Greenland several months before the arrival of the sulphate aerosols [Hammer et al., 2003]. For an Alaskan eruption it would be expected that tephra and sulphate aerosols arrive simultaneously as they are transported to Greenland by the prevailing tropospheric flow (the polar jet). A delay in sulphate arrival can only take place if the sulphate aerosols are transported through the stratosphere, indicative of a highly explosive low latitude eruption.

Plots of 20-year averages of DYE-3, GRIP and NGRIP δ^{18}O data on the synchronized GICC05 timescale are shown in Fig. 4.7. It can be seen that the past 8000 years are most of all characterized by very stable δ^{18}O values. A slight decline in average δ^{18}O from 8000 b2k to present is, however, discernible in the profiles, most notable in the NGRIP δ^{18}O record.

Before 8000 b2k, the δ^{18}O values are less stable. Significant deviations from the mean DYE-3, GRIP and NGRIP δ^{18}O and annual layer thickness profiles have been found for three events (S. O. Rasmussen, preprint, 2005):
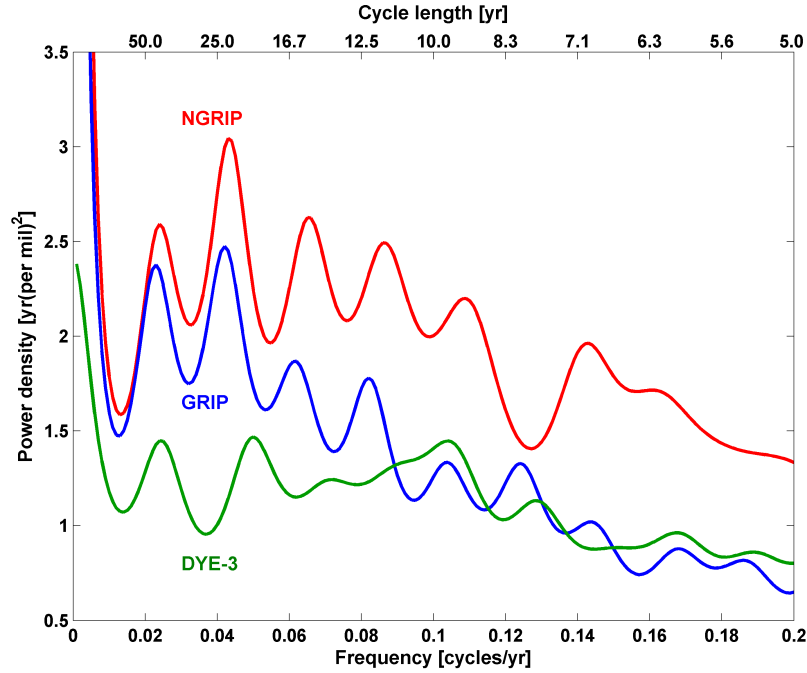
Figure 4.8: MEM power spectra (AR=50) for the past 8000 years of the DYE-3, GRIP and NGRIP annually resolved $\delta^{18}O$ records.

The 8.2 ka event, the 9.3 ka event and the 11.4 ka Preboreal Oscillation; all clearly visible in Fig. 4.7.

Having three synchronized $\delta^{18}O$ records offers the possibility of investigating periodicities without having to speculate whether dating discrepancies shift cycles in between the records. Maximum entropy method (MEM) power spectra using 50 auto regressive (AR) coefficients of annually resolved $\delta^{18}O$ data (1-3 year effective resolution) for the latest 8000 years are shown in Fig. 4.7. There is a striking lack of coherency between the three power spectra. A 40-45 year cycle is the only feature common to all three spectra, disregarding the zero frequency general trend peak. As the peak corresponding to the 40-45 year cycle splits up with increasing auto regressive order, it does not seem to represent a strictly periodic component.

It is also worth noting, that no clear imprint of the 11-12 year solar cycle is discernible. It is only because three synchronized records are available for investigation, that the existence of a 11-12 year cycle can be rejected. Looking only at the GRIP or NGRIP spectra one could easily attribute the peaks to the solar cycle.

Table 4.5: Comparison of counted timescales for the GRIP and GISP2 ice cores at selected GRIP and GISP2 reference horizons

Event	GRIP Depth (m)	GISP2 Depth (m)	GICC05 Age (b2k)
Vesuvius[d]	429.08	453.42	1921
Thera (?)	736.47	774.53	3640 ± 5^e
Unknown	1074.60	1126.04	5992 ± 16^e
8.2 ka ECM peak	1334.04	1392.66	8236 ± 47^e
Termination[g]	1624.27	1678.05	11703 ± 99^e

Event	GRIP[a] Age (b2k)	GISP2[b] Age (b2k)	GISP2A[c] Age (b2k)
Vesuvius[d]	1921	1920	1922
Thera (?)	3635 ± 7	3669 ± 21^f	3672 ± 21^f
Unknown	5974 ± 19	6034 ± 68^f	6039 ± 69^f
8.2 ka ECM peak	8214 ± 30	8271 ± 113^f	8298 ± 114^f
Termination[g]	11573 ± 70	11704 ± 182^f	11760 ± 183^f

[a]The counted GRIP timescale presented in Johnsen et al. [1992a].

[b]The official GISP2 time scale by Meese et al. [1997].

[c]GISP2 time scale by Alley et al. [1997; pers. comm.], based on visual stratigraphy only.

[d]The A.D. 79 Vesuvius eruption has been used as a historical tie point for all timescales.

[e]Maximum counting errors.

[f]Based on error estimate given in Table 2 in Meese et al. [1997] (1% error down to 3339 b2k, 2% error below 3339 b2k).

[g]The termination of the Younger Dryas as determined by a shift in deuterium excess values.

4.7 Discussion

Comparisons between the new GICC05 timescale and existing counted GRIP and GISP2 timescales are given in Table 4.5 and 4.6. The GICC05 timescale is seen to be in close agreement with the previous dating of the GRIP ice core [Johnsen et al., 1992a] for all parts of the Holocene, except for the oldest section (see Table 4.6). In Rasmussen et al. [2006] this issue is discussed and the disagreement is attributed to an erroneous interpretation of the GRIP CFA data during the original GRIP dating effort.

Table 4.5 shows an astounding agreement between the GICC05 and the official GISP2 dates for the termination of Younger Dryas. However, when comparing different subsections of the GICC05 timescale and the official GISP2 dating [Meese et al., 1997], it is seen that the agreement is less impressive. In the section between the reference horizons of Thera and Vesuvius, the official GISP2 timescale includes 30 more years than observed in GICC05. This is beyond the limits given by the 5 year GICC05 maximum

Table 4.6: Comparison of counted timescales for the GRIP and GISP2 ice cores between selected GRIP and GISP2 reference horizons

Events deliminating period	GICC05 Duration (yr)	GRIP[a] Duration (yr)
Vesuvius to Thera (?)	1719 ± 5^{d}	1714 ± 7
Thera (?) to Unknown	2352 ± 12^{d}	2339 ± 12
Unknown to 8.2 ka peak	2244 ± 32^{d}	2240 ± 11
8.2 ka peak to Term.^{f}	3467 ± 52^{d}	3359 ± 40
Events deliminating period	GISP2[b] Duration (yr)	GISP2A[c] Duration (yr)
Vesuvius to Thera (?)	1749 ± 21^{e}	1750 ± 21^{e}
Thera (?) to Unknown	2365 ± 48^{e}	2367 ± 48^{e}
Unknown to 8.2 ka peak	2237 ± 45^{e}	2259 ± 46^{e}
8.2 ka peak to Term.^{f}	3433 ± 69^{e}	3462 ± 70^{e}

[a]The counted GRIP timescale presented in Johnsen et al. [1992a].

[b]The official GISP2 time scale by Meese et al. [1997].

[c]GISP2 time scale by Alley et al. [1997; pers. comm.], based on visual stratigraphy only.

[d]Maximum counting errors.

[e]Based on uncertainty estimate given in Table 2 in Meese et al. [1997] (1% error down to 3339 b2k, 2% error below 3339 b2k).

[f]The termination of Younger Dryas as determined by a shift in deuterium excess values.

counting error and the 21 year GISP2 uncertainty for that period. The GISP2 dating is hampered by many sections of significant core loss during this period [Alley et al. 1997], while the GICC05 dating is based on complete and highly resolved δ^{18}O and ECM records from two cores for the entire section in question. It is therefore believed that the 30 year discrepancy mainly stems from the difficulties affecting the GISP2 dating.

The GISP2 sections below the Thera eruption do agree with GICC05 within the uncertainties of the GISP2 dating. It is interesting that the GICC05 dating finds more years than the official GISP2 dating in the earliest part of the Holocene. Alley et al. [1997] specifically pointed towards this possibility, as problems with lacking visible annual bands in the GISP2 core hampered the initial dating of this specific core section (GISP2 visual stratigraphy has been used for annual layer counting). As storage of the GISP2 core made annual layers more visible (due to clatherate dissociation), a recount of the annual layers observed in the GISP2 core was carried out a couple of years later (GISP2A in Table 4.5 and 4.6) [Alley et al., 1997; pers. comm.]. The GISP2A timescale is seen to agree much better with the early Holocene GICC05 dating.

4.8 Conclusion

A new synchronized counted timescale has been constructed as a contribution to the Greenland Ice Core Chronology 2005 (GICC05). The new timescale is based on annual layer counting in the DYE-3, GRIP and NGRIP ice core records. The three ice core records have been stratigraphically linked by volcanic reference horizons, in order to form a synchronized timescale spanning the Holocene parts of all three cores.

Highly resolved records of stable isotope measurements have been used for the annual layer counting of the most recent 8000 years of the Holocene, while measurements of chemical impurities are used for the dating of the early part of the Holocene.

The maximum counting error is 0.5% or less for the past 6900 years, increasing to 2.0% in some of the older sections of the timescale. The Minoan Thera eruption is dated to 3641 b2k (1642 B.C.) with a maximum counting error of 5 years, while a volcanic reference horizon during the culmination of the 8.2 ka cold event is dated to 8236 b2k with a maximum counting error of 47 years. The Yonger Dryas termination is found at 11,703 b2k with a maximum counting error of 99 years.

4.9 The dating of the Renland ice core

In 1988 a 325 meter long ice core was drilled through the small Renland ice cap situated near Scoresbysund, Eastern Greenland (see figure 2.1 for exact location). Despite the modest size and thickness of the Renland ice cap, both the entire Holocene and the most recent ∼50,000 years of the last glacial period was found as an unbroken chronology in the Renland core. Furthermore ice of Eemian origin was found in the bottom-most part of the core. The very prominent Dansgaard-Oeschger cycles in the glacial period makes the dating of the glacial section of the Renland ice core rather straight forward (see figure A.5 in the appendix). The dating of the Holocene section of the core is more difficult, as changes in $\delta^{18}O$ are much more modest in the Holocene than during the glacial period. The usual method of counting annual layers in the $\delta^{18}O$ record of the core allows reliable dating some 900 years back in time, as the rapid thinning rate in the ice cap makes the annual layer thickness decrease rapidly, severely hampering the dating effort. For most of the Holocene the dating therefore has to rely on a matching of volcanic reference horizons in the Renland ECM record to other well-dated Greenland ice cores, a task which up until now has not been accomplished.

Given the new synchronized dating (GICC05) of the Dye-3, GRIP and NGRIP cores presented in the previous sections, it was decided to match the Holocene ECM record to the GICC05 time scale, using the volcanic signal in the ECM records from the cores. The matching effort turned out to be all but easy until it was realized that the annual layer thickness in the Renland

Table 4.7: Renland depths and GICC05 ages for Renland ECM fixpoints.

Age (AD/-BC)	Depth (m)	Fixpoint obs. in (cores)
1179	201.20	Dye-3, GRIP, NGRIP
933	218.85	Dye-3, GRIP, NGRIP
871	222.50	GRIP, NGRIP
529	233.80	Dye-3, GRIP, NGRIP
358	237.48	Dye-3, NGRIP
259	239.17	Dye-3, GRIP, NGRIP
177	240.51	Dye-3
-253	247.28	Dye-3, GRIP, NGRIP
-584	251.74	Dye-3, GRIP, NGRIP
-733	253.35	Dye-3, GRIP, NGRIP
-900	254.92	GRIP
-1077	256.68	Dye-3, GRIP, NGRIP
-1432	259.66	Dye-3, GRIP, NGRIP
-1641	261.29	Dye-3, GRIP, NGRIP
-2050	264.07	Dye-3, GRIP, NGRIP
-3174	271.71	GRIP
-3240	272.05	Dye-3
-3503	273.40	GRIP, NGRIP
-3838	275.02	Dye-3, GRIP, NGRIP
-3993	275.74	Dye-3, GRIP, NGRIP
-4222	276.67	Dye-3, NGRIP
-4363	277.20	Dye-3, GRIP, NGRIP
-4562	277.83	Dye-3, GRIP, NGRIP
-4734	278.34	Dye-3, GRIP, NGRIP
-5247	279.98	Dye-3, GRIP, NGRIP
-5636	281.22	Dye-3, GRIP, NGRIP
-5880	281.97	GRIP, NGRIP
-6237	283.28	Dye-3, GRIP, NGRIP
-6265	283.38	GRIP, NGRIP
-6442	284.58	Dye-3, GRIP, NGRIP
-6583	285.56	Dye-3, GRIP, NGRIP
-6699	286.58	Dye-3, GRIP, NGRIP
-7056	289.86	GRIP, NGRIP
-7180	291.00	GRIP
-7240	291.53	GRIP
-7371	292.30	GRIP, NGRIP
-7437	293.61	GRIP, NGRIP
-7485	294.19	Dye-3, GRIP
-7540	294.84	Dye-3, GRIP, NGRIP
-8063	300.35	Dye-3, GRIP, NGRIP
-8361	303.06	GRIP, NGRIP
-8485	303.57	Dye-3, GRIP, NGRIP
-9307	306.07	Dye-3, GRIP, NGRIP
-9571	306.37	GRIP, NGRIP
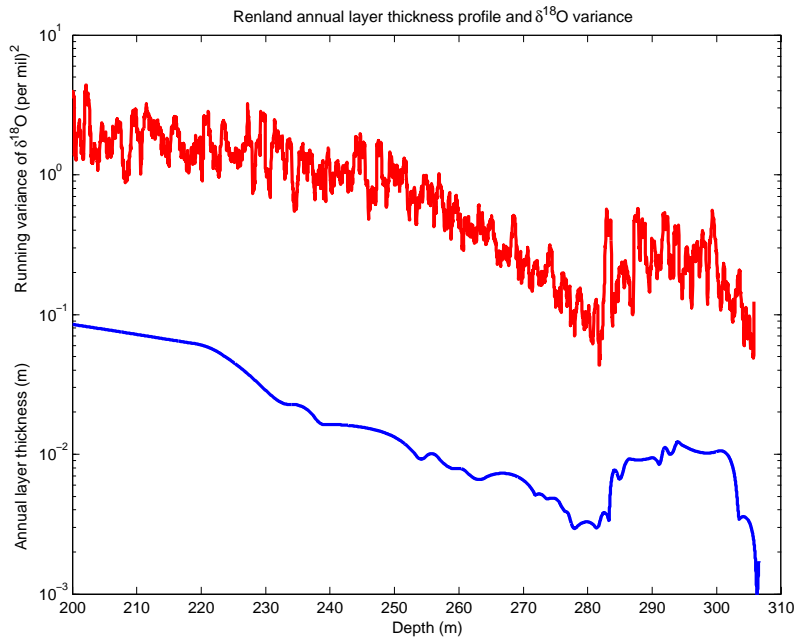
Figure 4.9: The Renland annual layer thickness profile (blue curve) for the oldest part of the Holocene, compared to the variance of the Renland $\delta^{18}O$ record (red curve).

core not necessarily had to decrease with depths! In fact, when studying the variability of the Renland $\delta^{18}O$ record it was discovered that the record had a variability minimum at a depth of $\sim$280 meters (see figure 4.9). As the $\delta^{18}O$ varibility in a climatically stable period is a good indication of the number of years each sample represents (more years per sample yields less variable $\delta^{18}O$ values), the variability minimum suggested that the annual layer thickness in the Renland core decreases only to a depth of $\sim$280 meters. From $\sim$280 meters down to $\sim$305 meters the variability has a local maximum suggestive of a larger annual layer thickness in that section.

Keeping the variability pattern in mind, the volcanic match to the Dye-3, GRIP and NGRIP was reasonably easy to establish. The matched reference horizons are given in table 4.7 and the resulting Renland annual layer thickness profile is shown in figure 4.9 (using cubic spline interpolation between the fixpoints in table 4.7).

The very large fluctuations in annual layer thickness which can be seen in figure 4.9 are believed to be an effect of ice flowing over the very mountainous bedrock under the small ice cap [Johnsen et al., 1992b].

The Renland $\delta^{18}O$ record matched to GICC05 is shown in figure 4.10 and compared to the Dye-3, GRIP and NGRIP $\delta^{18}O$ records. The three recognizable cold-events in Greenland $\delta^{18}O$ records during the Holocene (8.2k,
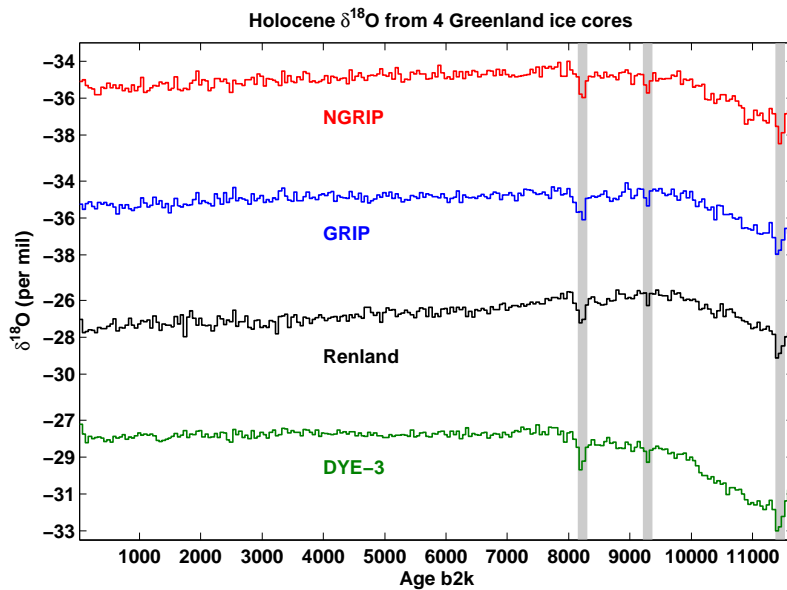
Figure 4.10: The Holocene δ^{18}O record from the Renland ice core comapared to Dye-3, GRIP and NGRIP δ^{18}O after the Renland core has been synchronized to the GICC05 timescale.

9.3k and the Preboreal Oscillation), are seen to line up perfectly, further supporting the validity of the ECM match.

4.10 Comparison of the GICC05 and Intcal04 time scales

Using measurements of the cosmogenic ^{10}Be isotope in the GRIP and GISP2 ice cores it is possible to compare the GICC05 time scale to tree ring count based Intcal04 ^{14}C calibration. This can be done if a carbon cycle model is used to convert the ^{10}Be isotope values (which are proportional to the ^{14}C production rate) to Δ^{14}C values [Muscheler et al., 2000].

A thorough matching of ice core based and tree-ring based Δ^{14}C curves for the Holocene is yet to be carried out, but a preliminary matching has been carried out by Raimund Muscheler (pers. comm., 2006). The GICC05 maximum counting error and the age difference estimates between the GICC05 dating and Intcal04 can be seen in figure 4.11. This comparsion suggests that the GICC05 dating could be 70±20 years too old at the transition and that the age difference between GICC05 and Intcal04 does not exceed ~40 years for the past 9000 years. Curiously the comparison suggests a more than 20 year offset some 1900 years ago, which is unlikely at best, as the discovery of Vesuvius tephra at 79 A.D. in the GRIP ice core should assure that the
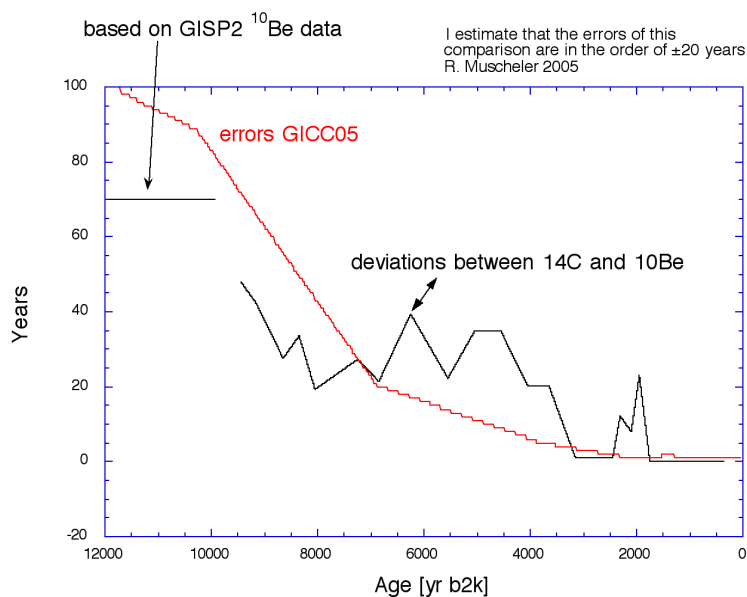
Figure 4.11: Deviations between the GICC05 and Intcal04 timescales (black curve) based on a comparison between ice core ^{10}Be and Δ^{14}C from trees compared to the GICC05 maximum counting error estimate (red curve). Figure courtesy to Raimund Muscheler (pers. comm. 2006).

GICC05 time scale has no dating error 1900 years ago. The mismatch at 79. A.D. is therefore an indication that the Δ^{14}C matching uncertainty is about 20 years, as stated by R. Muscheler (see figure 4.11). Taking this matching uncertainty into account, it can be argued that GICC05 and Intcal04 agrees within the combined uncertainties in the GICC05 dating (the maximum counting errors) and the matching uncertainty ($\sim$ 20 years). Some uncertainty crated by past changes in the carbon cycle (which are hard to estimate and would affect the carbon cycle model that is used to convert ^{10}Be isotope values to Δ^{14}C) should also be anticipated, but it is difficult to estimate.

4.11 Summary

A new synchronous dating (GICC05) of the Holocene part of the Dye-3, GRIP and NGRIP ice cores has been constructed. The three cores were synchronized mainly through matching of volcanic reference horizons found in the ECM records of the cores and thereafter the annual layer count was determined using the best data available in all three cores. Some additional

measurements were carried out on the Dye-3 core to complete its detailed stable isotope profile, which is excellent for accurate dating. Thereafter the Renland ice core was matched to the GICC05 timescale using its ECM record.

A comparison between Intcal04 and the GICC05 time scale suggested that GICC05 date of the transition (11703 b2k) is approximately 70 years too old, which is within the estimated maximum counting error of 99 years. This discrepancy between GICC05 and Intcal04 builds up from ∼3000 b2k to the transition.

Chapter 5

Constraints on millennial scale changes of Greenland ice sheet topography

In chapter 2 it was documented that highly resolved Greenland ice core $\delta^{18}O$ records are closely related to both Greenland and Icelandic temperatures during the past $\sim$200 years. In this light it seems feasible to use $\delta^{18}O$ records from the four ice cores (Dye-3, GRIP, NGRIP and Renland) that are all synchronized on the GICC05 timescale (see chapter 4) to estimate Greenland temperature conditions throughout the Holocene.

The interpretation of $\delta^{18}O$ records that span several millennia is however complicated by the fact that the Greenland ice sheet has not been in a steady state throughout the Holocene. After the transition from glacial to Holocene climatic conditions the Greenland ice sheet adjusted its size and shape over several millennia; the margins of the ice sheet retreated dramatically [Weidick, 1993] and the thickness of the ice sheet would have to respond both to increased precipitation and the retreating margins.

Keeping the dynamic nature of the ice sheet in mind, the ice core drill sites must therefore be expected to have experienced elevation changes during the Holocene. This is important because $\delta^{18}O$ (and temperature) on the Greenland ice sheet is closely related to elevation [Epstein and Sharp, 1959; Dansgaard, 1961].

In order to derive millennial scale climatic variations from Greenland ice core $\delta^{18}O$ records, it is therefore crucial to have solid knowledge of the Greenland ice sheet elevation history.

In this chapter borehole temperatures from the GRIP and NGRIP drill sites will be used in a combined effort to both find the best possible Holocene temperature-$\delta^{18}O$ calibration and determine the most likely Holocene elevation history for the two drill sites.

5.1 The sensitivity of $\delta^{18}O$ to height and temperature change

A large number of combined temperature, height and ice core $\delta^{18}O$ data from multiple locations on the Greenland ice sheet have been used to quantify the relationships between $\delta^{18}O$, temperature and height [Epstein and Sharp, 1959; Dansgaard, 1961; Johnsen et al., 1989]. In these studies the slope between temperature and $\delta^{18}O$ was found to be apprx. 1.5°C/‰ while the slope between $\delta^{18}O$ and height was found to be approx. -0.6 ‰/100m. Combining the two yields a temperature versus height slope of -0.9°C/100m, which is quite close to the dry adiabatic lapse rate, reflecting the fact that conditions on the ice sheet are dominated by cold dry air masses.

It is important to note that the slope between temperature and $\delta^{18}O$ found in the above studies is based on observing pairs of average temperature and $\delta^{18}O$ at different locations; not pairs of $\delta^{18}O$ and temperature at different times. In the following a slope determined in this manner will be referred to as the spatial temperature/$\delta^{18}O$ slope while temperature/$\delta^{18}O$ slopes derived using observations from different times at the same location will be referred to as temporal slopes.

The distinction between spatial and temporal temperature/$\delta^{18}O$ slopes is important because neither data nor meteorological considerations suggest that they necessarily should be identical. $\delta^{18}O$ values in precipitation are influenced by the condensation history from the source area to the precipitation site. This history is not the same for different locations on the ice sheet due to differences in the distance to the source area and differences in site elevation, while temporal climatic changes are a result of a restructuring of the organization of the weather systems. There is no good reason to expect these very different processes to influence $\delta^{18}O$ in the same way.

Observations of the seasonal cycle of $\delta^{18}O$ and temperature at the GRIP drill site (se figure 5.1) suggest a temporal slope of $\sim2°C‰$ while the Dahl-Jensen et al. [1998] estimate of Last Glacial Maximum temperatures at GRIP some 23°C colder than present (corresponding to a ~7 ‰ drop in $\delta^{18}O$) suggest a slope slightly larger than 3°C‰ or a slope that increases with colder climatic conditions [Johnsen et al., 1995].

5.2 Holocene height changes of the Greenland ice sheet

The ice thickness and volume history of the Greenland ice sheet have been the subject of several modelling efforts, both with highly sophisticated thermo-mechanical ice sheet models [Tarasov and Peltier, 2003; Greve, 2005] and very simple elevation models [e.g. Johnsen et al., 1995]. For the Holocene there are considerable differences between the ice thickness estimates be-
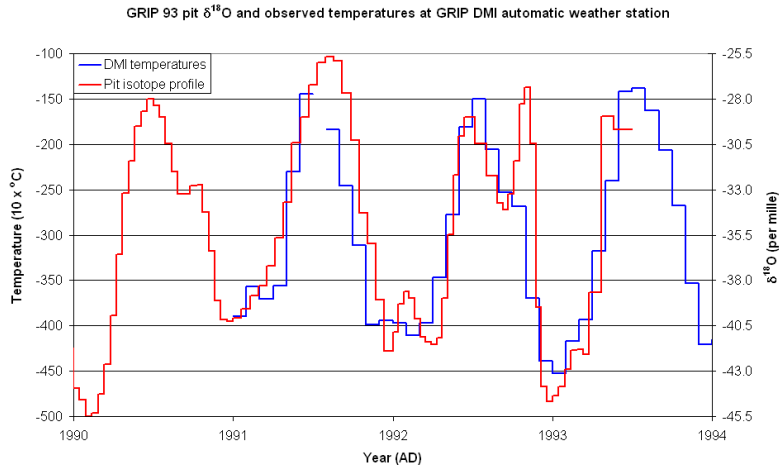
Figure 5.1: Observed temperatures at the GRIP drill site compared to $\delta^{18}O$ in the uppermost strata of a snow pit.

tween the models, with the two thermo-mechanical models yielding increasing elevations for the Greenland ice sheet summit (they are differing by almost a factor of two in the magnitude of the increase) while the Johnsen et al. [1995] elevation model estimates a slight increase in thickness followed by a steady decrease (Summit ice sheet thickness changes from the Greve [2005] and Johnsen et al. [1995] models can be seen in figure 5.2).
The large differences between the model estimates are most likely due both to differences in glacial boundary conditions (i.e. the situation of the ice margin) and the vast difference in model complexity. Either way the discrepancies between the models are discouraging in the context of establishing a firm Holocene elevation history for the Greenland ice sheet based on presently available modeling efforts only.

Studying the evolution of differences in $\delta^{18}O$ between the Renland and GRIP sites throughout the Holocene is an independent way of gaining information on the Greenland ice sheet elevation history. Changes in the $\delta^{18}O$ difference between the two sites can be translated into height estimates using the observed $\delta^{18}O$/elevation slope. Holocene $\delta^{18}O$ from Renland and GRIP and their $\delta^{18}O$ difference can be seen in figure 5.3. A comparison between the $\delta^{18}O$ difference based Holocene changes in height difference between GRIP and Renland and the Johnsen et al. [1995] modeled GRIP elevation can be seen in figure 5.4 (red and green curves).

The GRIP/Renland comparison is interesting because the topography of the Renland ice cap surroundings assures that the Renland ice cap can hardly gain in thickness [Johnsen et al., 1992b]. Furthermore the fact that the Renland ice core presents an unbroken stratigraphy of the past ∼60000 years and contains Eemian ice near the bedrock makes a strong case that

60
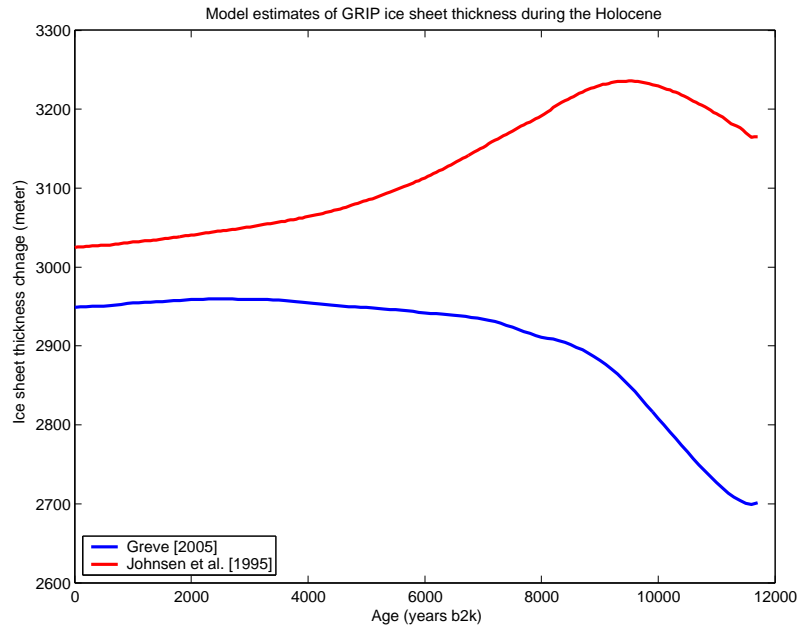
Figure 5.2: Modeled Holocene ice sheet thickness during the Holocene. The Greve [2005] estimate (blue curve) is made with a complex thermo mechanical ice sheet model, while the Johnsen et al. [1995] estimate (red curve) is made with a very simple ice sheet elevation model.

the small ice cap (thickness only ∼325m at the drill site) is very stable with respect to climate change. It is therefore most likely that the ice cap neither gained nor lost in altitude during the course of the Holocene. The entire Renland area did, however, experience significant post glacial rebound in the period from the glacial termination to about 6900 b2k (∼60m just west of the ice cap and ∼120m just east of ice cap [Funder, 1978; Funder and Hansen, 1996; Fleming and Lambeck, 2004]). Applying a linear correction for a post glacial rebound of 90m (hence using an average of the east and west observations) from 11700 b2k to 6900 b2k to the green curve in figure 5.4 yields the blue curve in the figure.

Assuming that the Renland ice cap did not change in thickness during the Holocene, the blue curve in figure 5.4 represents the best estimate of GRIP drill site elevation change during the Holocene; derived without any ice sheet modeling. It is surprising how well this estimate resembles the Johnsen et al. [1995] modeled GRIP elevation given that the two estimates are completely independent of each other. It is equally (or even more) surprising how far the Renland based GRIP elevation estimate is from the estimate of Greve [2005] (and in fact also from the estimate of Tarasov and Peltier [2003]) based on high-complexity modeling of the ice sheet.

The disagreement with the two independent sophisticated modeling ef-
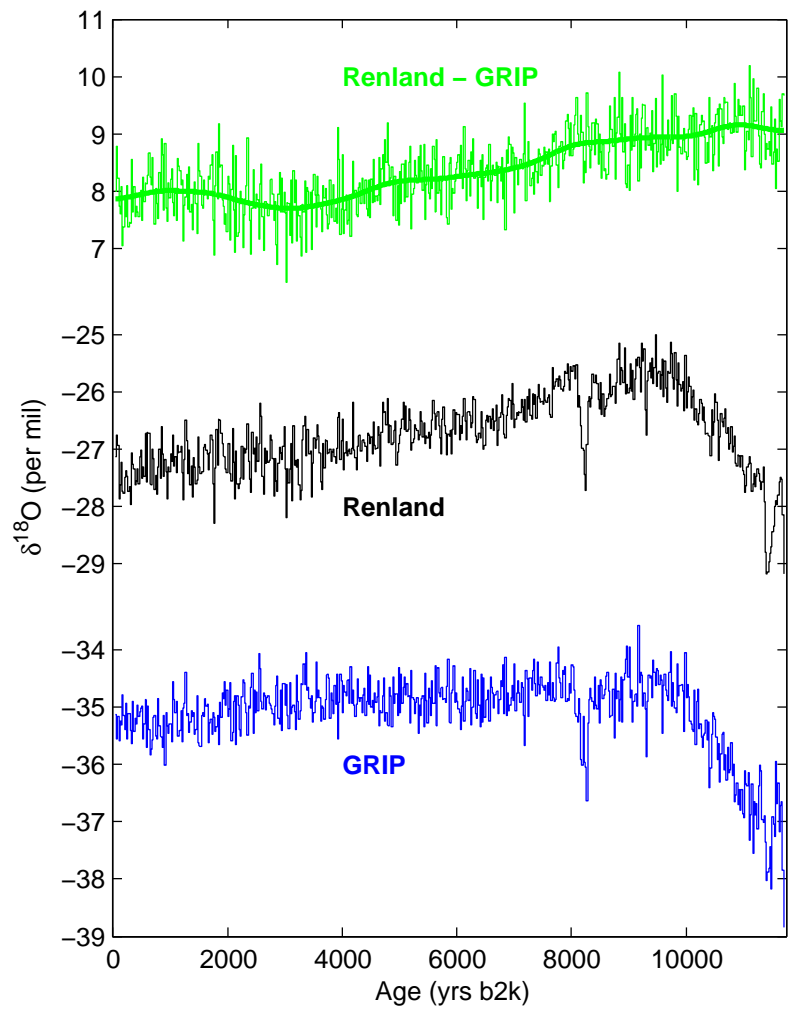
Figure 5.3: Holocene profiles of δ^{18}O from the Renland and GRIP ice cores and the difference between them. The thick line is filtered data ($T_{1/2} = 2000$ years - see appendix B for details).
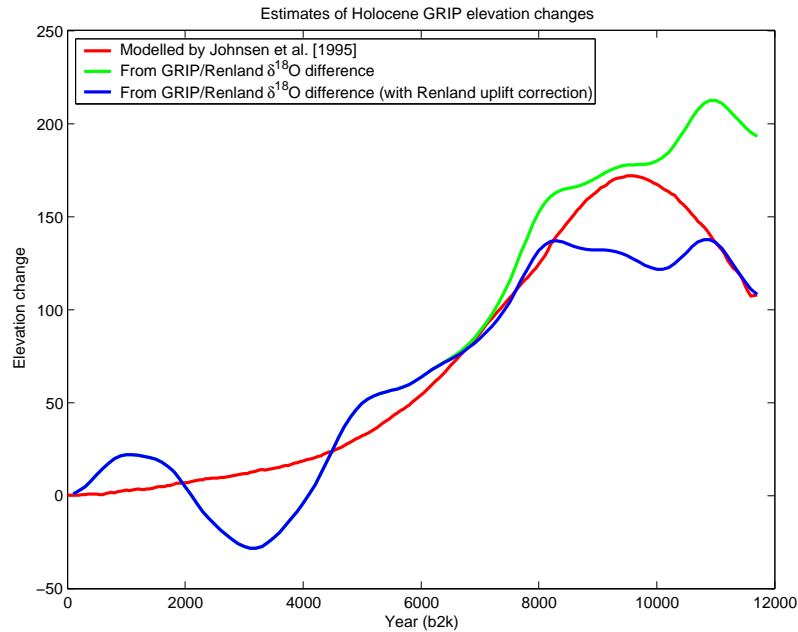
Figure 5.4: Estimates of GRIP surface elevation change during the Holocene. Red curve is based on a simple ice sheet elevation model, while the green and blue curves are derived from the changes in $\delta^{18}O$ difference between GRIP and Renland. Green curve assumes constant height at Renland (and is derived from the green curve in figure 5.3). Blue curve is identical to the green curve, except for the 6900-11700 b2k period, where the post-glacial rebound of Renland and its surroundings is subtracted.

forts calls for pause. Could the assumption that the Renland ice sheet was stable during the Holocene be in error? Or could climatic conditions at the Renland and GRIP drill sites have developed differently causing a change in $\delta^{18}O$ at one site, but not the other? Addressing the last question first, it seems unlikely that millennial scale trends in climate should be different at sites only ∼400km apart, especially in the light of the similarity between the large centennial scale $\delta^{18}O$ variations during the early Holocene at the two sites (see figure 5.5). In this context it should, however, be noted that the smaller observed Holocene changes in $\delta^{18}O$ difference between GRIP and NGRIP (∼320km apart) has recently been proposed to stem from climatic effects [Masson-Delmotte et al., 2005], but could equally well be a result of small changes in elevation between the GRIP and NGRIP drill sites during the Holocene. With respect to possible Renland height change, agreement with the Greve [2005] GRIP ice thickness estimate would demand that the Renland ice cap all but melted away during the early Holocene. A scenario which is very hard to reconcile with the fact that the stratigraphy is preserved for the past ∼60.000 years in the Renland ice core.
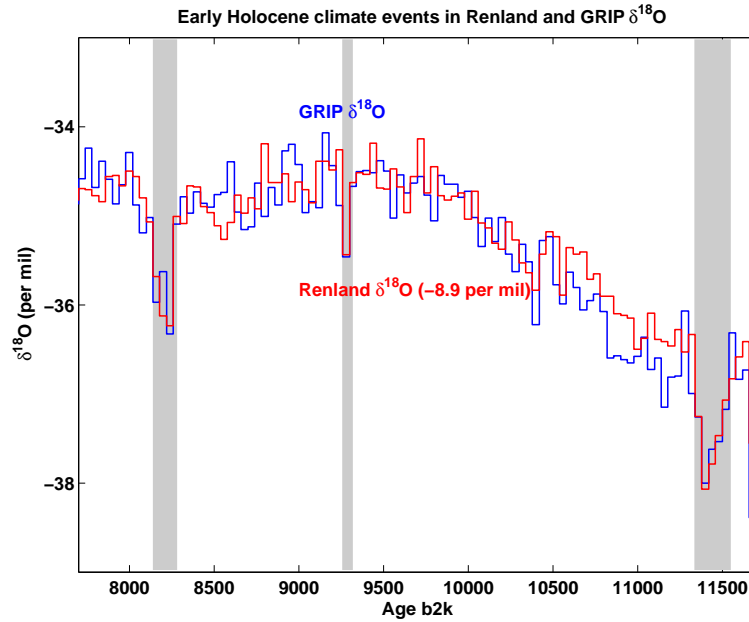
Figure 5.5: Plot of early Holocene $\delta^{18}O$ records from GRIP and Renland (in 40 year steps), note that Renland $\delta^{18}O$ has been shifted downwards.

5.3   Modeling borehole temperatures

In order to obtain an estimate of the temporal temperature/$\delta^{18}O$ slope and gain further insight on the height changes experienced by the Greenland ice sheet it is decided to use the two borehole temperature profiles from GRIP [Johnsen et al., 1995; Dahl-Jensen et al., 1998] and NGRIP [Dahl-Jensen et al., 2003] for calibration purposes. The corresponding Dye-3 borehole temperature profile will not be used, as modeling the complicated ice flow and upstream effects (Dye-3 drill site being located downstream from the ice divide) [Reeh et al. 1977; 1985, Reeh, 1989] would both be immensely difficult and add significantly to the uncertainties in the calibration.

As in Johnsen et al. [1995] a forward modeling approach is applied, where it is assumed that the ice core $\delta^{18}O$ profile can be translated into surface temperatures at the drill site. Contrary to the approach of Johnsen et al. [1995], it was decided not to use glacial part of the $\delta^{18}O$ records to model glacial temperatures, as Greenland $\delta^{18}O$ and chemical impurity records suggest that during very cold stages of the glacial, atmospheric flow north of the Laurentide ice sheet brought precipitation from the north to Greenland (as discussed in appendix A.4.3). Such precipitation cannot be expected to have the same temperature/$\delta^{18}O$ relation as precipitation arriving from the Atlantic sup-tropical region, making any temperature interpretation of

glacial ice core δ^{18}O difficult at best. Leaving out glacial δ^{18}O does, however pose a problem, as glacial temperature conditions are important for the initialization of the ice sheet temperature model. This problem will be circumvented by letting glacial temperature conditions being a parameter in the calibration.

As this modeling effort only focus on the Holocene section of the ice core, changes in the temperature/δ^{18}O slope are not allowed, as no dramatic changes in conditions at the precipitation source are expected during the Holocene, this is also contrary to the Johnsen et al. [1995] approach. The most significant difference between this experiment and the Johnsen et al. [1995] calibration is, however, that the spatial and temporal temperature/δ^{18}O slopes were (implicitly) assumed equal in the Johnsen et al. [1995] paper. This will not be the case in this experiment due to the observed differences outlined previously. The translation from δ^{18}O to temperature can then be written as:

$$T(t) = \frac{\partial T}{\partial \delta} \cdot (\delta(t) - \delta_0 - \frac{\partial \delta}{\partial H} \cdot \Delta H(t)) + T_0 + \frac{\partial T}{\partial H} \cdot \Delta H(t) \qquad (5.1)$$

Here $\frac{\partial T}{\partial \delta}$ is the temporal temperature/δ^{18}O slope, $\frac{\partial \delta}{\partial H}$=-0.006‰/m is the δ^{18}O/height slope, $\frac{\partial T}{\partial H}$=-0.009°C/m is the temperature/height slope, ΔH(t) is the change in site elevation at time t and δ_0 and T_0 are the present values of δ^{18}O and temperature at the drill site. Furthermore $\delta(t)$ is the δ^{18}O value at time t, corrected for the changing mean δ^{18}O value of seawater (a change which amounts to almost 0.5‰ during the early Holocene) [Waelbroeck et al., 2002].

An intriguing consequence of separating spatial and temporal δ^{18}O/temperature relations is that equal values of δ^{18}O can result in different temperatures due to changes in ΔH.

The temperature history found using 5.1 can then be applied as a boundary condition on a simple ice sheet model and the temperature profile in the ice found by numerical integration of the differential equation for heat conduction in moving firn and ice [Johnsen, 1977b] (neglecting horizontal temperature gradients and internal heat production in the ice sheet):

$$\frac{\partial T}{\partial t} = \kappa \cdot \frac{\partial^2 T}{\partial^2 z} + \left(\left(\frac{\kappa}{\rho} + \frac{\partial \kappa}{\partial \rho} \right) \frac{\partial \rho}{\partial z} - v_z \right) + \left(\frac{\partial \kappa}{\partial T} + \frac{\kappa}{c} \frac{dc}{dT} \right) \left(\frac{\partial T}{\partial z} \right)^2 \quad (5.2)$$

Where κ is the thermal diffusivity, ρ is the density, c is the specific heat capacity and T the temperature of the firn/ice. Furthermore z is the depth and v_z the vertical velocity in the ice sheet. A Dangaard-Johnsen type model with an integrated firn layer [Dansgaard and Johnsen, 1969; Johnsen and Dansgaard, 1992; Vinther, 2003] will be used to determine the density and vertical velocities as a function of depths.

The mass balance equation for the ice sheet in non-steady state is used to
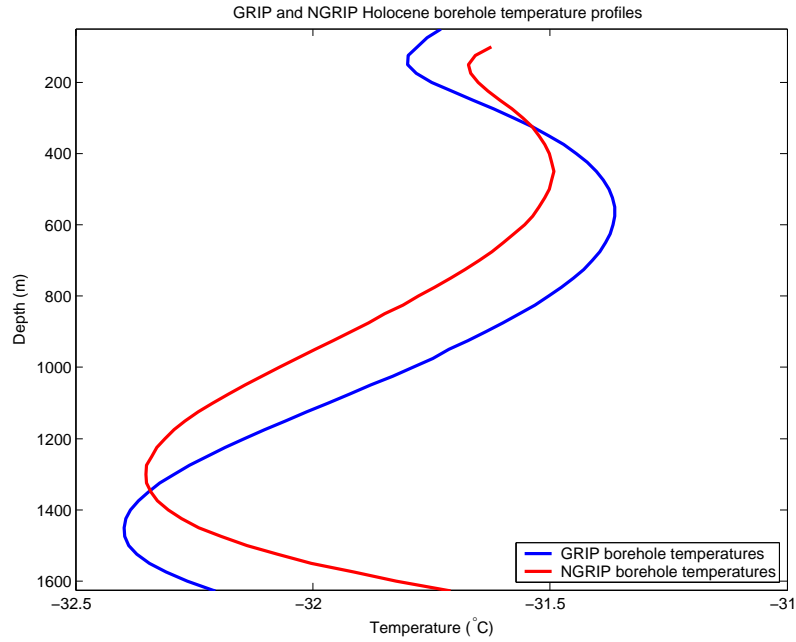
Figure 5.6: Plot of the Holocene sections of the observed GRIP and NGRIP borehole temperatures.

adjust the mean horizontal velocity ($\overline{v_x}$) in the Dansgaard-Johnsen model to account for changes in ice sheet thickness (which can be exemplified looking at the simplest case of two-dimensional flow):

$$A \cdot x - \overline{v_x} \cdot H = \frac{dH}{dt} \cdot x \tag{5.3}$$

Where A is the annual accumulation rate (assumed constant with regard to x, the distance from the ice divide), H the thickness of the ice sheet and $\frac{dH}{dt}$ the change in ice sheet thickness. For a constant accumulation rate it can be seen that a growing/shrinking ice sheet demands a smaller/larger than steady state ($\overline{v_x}$). As the strain-rate in a Dansgaard-Johnsen model is (linearly) dependant on v_x, changes in thickness of the ice sheet will directly influence the layer thinning rate in the ice sheet.

5.3.1 Modeling the GRIP borehole temperature profile

Three modeling experiments were carried out in the effort to reproduce the Holocene GRIP borehole temperature profile (see figure 5.6) from GRIP $\delta^{18}O$ data. The experiments used (5.1) to convert the Holocene GRIP $\delta^{18}O$ data to a temperature history and started at the transition 11700 years ago. The initial temperature profile was assumed to be a steady state glacial profile found using a mean accumulation rate of 10.7 cm ice eq./yr (the mean

GRIP accumulation rate for the 60,000 years preceding the Holocene using the ss09sea flow-model [Johnsen et al., 2001]). Furthermore a geothermal heat flux of 51.3mW/m^2 [Dahl-Jensen et al., 1998] was applied below a 3km thick slap of bedrock (the temperature profile was calculated down through both the ice sheet and the bedrock). For each experiment, the flow model was tuned to have the corrected depth (1624m) for the transition assuming the accumulation rate was unchanged at its present value (23 cm ice eq./yr) during the entire Holocene.

The three experiments had the following setup:

- Exp. 1: No elevation change at the GRIP drill site

- Exp. 2: GRIP elevation changes found through comparison between Renland and GRIP δ^{18}O records assuming Renland post-glacial rebound but no changes in thickness of the Renland ice cap.

- Exp. 3 GRIP elevation changes as found by Greve [2005].

Ice sheet surface elevation changes were assumed to equal the thickness changes of the ice sheet disregarding bedrock possible depression/uplift. This decision was made because it is not obvious how the bedrock under the centre of the ice sheet reacted to load changes that also affected the margins of the ice sheet. The maximum height/thickness error expected when not including bedrock movements in the calculations does not exceed a third of the estimated elevation change (this is the maximum possible depression/elevation forced by changes in the thickness due to the ratio of $\sim$1/3 between the ice and bedrock density.

For each of the three experiments, three parameters were found as to best fit the Holocene part of the borehole temperature profile (upper 1625 meters of the ice sheet): The temperature/δ^{18}O slope, the present temperature at the GRIP drill site and the mean glacial temperature. Results from the three model experiments, including the mean misfit to the observed Holocene borehole temperatures can be seen in table 5.1. Misfits as a function of depths for the three experiments can be seen in figure 5.7.

Table 5.1: Optimum fit parameters and average misfit between modeled and observed borehole temperatures from modeling experiments using the GRIP δ^{18}O profiles to model GRIP borehole temperatures.

Exp. No.	GRIP height change from	Glacial temp. (°C)	Present temp. (°C)	$\frac{\partial T}{\partial \delta}$ (°C/^{0}/$_{00}$)	Mean misfit (°C)
1	(No change)	-46.27	-32.27	4.05	0.036
2	Renland δ^{18}O	-46.77	-32.28	3.43	0.028
3	Greve [2005]	-44.71	-32.34	4.18	0.043
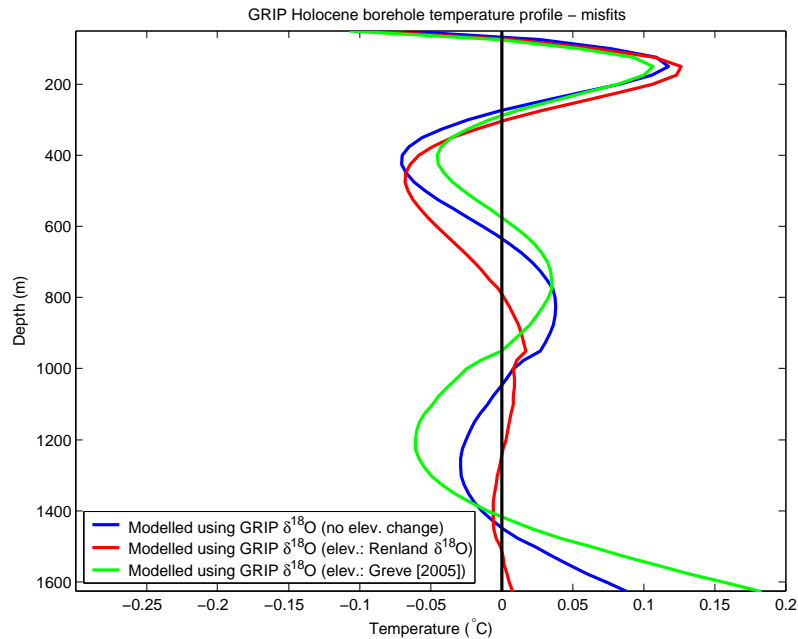
Figure 5.7: Plot of observed minimum misfit for modeled borehole temperatures (based on Holocene GRIP δ^{18}O) vs. observed GRIP borehole temperatures under three different GRIP surface height histories: No change in surface height at all (blue curve), changes as given by comparison with Renland δ^{18}O (red curve) and changes given by the Greve [2005] modeling effort (green curve).

5.3.2 Comparison with the GRIP borehole temperature inversion

Using a Monte Carlo inversion technique Dahl-Jensen et al. [1998] estimated past GRIP temperatures from the measured GRIP borehole temperature profile, an estimate which is completely independent of the GRIP δ^{18}O record. In order to correct the inverted GRIP temperatures for changes in elevation, the Johnsen et al., [1995] elevation model was used by Dahl-Jensen et al. [1998]. If this elevation correction is removed, a surface temperature record for the GRIP drill site is obtained. As this surface temperature record is independent of all assumptions concerning the elevation of the GRIP drill site, it is ideal for comparison with the surface temperature histories based on the GRIP δ^{18}O record.

Comparisions between the GRIP δ^{18}O based surface temperature estimates for the three different GRIP elevation histories tested in the previous section and the borehole inversion can be seen in figures 5.8 and 5.9. The comparison has been limited to the last 7000 years to avoid the subtle problem that the very cold Younger Dryas period is not resolved, but rather mixed into
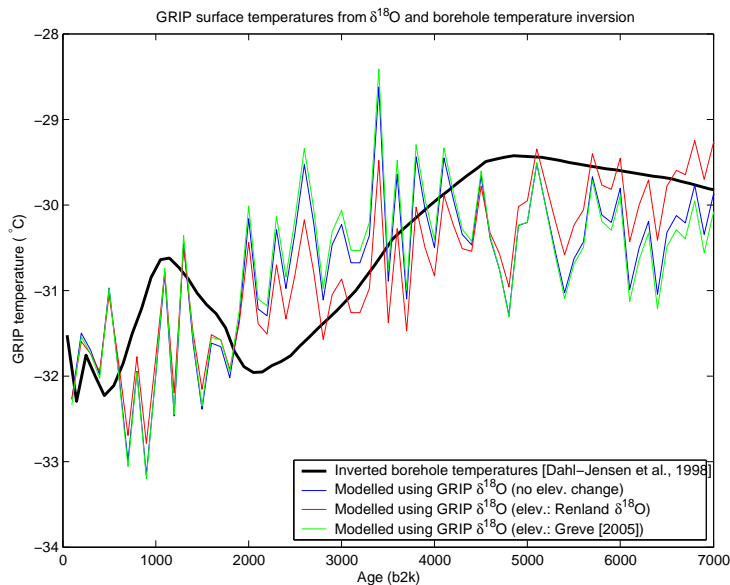
Figure 5.8: Plot of four estimates of GRIP surface temperatures. Black line is the Dahl-Jensen et al. [1998] GRIP borehole temperature inversion, while colored lines are estimates based on GRIP $\delta^{18}O$ under three different GRIP surface height histories: No change in surface height at all (blue curve), changes as given by comparison with Renland $\delta^{18}O$ (red curve) and changes given by the Greve [2005] modeling effort (green curve).

the early Holocene temperature inversion.

It is noteworthy that the GRIP $\delta^{18}O$ based temperature reconstruction which uses the Renland $\delta^{18}O$ record to estimate GRIP elevation change, does by far correlate best with the Dahl-Jensen et al. [1998] borehole temperature inversion (see figure 5.9).

5.3.3 Modeling the NGRIP borehole temperature profile

The three experiments carried out to model GRIP borehole temperatures were repeated with respect for the Holocene NGRIP borehole profile (see figure 5.6):

- Exp. 1: No elevation change at the NGRIP drill site

- Exp. 2: NGRIP elevation changes found through comparison between Renland and NGRIP $\delta^{18}O$ records (see figure 5.10) assuming Renland post-glacial rebound but no changes in thickness of the Renland ice cap (blue curve in figure 5.11).

- Exp. 3 NGRIP elevation changes as found by Greve [2005].

69
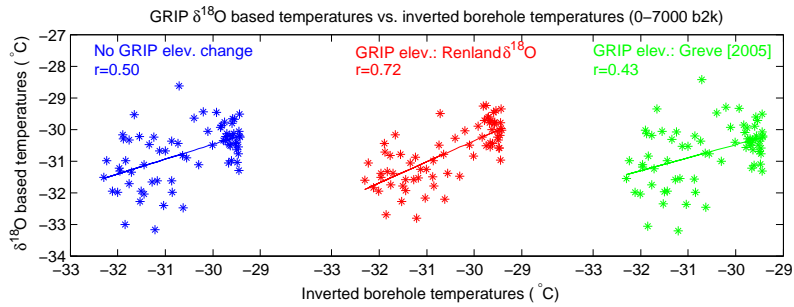
Figure 5.9: Scatter-plots and correlation coefficients for the three δ^{18}O based estimates of GRIP surface temperatures versus the Dahl-Jensen et al. [1998] GRIP borehole temperature inversion. Colours refer to three different GRIP height surface scenarios (as in figures 5.7 and 5.8)

As the ice sheet is subject to bottom melting at the NGRIP site ($\sim$ 7mm/yr) it was not necessary to include a slab of bedrock in the modeling, temperature always being at the pressure melting point for ice at the bottom of the ice sheet. The Dansgaard-Johnsen model was adjusted to allow for bottom melting. The accumulation rate was assumed to be constant at its present value (19.7 cm ice eq./yr) during the entire Holocene and for each experiment the flow model was tuned to give the correct depth for the transition (1492 m).

The initial temperature profile was assumed to be a steady state glacial profile found using a mean accumulation rate of 7.3 cm ice eq./yr (the mean NGRIP accumulation rate for the 60,000 years preceding the Holocene using the ss09sea flow-model [Johnsen et al., 2001]).

The results from the three experiments can be seen in table 5.2 and figure 5.12.

Table 5.2: Optimum fit parameters and average misfit between modeled and observed borehole temperatures from modeling experiments using the NGRIP δ^{18}O profiles to model NGRIP borehole temperatures.

Exp. No.	NGRIP height change from	Glacial temp. ($^\circ$C)	Present temp. ($^\circ$C)	$\frac{\partial T}{\partial \delta}$ ($^\circ$C/$^0\!/_{00}$)	Mean misfit ($^\circ$C)
1	(No change)	-47.65	-30.96	2.67	0.012
2	Renland δ^{18}O	-47.09	-31.04	2.67	0.0076
3	Greve [2005]	-47.20	-30.97	2.72	0.014
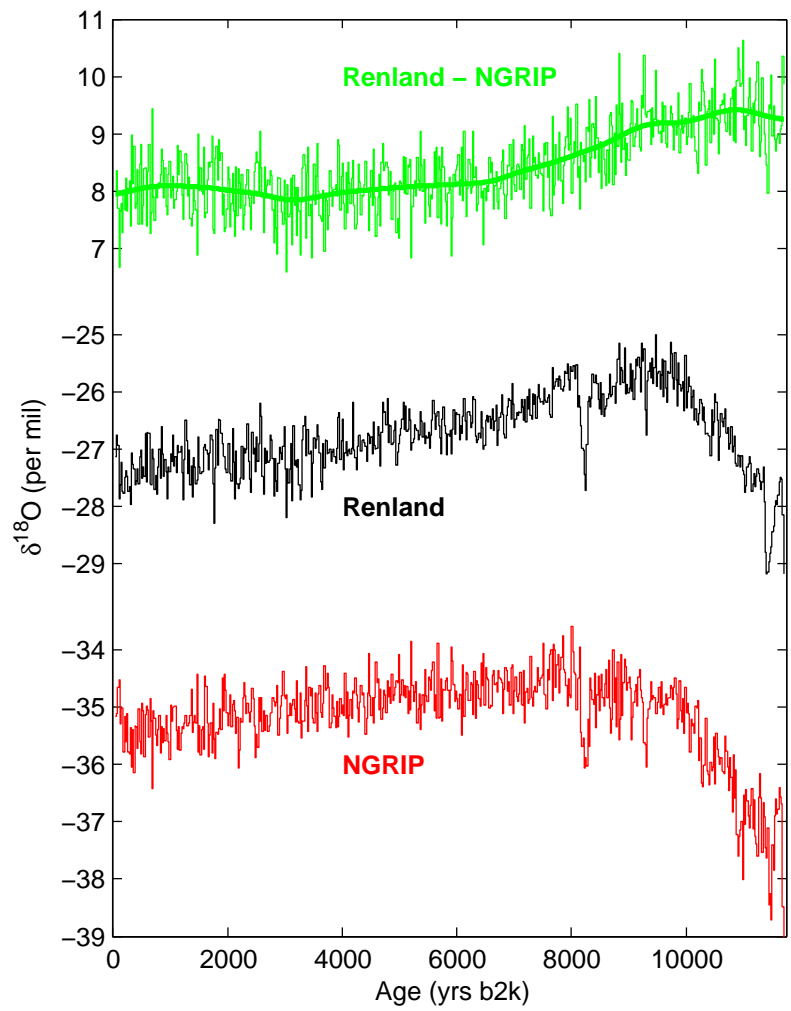
Figure 5.10: Holocene profiles of δ^{18}O from the Renland and NGRIP ice cores and the difference between them. The thick line is filtered data ($T_{1/2} = 2000$ years).

71
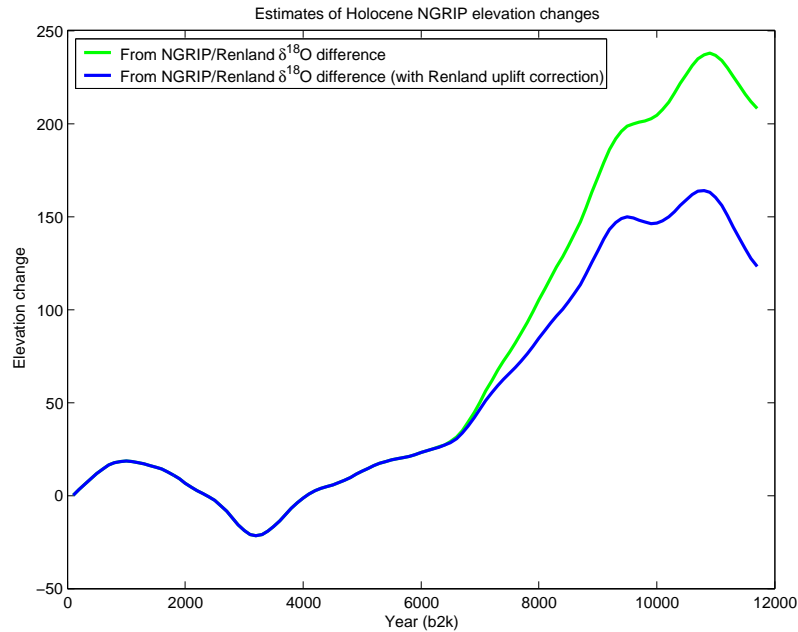
Figure 5.11: Estimates of NGRIP surface elevation change during the Holocene. The green and blue curves are derived from the changes in $\delta^{18}O$ difference between NGRIP and Renland. Green curve assumes constant height at Renland. Blue curve takes into account the post-glacial rebound of Renland and its surroundings.

5.3.4 Discussion of the experiments

The results from the borehole-temperature modeling are surprisingly unambiguous, the misfit between the modeled temperature profiles and observed GRIP and NGRIP profiles is smallest when the surface height is found through comparison with the uplift corrected Renland $\delta^{18}O$ record and largest when the Greve [2005] ice thickness data is used for height estimation, with the misfit from the steady height experiment being in between (see tables 5.1 and 5.2). Furthermore the difference between the estimated GRIP and NGRIP temperature/$\delta^{18}O$ slopes (which should be expected to be almost equal, due to the proximity of the drill sites) are by far most alike when hight calculations are based on the uplift corrected Renland $\delta^{18}O$ record. The same is true for the estimated glacial average temperature used for the initialisation of the temperature modeling experiments.

There are however two disturbing caveats: First of all, the GRIP and NGRIP estimated temperature/$\delta^{18}O$ slopes are quite different, even when GRIP and NGRIP heights are based on the Renland comparison. Secondly the average misfit for the modeled GRIP Holocene temperature profile (0.028°C) is far larger than the one sigma uncertainty of 0.005°C reported on the observed
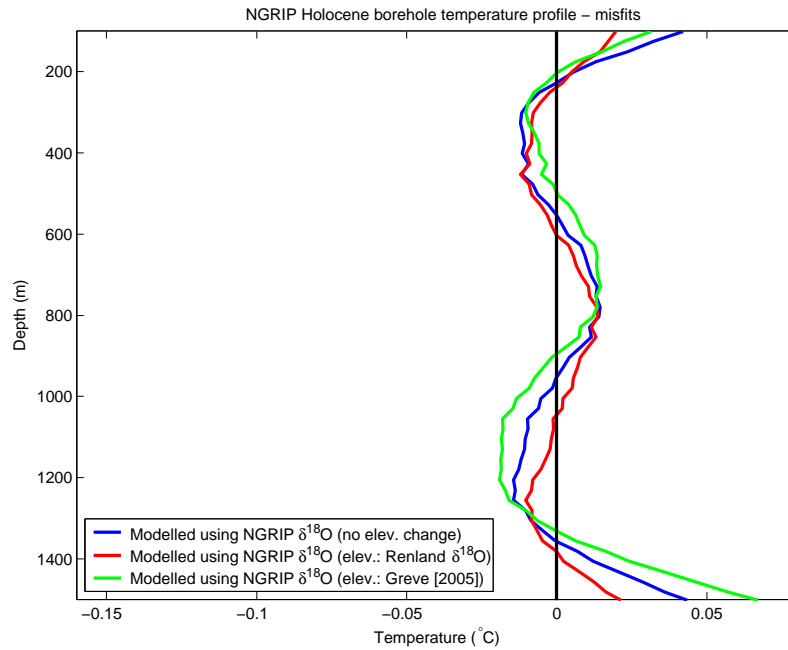
Figure 5.12: Plot of observed minimum misfit for modeled borehole temperatures (based on Holocene NGRIP δ^{18}O) vs. observed NGRIP borehole temperatures under three different NGRIP surface height histories: No change in surface height at all (blue curve), changes as given by comparison with uplift corrected Renland δ^{18}O (red curve) and changes given by the Greve [2005] modelling effort (green curve)..

GRIP borehole temperatures [Dahl-Jensen et al. 1998], while the NGRIP modeling produces an average misfit (0.0076°C) much closer to the measuring uncertainty [Dahl-Jensen et al. 2003].

The much better fit of the modeled NGRIP temperature profile, does suggest that temperature/δ^{18}O slope found for NGRIP probably should carry more weight than the GRIP based estimate. An assumption that is further underpinned by the fact, that the minimum GRIP plus NGRIP misfit found, when it is demanded that the same temperature/δ^{18}O slope applies to both locations ($\sim$2.9°C/$^0/_{00}$ - see figure 5.13) is much closer to the NGRIP estimate than the GRIP estimate (tables 5.1 and 5.2).

Further examining the rather large GRIP misfit, it is evident that it is in the top part of the GRIP borehole temperature profile where it is problematic to obtain a good fit. As δ^{18}O data from the Greenland summit region is known to have a rather poor signal to noise ratio [Fisher et al., 1985; 1996], it is worth noting that δ^{18}O data spanning relatively short time periods (decades to centuries) are used to model the top of a borehole temperature profile, while the bottom part of the temperature profiles integrates climatic condi-
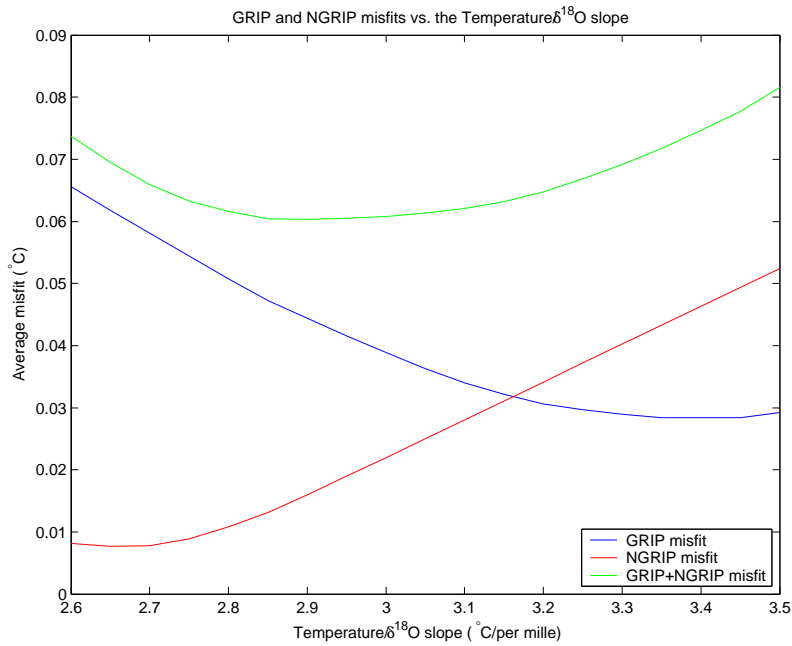
Figure 5.13: The GRIP, NGRIP and the GRIP+NGRIP modeled borehole temperature average misfits as a function of the temperature/δ^{18}O slope. The GRIP and NGRIP height estimates are based on a comparison with the uplift corrected Renland δ^{18}O record

tions through several millennia of data (i.e. the climatic optimum). Being susceptible to shorter time-scale δ^{18}O fluctuations, the modeling of the top few hundred meters of the borehole temperature profile will therefore be most prone to noise in the δ^{18}O record.

Fortunately two parallel GRIP shallow-core δ^{18}O records spanning the last millennium (see figure 5.14) can be used to test the significance of noise in the GRIP δ^{18}O record. From figure 5.15 it can in fact be seen that the misfit between modeled and observed GRIP borehole temperatures is very dependent on which GRIP δ^{18}O record is used for the last millennium, with the combination of the GRIP Main Core (11700-900 b2k) and the GRIP S93 shallow-core (900-0 b2k) yielding a mean misfit of only 0.011°C for the Holocene section of the GRIP borehole temperature profile; much more in line with both the NGRIP misfit and the stated uncertainties for the GRIP borehole temperatures.

The large difference between the modeled misfits in the top few hundred meters of the GRIP temperature profile raises the question of whether or not the top of the temperature profile should be used for temperature/δ^{18}O calibration purposes given the noise in the δ^{18}O records. However, it does turn out that the temperature/δ^{18}O calibration obtained for the three GRIP
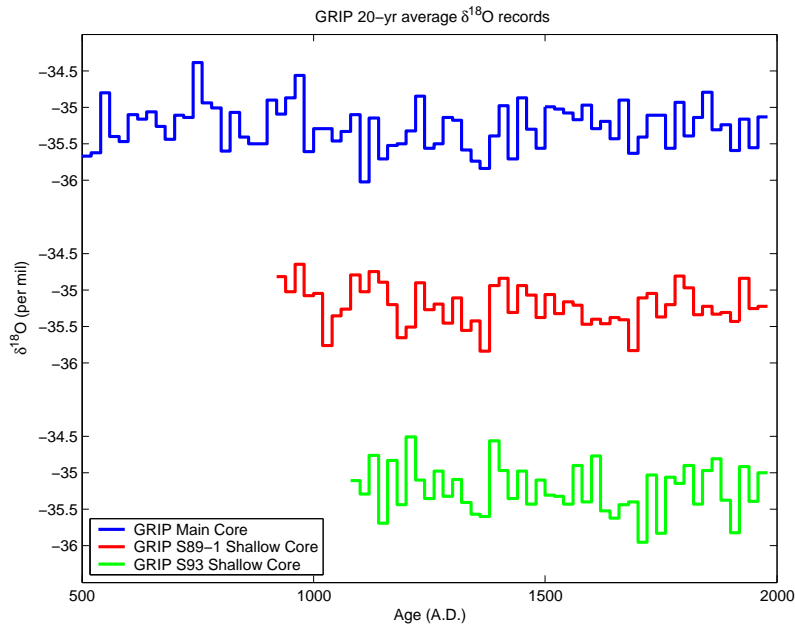
Figure 5.14: Three 20-yr averaged $\delta^{18}O$ records, covering the past ~ 1000 years from the GRIP drill site.

$\delta^{18}O$ records is almost identical, suggesting that the modeling of the climatic optimum is far more important for the calibration than the temperature fluctuations during the past millennium. Hence the decision to include the top of the borehole temperature profiles in the calibration experiments seems to have little impact on the obtained $\delta^{18}O$/temperature calibration.

It is speculated that the large GRIP temperature/$\delta^{18}O$ slope could be a consequence of not including bedrock movement in the temperature profile modeling, as it seems that the slope decreases with increasing early Holocene ice sheet thickness (the slope being largest when Greve [2005] thicknesses are assumed). Therefore it could be that a possible 40-50 meter depression of the bedrock (yielding a 40-50 meter increase in ice sheet thickness) would further reduce the GRIP temperature/$\delta^{18}O$ slope, bringing it more in line with the NGRIP estimate and maybe further reducing the GRIP misfit. This further stresses that the NGRIP slope estimate seems to be the most solid.

The decision to assume a constant accumulation rate throughout the Holocene in the modeling experiments could also be responsible for the difference in GRIP and NGRIP temperature/$\delta^{18}O$ slopes. The annual layer thicknesses at GRIP and NGRIP (see figure 4.6 in the previous chapter) does show some differences in trends during the Holocene, that could have an impact on the modeling if converted to differences in accumulation rate histories.

A more general concern is the validity of the pre-Holocene initial conditions,

75
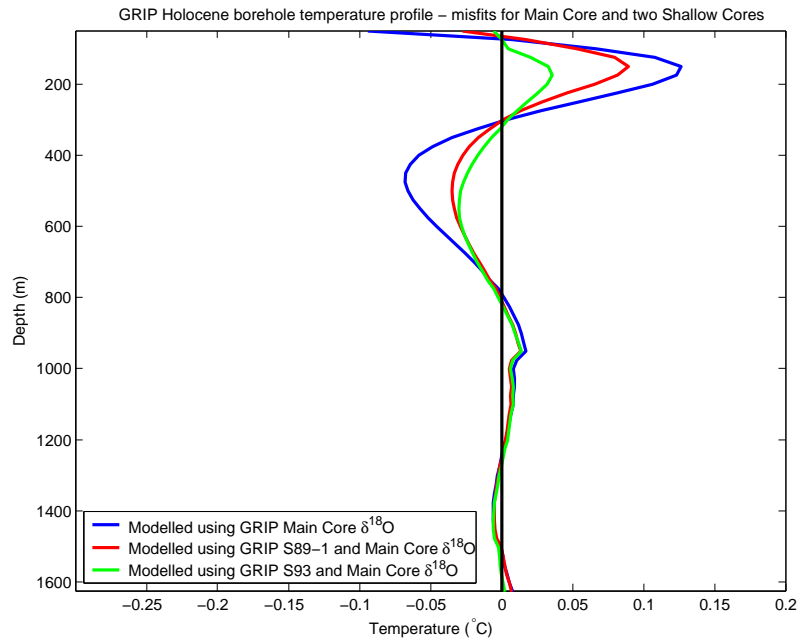
Figure 5.15: Misfit of the GRIP δ^{18}O based temperature history as compared to the GRIP borehole temperatures when Renland δ^{18}O is used to estimate the GRIP elevation history (blue curve). The red and green curves are minimum misfits generated by substituting the past $\sim$1000 years of the GRIP Main Core δ^{18}O record with S89-1 and S93 GRIP shallow core δ^{18}O before the temperature calibration.

which were simply calculated with an average glacial accumulation rate and a fixed temperature found through the tuning. This configuration completely ignores the Younger Dryas/Allerød-Bølling climatic oscillation before the inception of the Holocene. It can, however, be argued that by having the initial temperature as a tuning parameter, a reasonable compromise between the cold Younger Dryas and the mild Allerød-Bølling temperatures should be achieved. An assertion that is also supported by the fact that the optimum initial temperature was found to be significantly warmer ($\sim$-47°C) than the glacial temperature estimate of $\sim$-55°C from the Dahl-Jensen et al. [1998] GRIP borehole temperature inversion. The good agreement between the Dahl-Jensen et al. [1998] GRIP borehole temperature inversion and the GRIP δ^{18}O based temperature reconstruction for the past 7000 years (when uplift corrected Renland δ^{18}O is used to estimate the GRIP elevation history - see figure 5.9) also supports the validity of the approach.
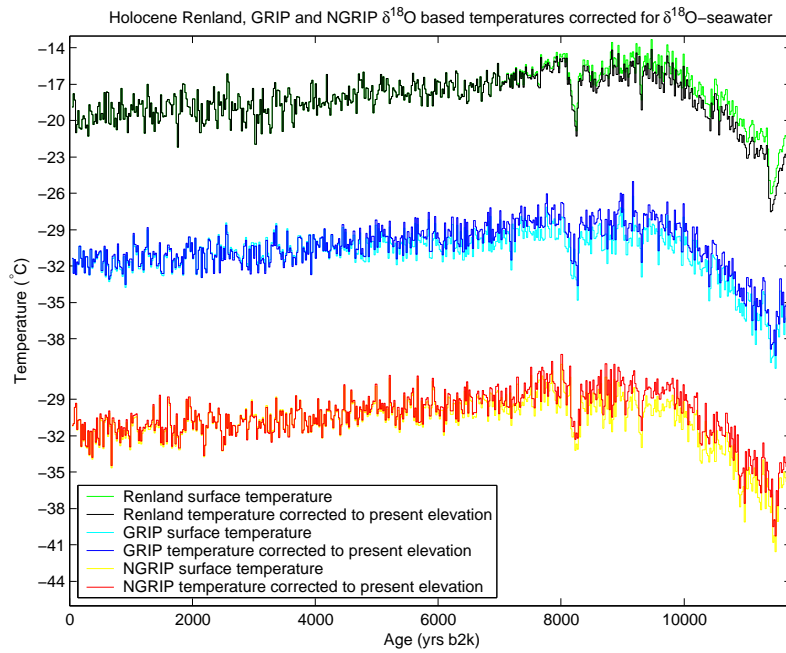
Figure 5.16: Best estimates of Holocene temperature history based on GRIP, NGRIP and Renland δ^{18}O records calibrated using GRIP and NGRIP borehole temperature profiles. For GRIP and NGRIP temperatures are based on surface height estimates found through comparison with uplift corrected Renland δ^{18}O. Surface temperatures Renland is based on height estimates from glacial rebound data (from Funder [1978]).

5.3.5 Best estimate of the temporal temperature/δ^{18}O slope

Based on the GRIP and NGRIP borehole temperature calibration experiments it is concluded that the Holocene temperature/δ^{18}O slope should be expected to be in the range 2.7-3.4°C/‰ with the most likely value being approximately 2.9°C/‰. This value for the temporal slope is almost twice as large as the spatial slope (1.5°C/‰) found through investigation of temperature and δ^{18}O averages at multiple Greenland drill sites [Johnsen et al., 1989]. The 2.9°C/‰ are, however, almost identical to the slope for shifts from glacial to inter-glacial conditions found using the Dahl-Jensen et al. [1998] estimate for Last Glacial Maximum temperatures at the GRIP drill site. Figure 5.16 shows temperature estimates for the GRIP, NGRIP and Renland drill sites using a temporal slope of 2.9°C/‰ and Renland δ^{18}O based surface height estimates for GRIP and NGRIP (and glacial rebound based surface heights for Renland).
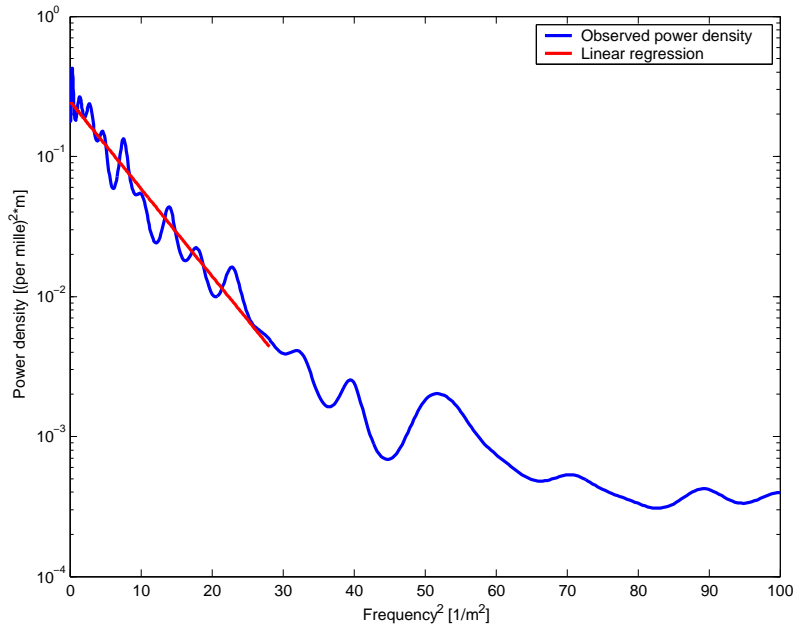
Figure 5.17: Power spectrum (blue curve) for the 5200-5600 b2k period in the NGRIP curve and best fit estimate of the reduction in spectral density due to firn diffusion (red rurve).

5.4 Surface temperatures from firn diffusion

It is possible to carry out a final independent check of the Holocene temperature/δ^{18}O slope derived from the calibration experiments in the previous section. In the upper $\sim$60m of the ice sheet temperature dependant diffusive processes in the snow and firn works to smooth the δ^{18}O profiles (see appendix A.3). At the depth of pore close off ($\sim$60m) this diffusive process stops and the much slower process of diffusion in solid ice takes over. However, in the GRIP and NGRIP cores the ice diffusion is negliable in the Holocene sections of the cores, as the ice diffusion works very slowly at a temperature of -30°C observed in the top half of the ice sheet. The smoothing of the δ^{18}O profile that happened in the snow and firn layers is therefore preserved in the deeper ice, opening a possibility to gain information of past surface temperatures throughout the Holocene (and in fact even far into the glacial for both the GRIP and NGRIP cores).

As shown in appendix A.3, the Johnsen et al. [2000] model of the diffusive processes in the snow and firn is extremely accurate in its predictions of the degree of smoothing of the isotope signal (in fact both for δ^{18}O and δD) given the particular surface and flow conditions at a given drill site. In Vinther [2003] a full derivation of the diffusion length (the typical length scale a water molecule will move vertically in the ice sheet) in the snow

and firn was presented for the Johnsen et al. [2000] diffusion model. The final diffusion length (σ) at pore close off found in Vinther [2003] can be summarized as:

$$\sigma_i^2 = \frac{f(T, P, A, H_{eff})}{q_i \cdot \alpha_i} \tag{5.4}$$

Hence the diffusion length (σ_i) at pore close off is a function of temperature (T), surface pressure (P), annual accumulation rate (A) and effective height (H_{eff}), which is a Dansgaard-Johnsen flow model parameter. Furthermore σ_i depends on the fractionation factor (α_i) and the constant (q_i) both depending on the isotope in question [Merlivat and Jouzel, 1979]:

$$q_{O^{18}} = 1.0285 \quad and \quad q_D = 1.0251 \tag{5.5}$$

$$\alpha_{O^{18}} = 0.9722 \cdot e^{\frac{11.839}{T}} \tag{5.6}$$

$$\alpha_D = 0.9098 \cdot e^{\frac{16288}{T^2}} \tag{5.7}$$

As noted in Johnsen et al. [2000] it is intriguing that the ratio between the diffusion lengths for $\delta^{18}O$ and δD is dependant only on the surface temperature (T):

$$\frac{\sigma_{O_{18}}}{\sigma_D} = \sqrt{\frac{q_D \cdot \alpha_D}{q_{O_{18}} \cdot \alpha_{O_{18}}}} = \sqrt{0.9327 \cdot e^{\frac{16288}{T^2} - \frac{11.839}{T}}} \tag{5.8}$$

Hence the diffusion lengths observed in Holocene records of $\delta^{18}O$ and δD can be combined to yield a direct estimate of the past surface temperatures that governed the diffusive processes in the top $\sim$60m of the ice sheet.
The determination of past diffusion lengths can be made by studying the power spectrum of $\delta^{18}O/\delta D$ records [Johnsen et al., 2000]:

$$P(k) = P_0 \cdot e^{k^2 \sigma^2} \Leftrightarrow k^2 = \sigma^2 \cdot (log(P(k)) - log(P_0)) \tag{5.9}$$

Here P(k) is the power density as a function of wave number (k), and the noise in the isotope data has been ignored, as the noise problem can be (almost completely) circumvented by only using the low frequency part of the spectrum for determining the diffusion length. From (5.9) it can be seen that σ^2 can be determined by linear regression, as shown in figure 5.17, being mindful not to carry out the regression into the flat noise spectrum at high frequencies.
Unfortunately the elegant approach of using diffusions lengths for both $\delta^{18}O$ and δD is not viable at present, as no continuous series of Holocene δD data at sufficient resolution is available for the GRIP and NGRIP cores. As a second best option it is still possible to solve the full equation (5.4) with respect to T using the detailed Holocene NGRIP $\delta^{18}O$ profile for diffusion length estimation. This is less desirable as uncertainties in the ice flow modeling and
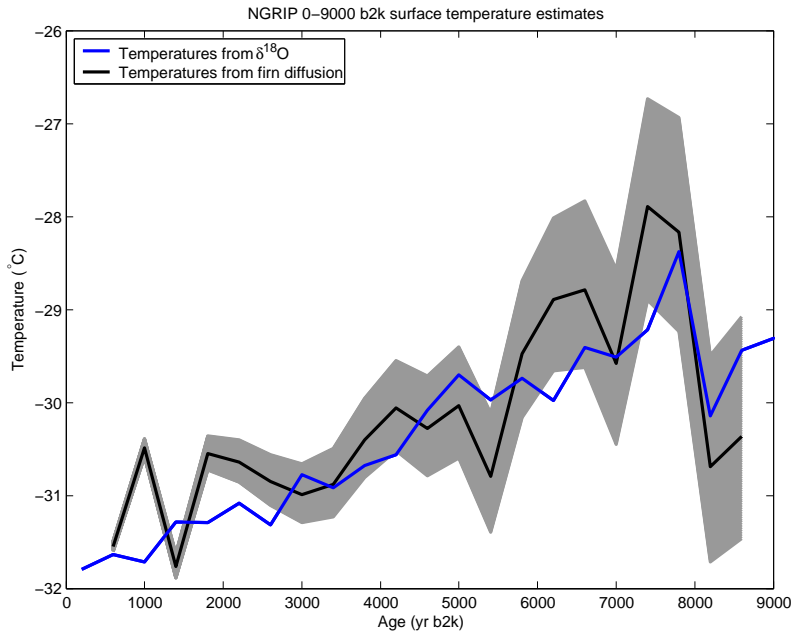
Figure 5.18: Past temperatures from the NGRIP δ^{18}O record (blue curve), and from firn diffusion of the δ^{18}O record (black curve), both in 400 year steps. The grey shading indicates the uncertainty in the temperature estimate (due to flow model and accumulation rate uncertainties).

accumulation history will propagate into the temperature estimate. Nevertheless, using the lower frequency (less than 0.7 cycles per year - avoiding the annual peak at 1 cycle per year and the noise) part of the power spectrum it is possible to give a reasonable estimate of NGRIP surface temperatures during the past ∼9000 years (see figure 5.18). The temperature estimate is, however, subject to considerable uncertainty due to uncertainties in the determination of past accumulation rates and the flow model parameter, H_{eff}, underlining the importance of having measurements of both δ^{18}O and δD at sufficient resolution for diffusion studies.

Despite the uncertainty in the NGRIP surface temperature estimate, it is encouraging to see (figure 5.18) that it to a large degree confirms the general temperature development during the past 9000 years predicted using the temperature/δ^{18}O slope of ∼2.9°C/‰ derived from borehole temperature modelling (using the Renland δ^{18}O based surface height estimate) in the previous section.

5.5 Summary

A simple ice flow and temperature model was used to calculate GRIP and NGRIP borehole temperatures based on Holocene δ^{18}O histories. The modeling showed that it is possible to obtain a Holocene δ^{18}O to temperature calibration that results in consistency between the modeled and observed borehole temperatures, taking into account the limitations set forth by the high level of noise in the δ^{18}O data.

When using ice core δ^{18}O to calculate Holocene temperature histories, one has to use different temporal and spatial temperature/δ^{18}O slopes, as studies of both fast and slow temperature variations show that the temporal temperature/δ^{18}O slope is significantly different from the observed spatial slope. As a consequence δ^{18}O records have to be corrected for past changes in surface elevation with the observed slope of -0.6 $^0\!/_{00}$/100m before temperature calculations are carried out; even when past surface temperatures are calculated from δ^{18}O records.

The best estimate of the temporal temperature/δ^{18}O slope was found to be $\sim$2.9°C/$^0\!/_{00}$. A temperature history based on this slope was verified against an independent temperature estimate based on a study of the (temperature dependent) diffusive smoothing of the detailed NGRIP δ^{18}O record. Despite significant uncertainties in the diffusion based temperature estimate, it did to a large degree confirm the temperature/δ^{18}O slope of $\sim$2.9°C/$^0\!/_{00}$.

The bore hole temperature modeling effort was also able to identify the most likely of three proposed elevation histories for the GRIP and NGRIP sites, as the best approximations of observed borehole temperatures always occurred when GRIP and NGRIP elevation histories were based on comparisons with uplift corrected Renland δ^{18}O data.

Modeling assuming constant ice sheet thickness and modeling based on ice sheet thickness data from the Greve [2005] thermo-mechanical ice sheet model consistently produced worse approximations to both GRIP and NGRIP borehole temperatures. Furthermore the agreement between δ^{18}O based GRIP temperatures and the Dahl-Jensen et al. [1998] GRIP temperature inversion was by far most convincing when the GRIP elevation history was found using the uplift corrected Renland δ^{18}O data.

The preferred elevation history of the GRIP drill site (based on a comparison between GRIP and uplift corrected Renland δ^{18}O) is very similar to a GRIP elevation history from a simple ice sheet model presented by Johnsen et al. [1995].

The combined evidence of the modeling effort gives a strong indication that (1) the Renland ice cap did not significantly change its thickness during the Holocene and the surface elevation of the ice cap only changed due to postglacial rebound of the entire Scoresbysund area. (2) The extremely simple Johnsen et al. [1995] GRIP elevation model gives a very good approximation of the GRIP ice sheet elevation history. (3) Complex thermo-mechanical ice

sheet models have significant problems in reproducing Greenland Holocene ice sheet dynamics.

Finally it should be noted that the very narrow constraints on Renland elevation throughout the Holocene, makes the Renland δ^{18}O record extremely easy to interpret climatically as all Renland Holocene δ^{18}O variations can be expected to reflect climatic changes, when the Renland δ^{18}O record has been uplift corrected. This very special quality of the Holocene Renland δ^{18}O record will be exploited almost ruthlessly in the next chapter.

Chapter 6

Seasonally resolved proxies for North Atlantic climatic conditions during 8 millennia

In chapter 2 it was demonstrated that the climatic interpretation of stable isotope data from Greenland ice cores is eased significantly by separating the summer and winter seasons in the data. Furthermore it was discovered that seasonal $\delta^{18}O$ data from the high accumulation Dye-3 site in southern Greenland had a very favorable signal to noise ratio. Hence this chapter will focus on the development of long series of seasonal stable isotope data from the Dye-3 deep ice core high resolution $\delta^{18}O$ and δD data sets, including the new measurements performed as par of this project (see chapter 3).

The setting of the Dye-3 drill site does, however, complicate this effort. The drill site is about 40 km east of the ice divide and the bedrock is all but flat. Hence the flow pattern influencing the Dye-3 core is complicated and the stable isotope data are significantly influenced by various upstream effects [Reeh et al., 1977; 1985]. Furthermore there is a possibility that the southern part of the Greenland ice sheet has undergone changes in altitude and thereby flow pattern during the Holocene, just as it probably was the case for the central parts of the Greenland ice sheet (see chapter 5).

Rather than facing the daunting task of modeling the complex and changing flow pattern in the Dye-3 area, it will therefore be proposed to use the Renland stable isotope data to circumvent the problem. In chapter 5 it was demonstrated that the Holocene Renland $\delta^{18}O$ record has been influenced only by quite well constrained elevation changes (the post glacial rebound of the entire Scoresbysund area). Hence the Renland $\delta^{18}O$ record is expected to be a good indicator of east Greenland Holocene temperatures, when corrected for the post glacial uplift. In this chapter it will therefore be proposed to combine the low frequency variability seen in the Renland record with the high frequency variability discernible in the Dye-3 stable isotope data, in order to form Greenland stable isotope records with a maximum of tem-

perature related information on all frequencies.

6.1 The Dye-3 stable isotope data

The Dye-3 deep ice core δ^{18}O data set spans the entire core from top to bottom. The δ^{18}O samples have, however, been cut in changing resolution with depth. From the top (21 b2k) and back to 5815 b2k and from 6906 to 7898 b2k the resolution is 8 samples per year or higher, while the 5816-6905 b2k section and the 7899-8313 b2k section is cut in 1-2 samples per year. As part of this Ph.D. project δD measurements in a resolution of 8 samples per year have been carried out on the 5816-6905 b2k and 7899-8313 b2k sections (see chapter 3).

In order to form a homogeneous high resolution isotopic data set for the entire 21-8313 b2k period it was decided to scale down the δD measurements by a factor of 8 (which is the best estimate for the slope between δD and δ^{18}O [Dansgaard, 1964]) and adjust the resulting series to have the same average as the lower resolution δ^{18}O data in the corresponding sections; thus effectively converting the δD measurements to δ^{18}O data.

6.2 Correcting the Dye-3 stable isotope data for firn and ice diffusion

Due to the relatively high temperatures and the rapid thinning rate at the Dye-3 drill site, single crystal ice diffusion [Ramseier, 1967] must be expected to affect the annual cycle in the Holocene stable isotope data. Hence the Dye-3 stable isotope data have to be corrected both for the diffusion in the snow and firn layers and for progressing single crystal ice diffusion in the entire core.

The correction for diffusion in the snow and firn layers will act to artificially smoothen the part of the profile for which this diffusion has not ceased (the top ∼60m) as to conform with the smoothed data below ∼60m. Traditional diffusion correction where the entire profile is corrected, as to eliminate the firn diffusion [Johnsen et al., 2000] is not viable due to occasional melt layers in the Dye-3 core (melt layers tend to create steep gradients in the stable isotope data, which in turn result in spurious high frequency ringing in traditionally diffusion corrected data).

To determine the degree of single crystal ice diffusion experienced by the Dye-3 stable isotope data, the amplitude of the annual cycle has been determined (using the analytical maximum entropy peak determination method outlined by Johnsen and Andersen [1978]) for each 100 year section in the Dye-3 record back to 8313 b2k (see figure 6.1). The expected annual cycle amplitudes when taking into account the single crystal ice diffusion (and assuming that the initial amplitude of the annual cycle has remained constant during the past 8 millennia) have thereafter been calculated and plotted
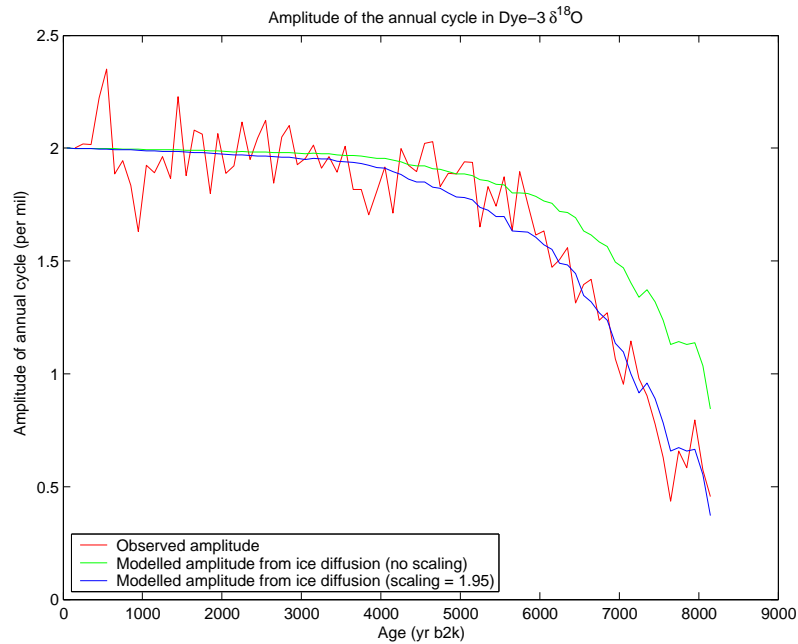
Figure 6.1: Observed amplitudes of the annual cycle in highly resolved Dye-3 δ^{18}O data (for some sections δD/8) compared to modeled amplitudes estimates.

in figure 6.1 for comparison The modeled amplitudes are based on modeled diffusion lengths and observed annual layer thicknesses (that causes the high frequency variability in the modeled amplitudes).

Looking at figure 6.1 it is immediately clear that the modeled single crystal ice diffusion yields a very unsatisfactory approximation to the diffusion seen in the data below ∼6000 b2k. It is speculated that the discrepancy is due both to an increase in firn diffusion due to warmer temperatures some 6000 years ago and upstream features in the ice flow affecting the Dye-3 site, which cannot be resolved by the amplitude modeling as it is based on a simple two dimensional Dansgaard-Johnsen flow model.

As the modeled diffusion severely underestimates the decrease in annual cycle amplitude, it was decided to artificially scale up the Ramseier [1967] diffusivity in an effort to better model the observed amplitudes. Using a scaling factor of 1.95 proved to yield the best approximation to the observed data (see figure 6.1). As the amplitudes modeled using the 1.95 scaling are very close to the observed amplitudes, it was decided to use this scaling for the diffusion correction. Even though it is very unsatisfactory to introduce such a fuzz factor in the diffusion correction, it is still much better than to live with diffusion estimates that are obviously wrong, as poor estimates immediately will result in artificial trends in the seasonal data series.

Figure 6.2: Gaussian filtered ($T_{1/2} = 300$ years - see appendix B for details) Renland δ^{18}O corrected for post glacial uplift (blue curve) and Dye-3 δ^{18}O data (red curve). The green curve gives the difference in between the filtered Renland and Dye-3 δ^{18}O series.

Finally it should be noted that in making such a best fit as was done through the diffusivity scaling, it is implicitly assumed that the initial annual amplitudes in the stable isotope data before any diffusion has taken place has been unchanged during the past 8000 years.

6.3 Eliminating flow related trends in the Dye-3 stable isotope data

As previously mentioned and thoroughly documented by Reeh et al. [1985] it is an immense task to model the complicated ice flow that affects the Dye-3 ice core. This is unfortunate as undulations of the ice sheet surface upstream from the Dye-3 drill site are known to affect the upstream accumulation rate [Reeh et al.; 1977, 1985] and could also affect the seasonality of the accumulation and thereby change the average δ^{18}O values. Hence it cannot be ruled out that some of the low frequency oscillations (500 years or longer) in the Dye-3 δ^{18}O record are due to upstream effects. Furthermore the increasing upstream elevation will with certainty gradually lower the δ^{18}O values observed with increasing depths in the Dye-3 core. Progressively deeper layers will originate from positions further and further
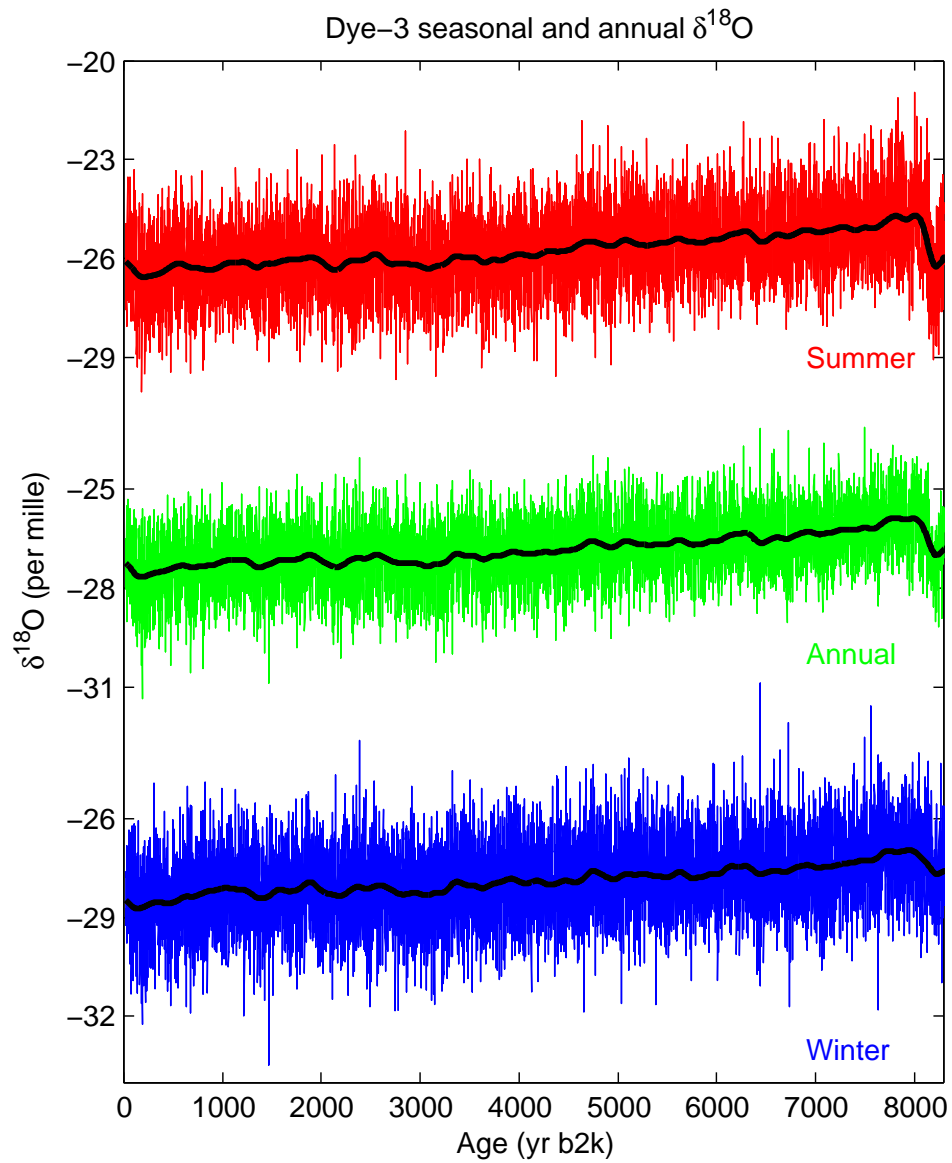
Figure 6.3: Summer season (red), annual (green) and winter season (blue)
$\delta^{18}O$ from the Dye-3 ice core. Thick black curves are gaussian filtered data
($T_{1/2} = 300$ years).
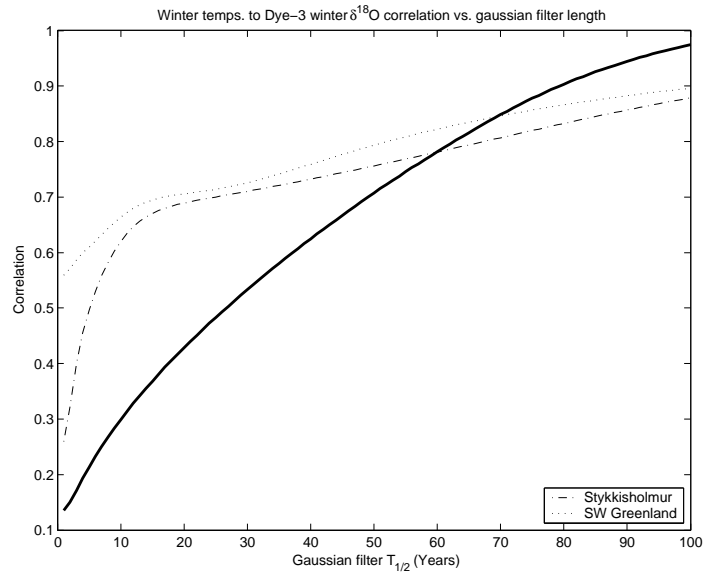
Figure 6.4: Correlations between Dye-3 winter season δ^{18}O and SW Greenland and Stykkisholmur Nov-Apr temperatures from 1830 to 1978 as a function of the degree of gaussian smothing applied to the data (quantified by ($T_{1/2}$). Thick black line gives the 90% confidence limit for the correlations (limit increases when the smoothing decreases the number of degrees of freedom left in the data sets.

upstream at higher and higher elevation with corresponding lower average δ^{18}O values (as average δ^{18}O decreases with $0.6^0/_{00}$ per 100m elevation).

To completely avoid the complications posed by the ice flow at Dye-3 it is therefore decided to replace the low frequency variations in the Dye-3 stable isotope data with the post glacial uplift corrected Renland δ^{18}O low frequency variations (see figure 6.2). A $T_{1/2}$ of 300 years is chosen to make sure that the bulk (almost 80%) of the variability on 500 year times scales is removed from the Dye-3 δ^{18}O, while the centinnial varibility in Dye-3 δ^{18}O is completely preserved (less than 0.2% is removed). Uplift corrected Renland δ^{18}O is very likely to represent true temperature variations, not masked by further changes in elevation, due to specific topographic constraints on the Renland ice cap (see chapter 5 and [Johnsen et al. 1992b] for details).

This low frequency replacement is employed by adding the difference between low pass filtered Renland and Dye-3 δ^{18}O data (green curve in figure 6.2) to the Dye-3 δ^{18}O series. The resulting seasonal and annual Dye-3 δ^{18}O series can be seen in figure 6.3.
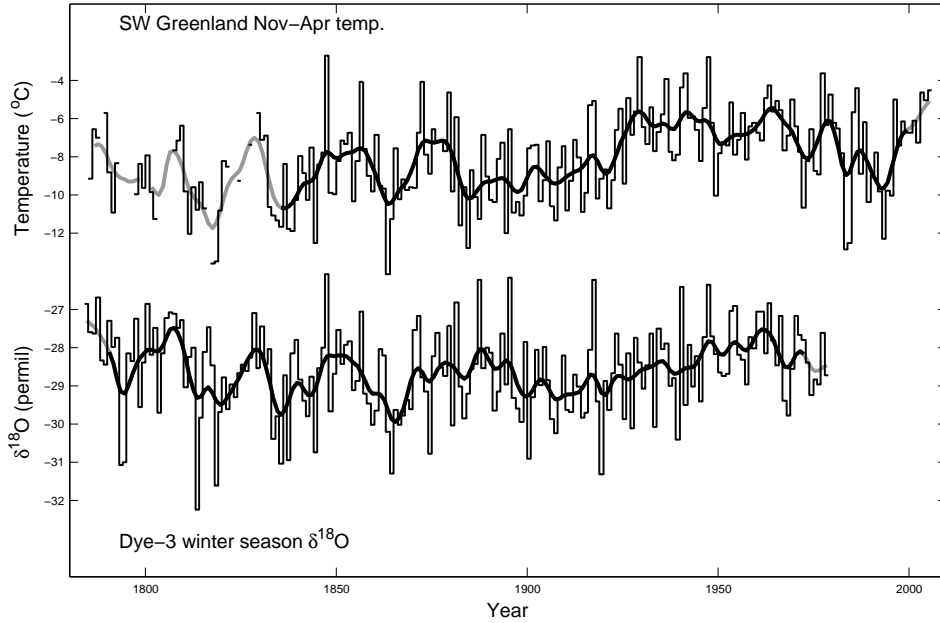
Figure 6.5: SW Greenland Nov-Apr temperatures and Dye-3 winter season δ^{18}O. Thick lines are decadally filtered data (lines are grey if the filtered values are based on incomplete data).

6.4 Meteorological data

Details concerning the data sets and series for temperature and sea level pressure (SLP), which will be used for comparison with the seasonally and annually resolved stable isotope series (shown in figure 6.3) can be found in section 2.2.

6.5 The seasonal data

It is very satisfactory to see that the high frequency variability in the 8 millennia long summer and winter season δ^{18}O data series (shown in figure 6.3) seems to be quite steady throughout the past ~8000 years. This suggest that the diffusion correction of the Dye-3 data is in fact capable of retrieving the seasonal oscillation in the high resolution δ^{18}O data. The only period of some concern in the seasonal data is the 8.2kyr cold event. During this event the variability drops and the summer to winter difference in δ^{18}O average lessens. This could be a real climate signal, suggesting that it was the summers that cooled markedly during the 8.2kyr cold event, but there is also a considerable risk, that it is an expression for the failure of the diffusion correction to completely resolve the seasons, due to a significant decrease in accumulation rate during the event [Rasmussen et al., 2006b]. A decrease
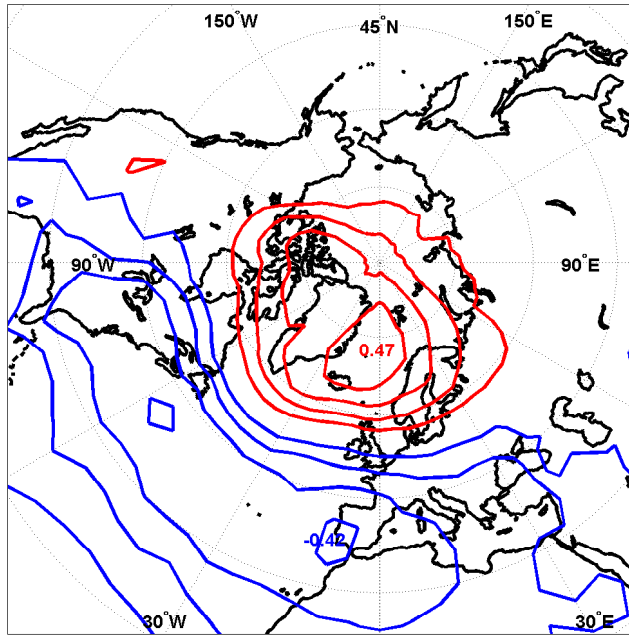
Figure 6.6: Spatial correlation map of 1851-1978 Nov-Apr sea level pressure (contours with 0.1 interval, red lines indicate positive correlations, blue lines negative) and winter season δ^{18}O from the Dye-3 ice core.

in accumulation rate would allow diffusive processes in the snow and firn to be more effective in dampening the annual cycle in the δ^{18}O data, a feature which cannot be fully resolved by the diffusion modeling.

6.5.1 Investigation of the winter season data

In figure 6.4 correlations as a function of gaussian smoothing (see appendix B for details) between Dye-3 winter season δ^{18}O and both Stykkisholmur and SW Greenland Nov-Apr temperatures are shown. It can be seen that winter season δ^{18}O correlations with SW Greenland temperatures are stronger than correlations with Stykkisholmur temperatures on all investigated time scales.

It is encouraging that correlations in figure 6.4 increase with increased smoothing, a sign that the δ^{18}O data are closely related to the regional temperatures. It should be noted that the failure of correlations to reach significance for the longest time scales most of all is due to the relatively small time period ($\sim$150 years) spanned by the temperature data.

It is interesting that correlations almost have a local maximum for 10-20 year gaussian smoothing and it is speculated that variations on this timescale are characteristic for the North Atlantic area. Plots of raw and decadally smoothed SW Greenland Nov-Apr temperatures and Dye-3 winter season
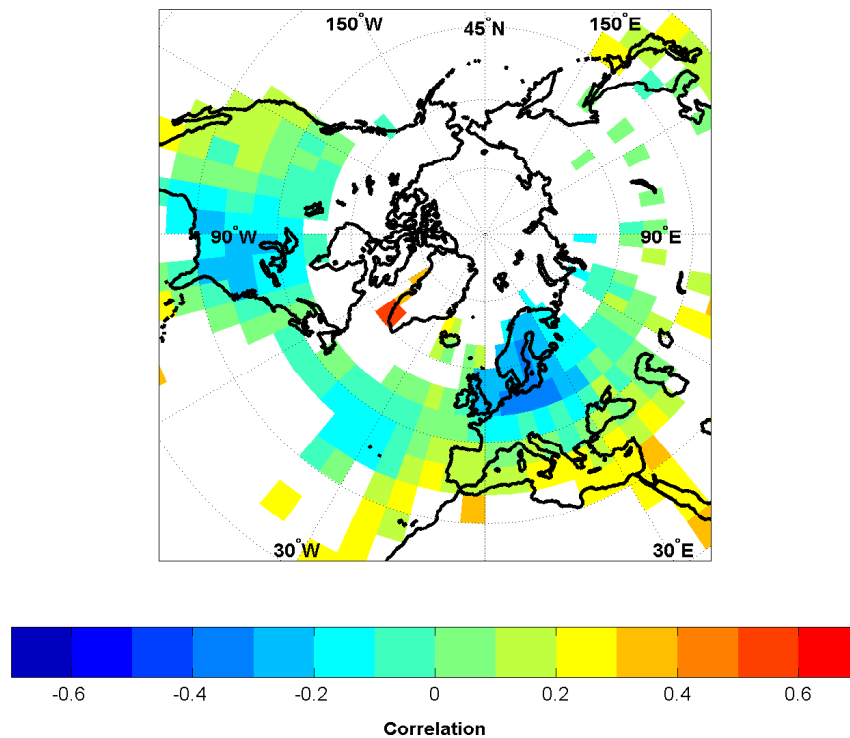
Figure 6.7: Spatial correlation map of 1871-1978 Nov-Apr surface temperature and winter season δ^{18}O from the Dye-3 ice core. Grid-points with more than 20% missing values are left blank.)

δ^{18}O can be seen in figure 6.5.

Plots of spatial correlation patterns between Dye-3 winter season δ^{18}O and regional SLP and temperature patterns can be seen in figures 6.6 and 6.7 respectively. Clear North Atlantic Oscillation (NAO) patterns stand out in both correlation plots; a promising indication that the Dye-3 winter season δ^{18}O data can be used to gain information on past NAO conditions.

To further investigate relations between the Dye-3 winter season δ^{18}O data and the NAO, correlations as a function of gaussian smoothing were calculated between the Iberian/Icelandic Nov-Apr NAO index [Jones et al. 1997; Vinther et al. 2003b] and the winter season δ^{18}O data (see figure 6.8). The most striking feature in figure 6.8 is without doubt the marked correlation minimum for decadal time scales. Hence the strong correlation between Dye-3 winter season δ^{18}O and SW Greenland winter temperatures on decadal timescales is unrelated to the NAO. It is speculated that it is decadal variability in North Atlantic sea surface temperatures (SSTs) that causes temperature and δ^{18}O to co-vary and dominate the NAO signal on decadal timescales.

It is also interesting that correlations between the winter NAO index and
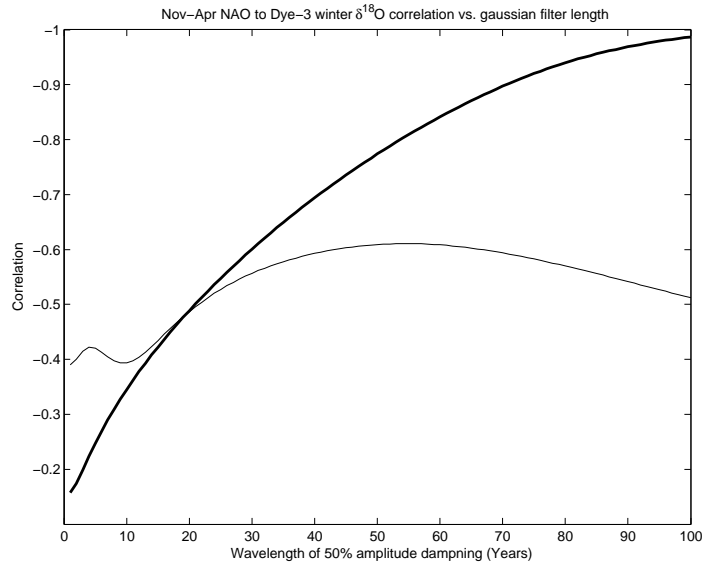
Figure 6.8: Correlations between Dye-3 winter season δ^{18}O and the NAO index (Nov-Apr) from 1823 to 1978 as a function of the degree of gaussian smothing applied to the data (quantified by $T_{1/2}$). Thick black line gives the 90% confidence limit for the correlations.

Figure 6.9: Nov-Apr NAO index (inverted) and Dye-3 winter season δ^{18}O. Thick lines are decadally filtered data (lines are grey if the filtered values are based on incomplete data).

Dye-3 winter season δ^{18}O decreases after peaking at half-century smoothing (albeit being below significance for $T_{1/2} \dot{\iota} 37$ years), which could be an indication that climatic fluctuations on centennial timescales are unrelated to the NAO. It could therefore be argued that the Dye-3 winter season δ^{18}O data should be high-pass filtered to obtain the best possible NAO proxy series. This would eliminate the need of using the low frequencies from Renland δ^{18}O data to correct the Dye-3 δ^{18}O data for upstream effects when NAO reconstructions are pursued.

A plot of the (inverted) Nov-Apr NAO index and the Dye-3 winter season δ^{18}O is shown in figure 6.9.

6.5.2 Investigation of the summer season data

In figure 6.10 correlations as a function of gaussian smoothing between Dye-3 summer season δ^{18}O and both Stykkisholmur and SW Greenland May-Oct temperatures are shown. Surprisingly it can be seen that while summer season δ^{18}O correlations with Stykkisholmur temperatures are highest on a year to year basis, SW Greenland temperatures correlate markedly better with Dye-3 summer season δ^{18}O on decadal or longer time scales. Hence the long term trends in the Dye-3 summer season δ^{18}O series correspond better to the long term evolution of SW Greenland climate than it does with Stykkisholmur climate. It is speculated that the high year to year correlation found between summer season δ^{18}O and Stykkisholmur summer temperatures could reflect common high frequency oscillation driven by variations in sea ice.
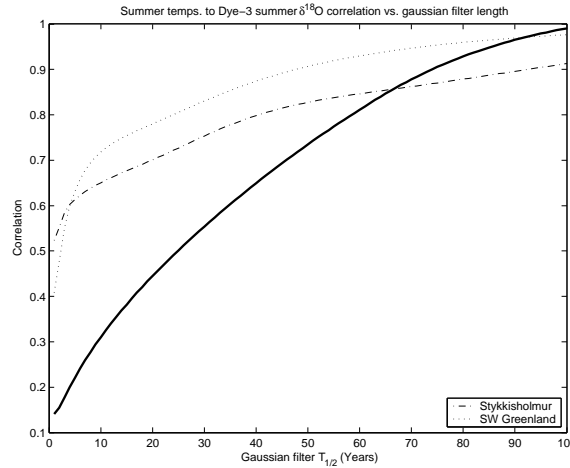
Figure 6.10: Correlations between Dye-3 summer season δ^{18}O and SW Greenland and Stykkisholmur May-Oct temperatures from 1840 to 1978 as a function of the degree of gaussian smothing applied to the data (quantified by $T_{1/2}$). Thick black line gives the 90% confidence limit for the correlations.
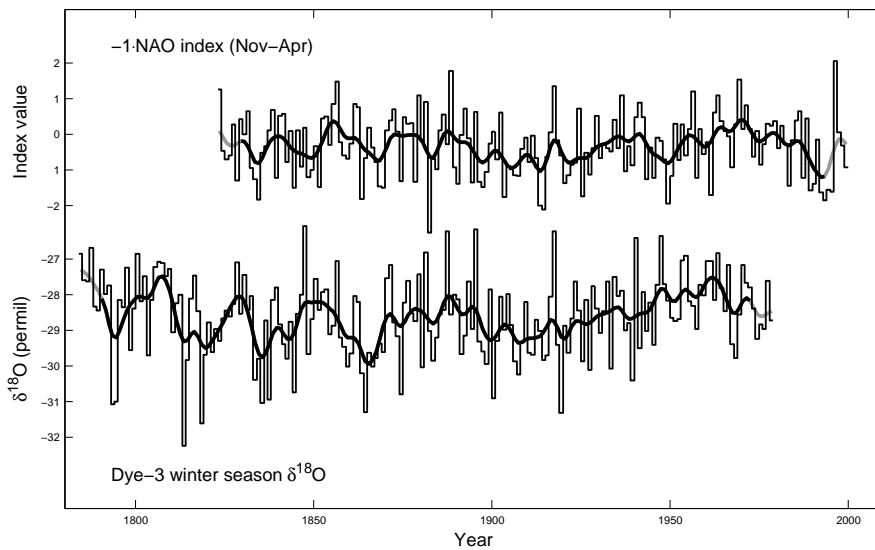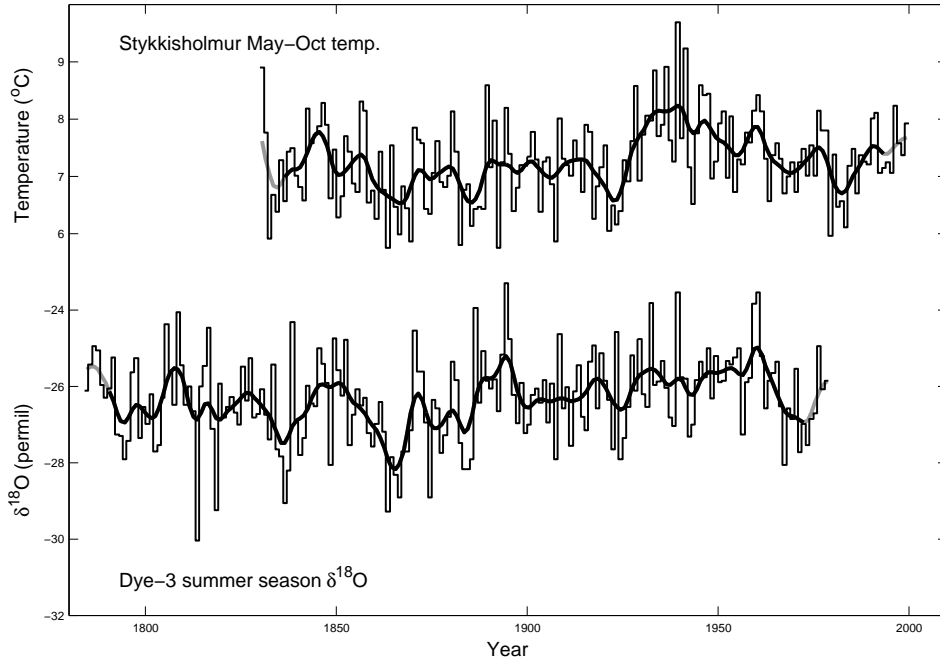
Figure 6.11: May-Oct Stykkisholmur temperatures and Dye-3 summer season δ^{18}O. Thick lines are decadally filtered data (lines are grey if the filtered values are based on incomplete data).

As was the case with the winter season data, the summer season correlations increase with increased gaussian smoothing. That this trend can be found for both winter and summer season δ^{18}O data is in fact very encouraging. It is clear evidence that the Dye-3 ice core δ^{18}O is an excellent proxy for especially SW Greenland temperatures, but also Stykkisholmur temperatures. A plot of both Stykkisholmur May-Oct temperatures and summer season Dye-3 δ^{18}O can be seen in figure 6.11.
Turning to relations between Dye-3 summer season δ^{18}O and regional May-Oct SLP and temperature patterns, spatial correlation plots both for regional SLP and temperatures can be seen in figures 6.12 and 6.13 respectively.

Correlations with May-Oct SLP data are generally weak but a discernible correlation maximum (r=0.30) over Iceland can be ascertained. Hence Dye-3 summer δ^{18}O seems to be slightly influenced by summer SLP conditions over Iceland. The relation between May-Oct temperatures in Icelandic waters and Dye-3 summer δ^{18}O is stronger (see figure 6.13) indicating that SST conditions exerts a larger influence on Dye-3 summer δ^{18}O values than summertime atmospheric flow patterns. However, it should be noted that the SSTs around Iceland could be related to the SLP conditions over Iceland and vice versa.

94

Figure 6.12: Spatial correlation map of 1850-1978 May-Oct sea level pressure (contours with 0.1 interval, red lines indicate positive correlations, blue lines negative) and summer season δ^{18}O from the Dye-3 ice core.

Figure 6.13: Spatial correlation map of 1870-1978 May-Oct surface temperature and summer season δ^{18}O from the Dye-3 ice core. Grid-points with more than 20% missing values are left blank.)
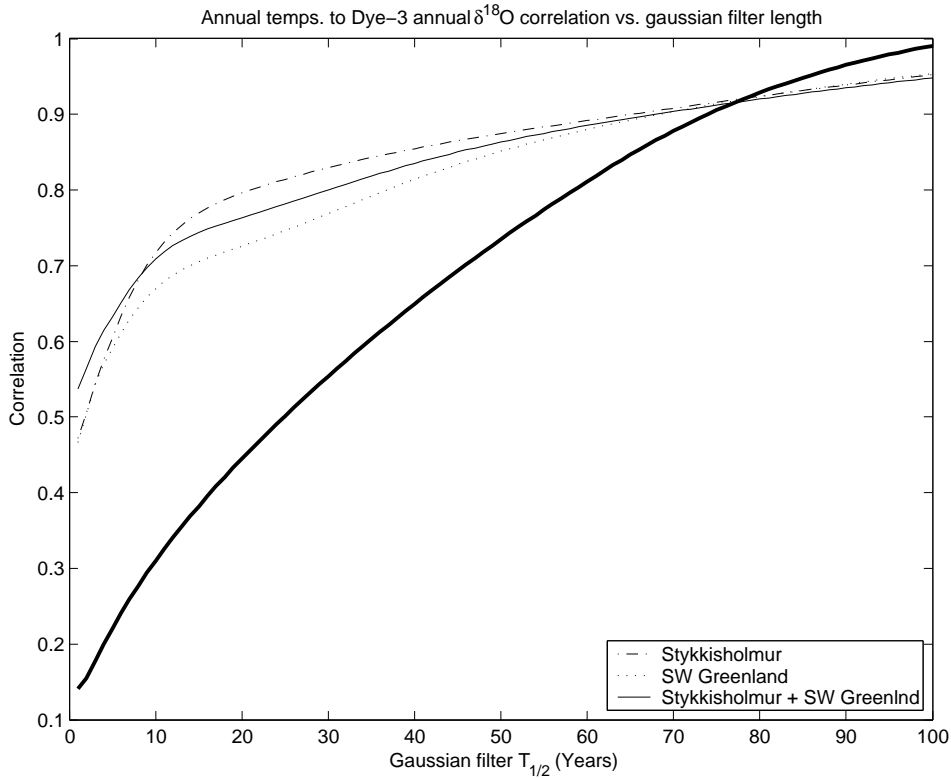
Figure 6.14: Correlations between Dye-3 annual $\delta^{18}O$ and SW Greenland annual temperatures (dotted line), Stykkisholmur annual temperatures (dashed line) the average of SW Greenland annual temperatures and Stykkisholmur annual temperatures (full line) from 1840 to 1978 as a function of $T_{1/2}$. Thick black line gives the 90% confidence limit for the correlations.

6.6 The annually resolved data

A time series of annually resolved Dye-3 $\delta^{18}O$ data has also been generated for the past ~8300 years (green curve in figure 6.3). Compared to seasonally resolved data, the annually resolved series has the advantage, that the stable isotope diffusion problem can be ignored, as diffusional smoothing cannot seriously affect annual average $\delta^{18}O$ values.

A correlation analysis between the Dye-3 annual $\delta^{18}O$ data and annual average temperatures from Stykkisholmur and SW Greenland can be seen in figure 6.14. Surprisingly it can be seen that on most timescales Dye-3 annual $\delta^{18}O$ correlates stronger with Stykkisholmur temperatures than with SW Greenland temperatures!

This is very interesting, as it has just been shown (in the previous sections), that Dye-3 seasonal $\delta^{18}O$ is correlated most significantly with SW Greenland
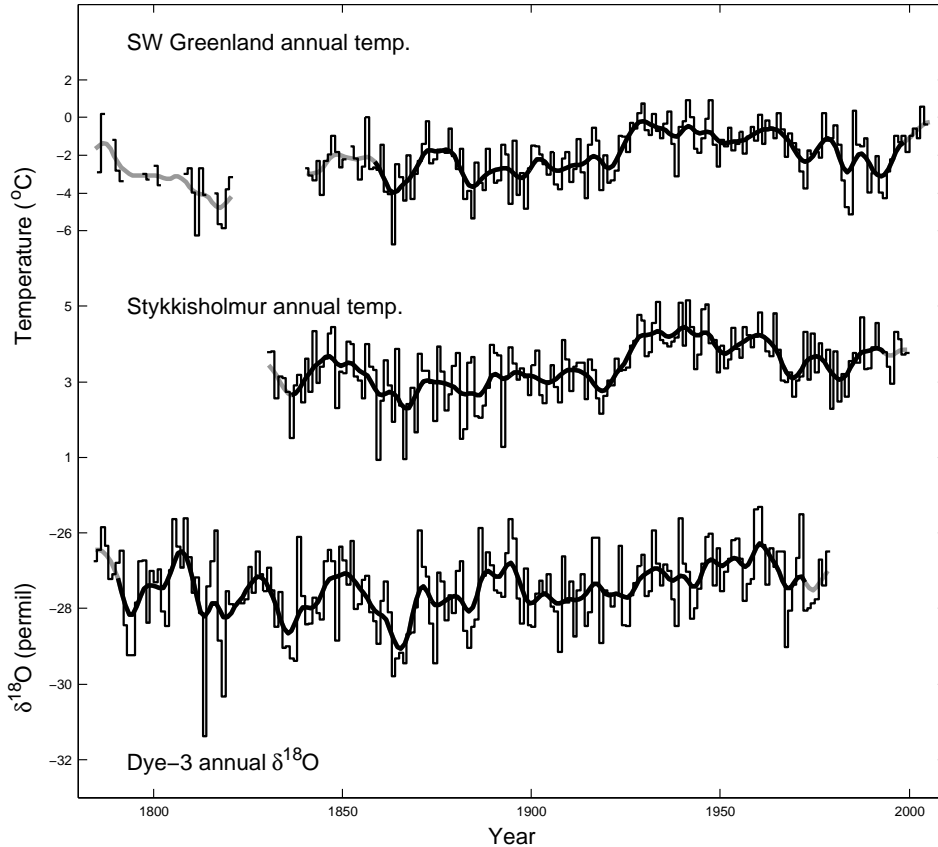
Figure 6.15: SW Greenland annual temperatures, Stykkisholmur annual temperatures and Dye-3 annual δ^{18}O. Thick lines are decadally filtered data (lines are grey if the filtered values are based on incomplete data).

temperatures, both for the summer and winter season on long time scales. The only explanation for this strange behavior is that the extreme winter to winter variability in SW Greenland temperatures (SW Greenland winter temperature variability is 2.5 times larger than the summer temperature variability) completely overshadows SW Greenland summer temperatures when the SW Greenland annual average is calculated. As Stykkisholmur winter temperature variability is more moderate (1.7 times the summer variability), the Stykkisholmur annual average is less unbalanced, giving some room for summer temperatures to impact the annual average. This seasonal weighting must simply be more in line with the weighting in the Dye-3 annual δ^{18}O data.

Another feature of the Dye-3 annual δ^{18}O, which can be determined from figure 6.14 is that on short timescales it is associated both with Stykkisholmur and SW Greenland temperatures; correlations are therefore highest when Dye-3 annual δ^{18}O data are compared to the average temperature from the
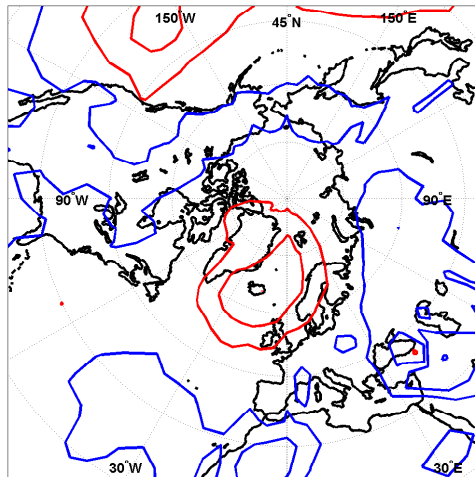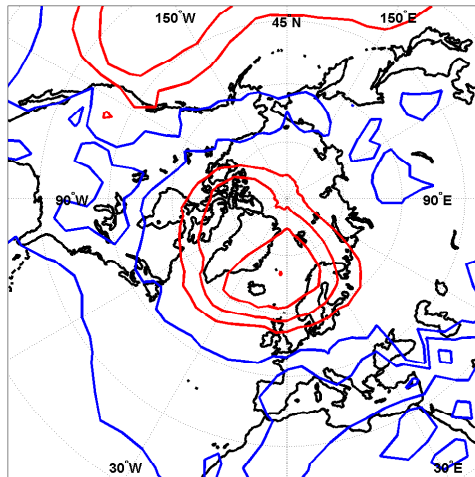
Figure 6.16: Spatial correlation map of 1850-1979 Jan-Dec sea level pressure (contours with 0.1 interval, red lines indicate positive correlations, blue lines negative) and annual δ^{18}O from the Dye-3 ice core.
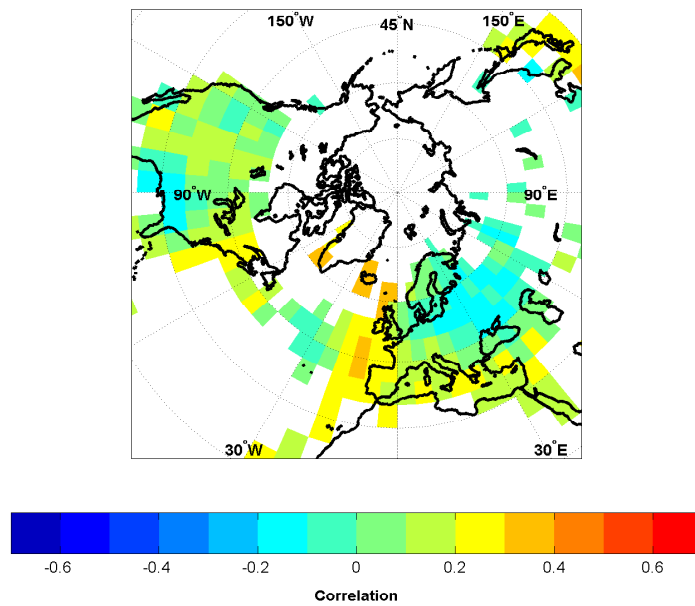
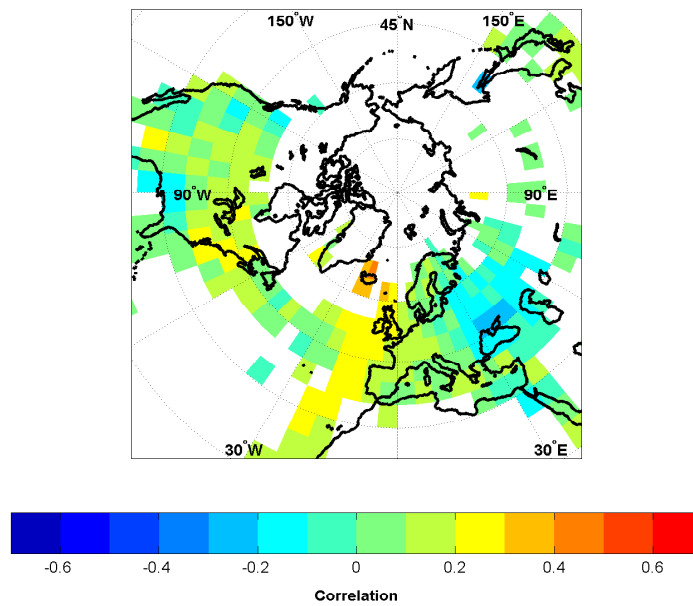Figure 6.17: Spatial correlation map of 1870-1979 Jan-Dec surface temperature and annual δ^{18}O from the Dye-3 ice core. Grid-points with more than 20% missing values are left blank.)
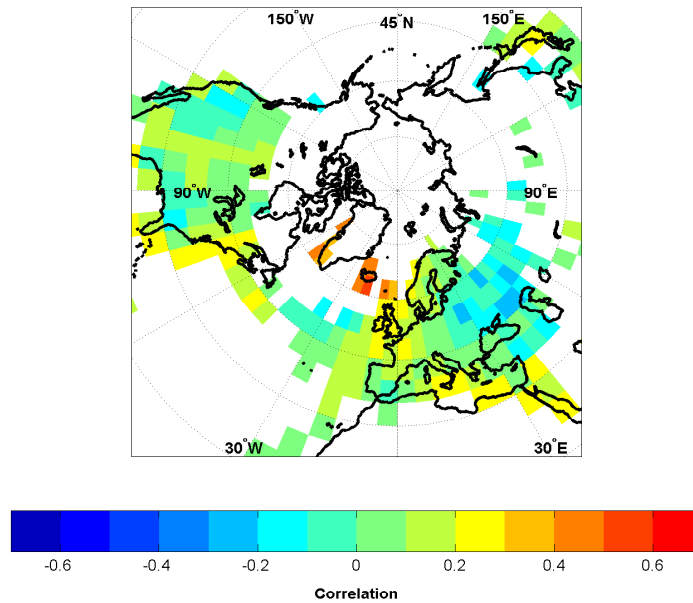
Figure 6.18: Spatial correlation map of 1870-1979 Jan-Dec surface temperature and annual δ^{18}O from the Renland ice core. Grid-points with more than 20% missing values are left blank.)

two temperature series. This is very much in line with the finding that high frequency oscillations in the seasonal δ^{18}O data are strongest related to Stykkisholmur temperatures during summer times and SW Greenland temperatures during the winter. The annual δ^{18}O data should therefore be expected to be associated with both temperature series. Dye-3 annual δ^{18}O as well as time series for both Stykkisholmur and SW Greenland annual average temperatures are plotted in figure 6.15.

In figures 6.16 and 6.17 spatial correlation patterns between Dye-3 annual δ^{18}O and respectively regional SLP and temperatures can be seen. Both correlation patterns can be seen to be composed of the winter and summer season correlation patterns discussed in the previous sections.

In figure 6.18 the relation between annually resolved Renland δ^{18}O and regional temperatures is presented. It is encouraging to see that the temperature correlation patterns associated with annually resolved Renland δ^{18}O almost resembles the pattern associated with Dye-3 annual δ^{18}O, as this is a strong indication that the two sites are influenced by the same regional climatic features. Hence using the Renland δ^{18}O series to correct the low frequency variability of Dye-3 δ^{18}O for upstream effects should not introduce climatic signals in the Dye-3 series, which are foreign to the Dye-3 site.

99

6.7 Summary

Three high resolution time series each spanning more than 8 millennia have been created, based on the highly resolved southern Greenland Dye-3 stable isotope record: Dye-3 winter season δ^{18}O, Dye-3 summer season δ^{18}O and Dye-3 annual δ^{18}O. All three series were found to be closely associated with SW Greenland and Stykkisholmur temperatures on all investigated time scales. Furthermore winter season δ^{18}O is associated with wintertime NAO conditions, mostly on a year to year basis, while decadal scale associations seem weaker. The associations between winter season δ^{18}O and the NAO also seem to weaken for time scales longer than $\sim$50 years.

As the Dye-3 stable isotope record is significantly influenced by ice-flow related upstream effects, which are very hard to quantify through modeling, it was decided to filter out the low frequency variations in the Dye-3 data and substitute them with the low frequency variations found in the uplift corrected Renland δ^{18}O series. The Renland series is ideal for this purpose as it has been shown (in chapter 5) to be very unlikely to have been affected by changes in altitude except for the well constrained post glacial uplift in the Scoresbysund area. Furthermore annually resolved Renland δ^{18}O have been shown to be associated with the same regional temperature variations as is Dye-3 annual δ^{18}O.

Finally it is worth noting that all three δ^{18}O series indicate that most of the past 8 millennia experienced climatic conditions as warm or even warmer than the most recent conditions seen in the records. The annual δ^{18}O record also indicate that Greenland climatic conditions in the late 18th and early 19th century probably represents the coldest period during the past 8300 years and were even colder than conditions during the 8.2kyr cold event.

Chapter 7

Discussion

As this dissertation consists of chapters covering many different subjects, it was decided to place most of the discussions in the chapters themselves. These discussions wont be repeated here, but can be found in the following sections:

Discussion of seasonal isotope date in 20 Greenland ice cores: Section 2.7.
Discussion of the new synchronized dating: Sections 4.7 and 4.10.
Discusion of δ^{18}O based borehole temperature modeling: Section 5.3.4.
Discussion of 8 millennias of seasonal Dye-3 δ^{18}O data. Sectiom 6.7.

Hence the following discussion will be devoted to two subjects only: The relationship between δ^{18}O and temperature and the interpretation of the Renland δ^{18}O record.
These subjects are of importance both to chapter 5 and chapter 6 and could therefore not be placed within one of the chapters.

The almost constant δ^{18}O value seen throughout the Holocene in many Greenland ice core δ^{18}O records have for a long time been the main argument against trusting δ^{18}O as a reliable proxy for Greenland temperatures, as the climatic optimum could hardly be discerned in flat δ^{18}O records from four of the best resolved Greenland ice cores (Dye-3, GRIP, GISP2 and NGRIP). A strong climatic optimum should be expected in the Holocene δ^{18}O because borehole temperatures from all four sites suggest a prominent climatic optimum with surface temperatures on the Greenland ice sheet 2-3 °C higher than present [e.g. Dahl-Jensen et al., 1998].
Based on the lacking climatic optimum in Greenland δ^{18}O, it could be argued that δ^{18}O should simply not be trusted as a temperature proxy during the Holocene. Using data for the past 150-200 years, a strong associations between δ^{18}O and regional temperature data was, however found on all investigated timescales in chapter 2 and chapter 6. Hence it seems much more likely that the lacking climatic optimum in many Greenland δ^{18}O records is due to non-climatic effects masking the temperature signal in the δ^{18}O

records.

In this dissertation a new framework for the interpretation of $\delta^{18}O$ in the Greenland ice sheet has been proposed. The corner-stone in this interpretation is that temporal changes in temperatures does not affect $\delta^{18}O$ on the Greenland ice sheet in the same manner as changes in temperature that are a consequence of altitude-changes. The subtle consequence of this is that two equal $\delta^{18}O$ values do not correspond to the same surface temperature at a drill site if the elevation of the drill site has changed in the meantime. This is in stark contrast with the previous understanding that the $\delta^{18}O$ record could be directly related to surface temperatures at the drill site, independently of changes in elevation.

The new interpretation therefore has the consequence that the almost flat Holocene $\delta^{18}O$ profiles from central Greenland can no longer be interpreted as evidence that surface temperatures derived from $\delta^{18}O$ were almost constant at the drill sites throughout the Holocene. Instead when applying proper corrections for changes in surface height, a clear climatic optimum is seen in the surface temperatures (see figure 5.16). The new interpretation is supported by the fact that it brings the central Greenland $\delta^{18}O$ based temperatures in good agreement with the borehole temperature profiles and other estimates of past surface temperatures.

As good agreement between $\delta^{18}O$ based temperatures and borehole temperatures can be obtained just through a height correction, it seems very likely that the dominant non-climatic effect affecting Holocene Greenland $\delta^{18}O$ is changes in drill site elevation. Other proposed effects on Holocene $\delta^{18}O$ such as changes in the conditions at the source area for Greenland precipitation, seems to be of second order.

In order to give solid estimates of Greenland temperatures based on ice core $\delta^{18}O$ records it is therefore imperative to have solid height estimates for the drill sites back in time. For the Holocene, the most reliable way of estimating surface height histories for the central Greenland drill sites was found to be through comparison with the uplift corrected Holocene record of $\delta^{18}O$ from the small Renland ice cap. This approach does, however, have the drawback that the central Greenland ice core $\delta^{18}O$ records are forced to yield the same millennial scale changes in temperature as found from the Renland $\delta^{18}O$ record. The uplift corrected Renland $\delta^{18}O$ series is therefore de facto elevated to be THE Greenland record of millennial trends in Holocene temperature!

It is therefore a matter of the utmost importance to make sure, that the Renland $\delta^{18}O$ record is interpreted correctly, i.e. that the only significant height change that affects the Holocene Renland $\delta^{18}O$ record is indeed the post glacial rebound, as was argued in chapter 5.

An avenue hitherto not used to verify the Renland $\delta^{18}O$ interpretation, is to compare Renland $\delta^{18}O$ to other Holocene records from small ice caps in the vicinity of Greenland. Such a comparison is presented in figure 7.1, where the Holocene ice core $\delta^{18}O$ records from the Penny, Devon and Agassiz ice
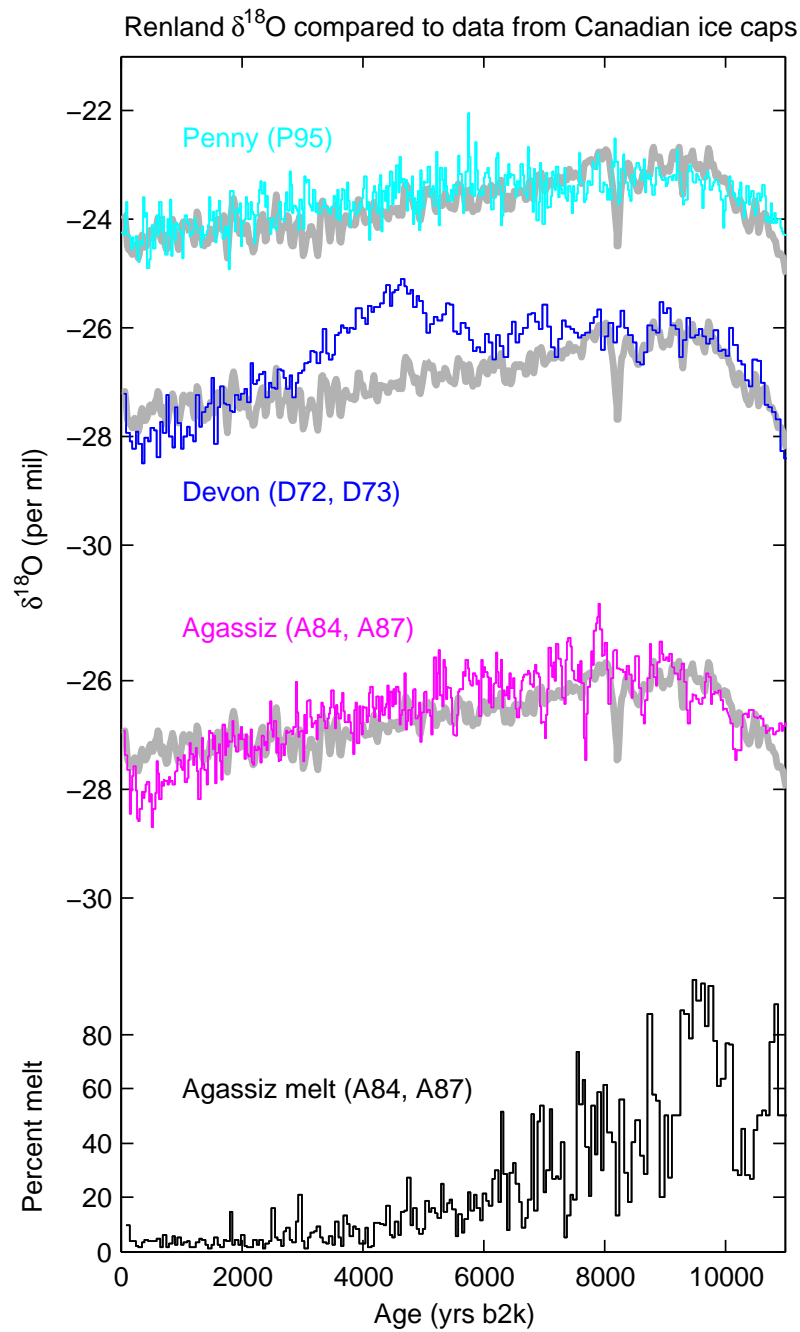
Figure 7.1: Holocene δ^{18}O data from three Canadian ice caps in the vicinity of Greenland (colored lines), compared to Renland δ^{18}O (grey lines) corrected for post glacial uplift and shifted to have the same modern δ^{18}O as observed in the Canadian ice cores. Black line is melt data from the Agassiz ice core. Timescales for the Canadian cores are adjusted to fit the GICC05 transition date and should not be considered to be very accurate.

caps [Fisher, 1979; Fisher et al., 1995; Fisher et al., 1998] are plotted on top of the uplift corrected Renland δ^{18}O record. The melt record from the Agassiz ice cap [Koerner and Fisher, 1990] is also plotted.

As the Agassiz ice cap on Ellesmere Island is only 127m thick at present [Koerner and Fisher, 1990] it should be expected the Agassiz minus Renland δ^{18}O difference should not increase much more than $\sim 0.5^0/_{00}$ on millennial time scales (assuming that climate at the two sites is evolving equally on millennial scales). This boundary on millennial scale variations does in fact seem to hold, the contrary would also has been a surprise, as a larger than $\sim 0.5^0/_{00}$ positive Aggassiz minus Renland δ^{18}O difference would imply that the Renland ice cap had gained in thickness, which is all but impossible due the fact that it already fills up the mountain valley and overflows its boundaries.

If on the other hand the Renland cap had thinned compared to Agassiz during the warmth of the climatic optimum, it would be expected that the Agassiz minus Renland δ^{18}O difference turned negative, but there is only a very slight indication of this being the case 10.000 to 9000 b2k, and never more than a few tenths of a $^0/_{00}$ (equivalent to less than 50 meters of elevation change).

With respect to the Aggassiz melt record it is encouraging that Renland δ^{18}O seems to correspond very nicely with this record; maybe even better than does the Agassiz δ^{18}O.

Turning to the Devon ice cap, a very spectacular difference in δ^{18}O develops from 6000 b2k to 4300 b2k and ends in 3000 b2k. The difference amounts to $\sim 1.5^0/_{00}$ corresponding to an elevation change of approx. 250m if no climatic effects play a role. The Devon ice cap can in fact have decreased its elevation some 250m, as the ice cap has a thickness of $\sim$300m at present. As no significant changes are seen neither in the Agassiz, nor in the Penny δ^{18}O ice core records, being from ice caps north and south of the Devon ice cap respectively, it does indeed seem likely that the curious Devon δ^{18}O values between 6000 b2k and 3000 b2k may be explained by local conditions, such as elevation change. Furthermore if Renland elevation change should explain the change, the Renland cap had to gain some 250m in height, which is impossible given its setting.

Again the it can be seen that during the climatic optimum Renland δ^{18}O is not higher than Devon δ^{18}O leaving no room for a Renland decrease in elevation not matched by a similar Devon elevation decrease. The changes in δ^{18}O differences between Renland and the Penny ice cap (on Baffin Island) δ^{18}O are also well within the boundaries of what can be explained by Penny ice cap elevation changes, as it has a thickness of more than 300m [Fisher et al., 1998].

To summarize, the comparison between Renland δ^{18}O and δ^{18}O from the three Canadian ice caps near Greenland, did nothing to contradict the hypothesis that uplift corrected Renland δ^{18}O can be regarded as unaffected by significant elevation changes during the Holocene.
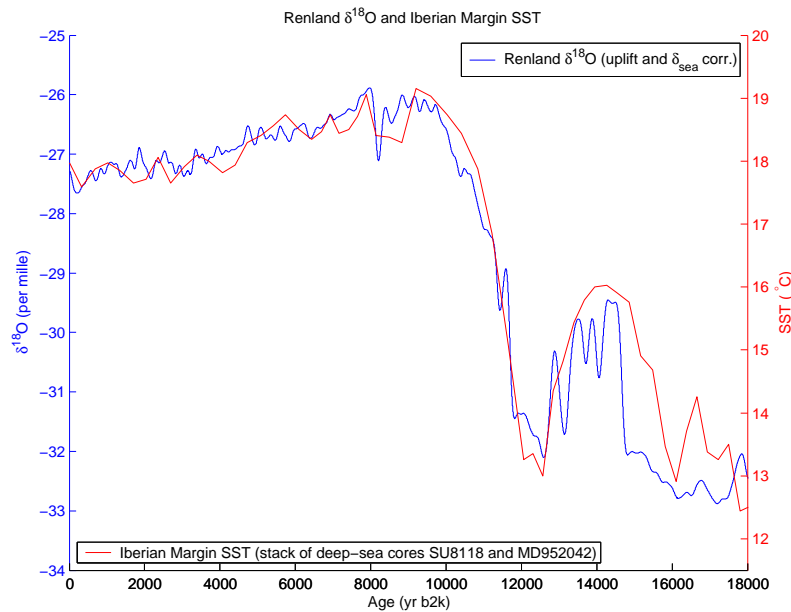
Figure 7.2: Smoothed Renland δ^{18}O ($T_{1/2} = 300$ years) corrected for post glacial uplift of the Scoresbysund area and the changes in mean sea water δ^{18}O (blue curve). Iberian Margin SST reconstruction from Bard [2002] (red curve) based on alkenone data from two sea sediment cores. The dating of the SST data are shifted slightly (≤ 150 years) to fit the GICC05 dating at the termination.

Having used all available ice core evidence in the vicinity of Greenland, it seems appropriate to turn to other proxy data for further investigation of the Renland δ^{18}O record. If the uplift corrected Renland δ^{18}O record in fact is not influenced by any other kind of elevation change, it should be expected to be directly translatable to atmospheric temperatures (except for a known correction for the change in mean δ^{18}O in seawater [Waelbroeck, et al., 2002]). And given the investigations in chapter 6, Renland δ^{18}O can be expected to be related to North Atlantic SST conditions.

In figure 7.2 Renland δ^{18}O is compared to the Iberian Margin SST reconstruction (based on the alkenone method) presented by Bard [2002]. The correspondence between the two data sets is astounding, given that this is a marine and a terrestrial data set situated some 4000km apart. Such a correspondence has to give the greatest confidence in both data sets, and surprisingly it leaves the impression that the same Renland δ^{18}O to temperature calibration can be used both during the Holocene and for glacial conditions. This reinforces the perception that Renland only has one source of precipitation: the subtropical Atlantic. Otherwise it would be hard to explain the nearly exact one-to-one correspondence with North Atlantic SST
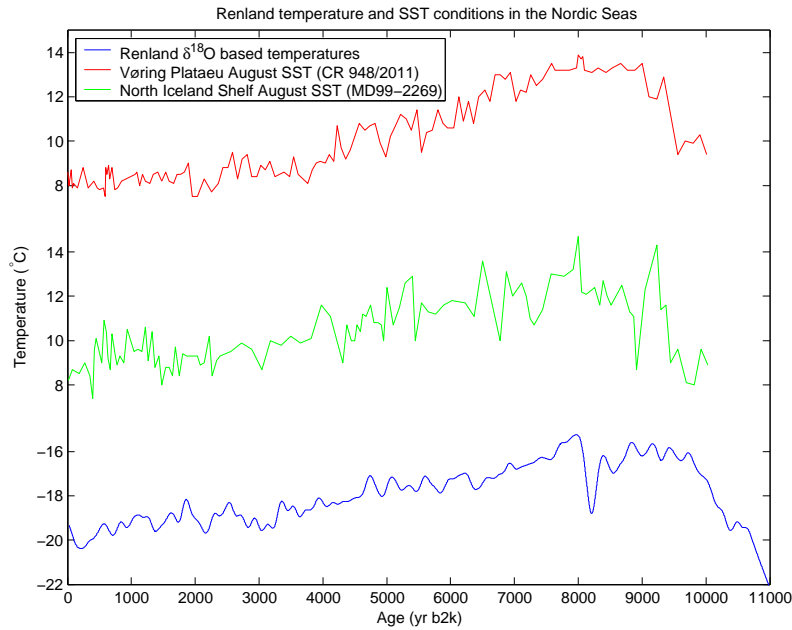
Figure 7.3: Smoothed Renland temperatures ($T_{1/2} = 300$ years) based on $\delta^{18}O$ corrected for post glacial uplift of the Scoresbysund area and the changes in mean sea water $\delta^{18}O$ (blue curve). Norwegian Sea (Vøring Plateau) and North Iceland shelf SST reconstructions digitized from figure 4 in Andersen et al. [2004] (red and green curves) based on fossil diatom assemblages sea sediment cores.

conditions.

A curious aspect of the close relation between Renland $\delta^{18}O$ and Iberian Margin SST, is that it yields a temperature to $\delta^{18}O$ slope of approx. $1°C/0/00$, which is much lower than the $2.9\ °C/0/00$ found through calibration with central Greenland borehole temperatures (chapter 5).

The marked difference is, however, most likely to be a consequence of the well known polar amplification of global temperature fluctuations. Turning to sea sediment evidence on approx. the same latitude as the Renland ice cap, it can be seen that the Renland Holocene temperatures calculated with a slope of $2.9\ °C/0/00$ correspond quite well to the estimated sea surface temperatures (see figure 7.3, data digitized from from Andersen et al. [2004]).

From figure 7.3 it can indeed be seen that the magnitude of the cooling from the climatic optimum to present conditions at Renland is very close to SST estimates west of Norway and just north of Iceland, supporting the calibration derived in chapter 5.

With all evidence pointing to the conclusion, that the elevation of the summit area of the Renland ice cap has been significantly affected by the glacial

rebound only, it seems that Renland δ^{18}O really deserves a special position among the Greenland δ^{18}O records. When the choice stands between having central Greenland Holocene δ^{18}O records with known disagreements with borehole temperatures during the climatic optimum or correcting the records to have the same millennial scale variability as the Renland δ^{18}O, the latter choice is clearly the most attractive. A fact that also became clear when the long seasonal δ^{18}O series were derived from the Dye-3 core in chapter 6.

The extreme importance of Renland δ^{18}O for the interpretation of all other Greenland δ^{18}O records does also highlight the urgent need of drilling a new Renland core, in order to make sure that the present interpretation and dating of the 1988 Renland core is absolutely correct.

Chapter 8

Conclusion

The main objective of this Ph.D.-project, was the development of seasonally resolved proxies for Greenland climatic conditions spanning the bulk of the Holocene, a goal which has been fulfilled through the creation of the Dye-3 seasonally resolved stable isotope series.

As often in research it is, however, not this planned achievement which is of most value. Instead the discoveries and byproducts, that were made working toward the goal, could turn out to be of greater value and interest.

One of the greatest byproducts is the new synchronized GICC05 chronology, that now comprises the Holocene sections of four Greenland ice cores. Having the Greenland ice cores on the same time scale is of immense importance, as has been demonstrated in this dissertation, where surface elevation estimates for central Greenland drill sites only could be made after the Renland core had been synchronized to GICC05. The synchronized dating paves the way for advanced interpretation of the Greenland ice core records.

An interesting discovery, which for sure demands further investigation, is the proposed difference between temporal and spatial temperature/δ^{18}O slopes. This new interpretation of the δ^{18}O records adds a new layer of complexity, when δ^{18}O values are converted to temperature estimates. According to this interpretation such a conversion can only take place when past changes in drill site elevation are known; even when surface temperatures are to be obtained.

The discovery with the most wide-ranging implications is probably that the uplift corrected Renland δ^{18}O record is an almost perfect indicator of centennial and millennial scale Greenland temperature conditions and thus can be used as a baseline for elevation estimates for the central Greenland cores. Comparison with an Iberian Margin sea sediment based SST reconstruction even suggests, that Renland δ^{18}O is a good proxy for regional temperatures under glacial conditions.

I therefore hope, that this conclusion is more of a beginning - signaling an era were the compilation of evidence from multiple ice cores and drill sites open new avenues for advanced interpretation of Greenland ice core records.

Appendix A

Stable isotope records from the Greenland Ice Cores

S. J. Johnsen and B. M. Vinther

A.1 Synopsis

Greenland ice cores contain a wealth of information on past climatic conditions throughout the northern hemisphere. A historical perspective on the climatic interpretation of stable isotopes in water and ice is presented in the introduction, while the remainder of the article is devoted to the current interpretation of stable isotope data from Greenland ice cores. The progress in our understanding of the stable isotope signals, on timescales from seasons to glacial cycles, is discussed and evaluated through numerous examples from Greenland ice cores. Stable isotope profiles from the Camp Century, DYE-3, GISP2, GRIP, NGRIP and Renland deep ice cores are emphasised, as they all provide climatic information back into the Eemian period.

A.2 The early isotope work

By doing stable isotope investigations of frontal precipitation over Copenhagen in the early fifties Willi Dansgaard discovered a correlation between the condensation temperatures and the isotopic ratios. Subsequently Dansgaard proposed in a ground breaking paper that palaeoclimate could be studied by doing stable isotope measurements on Greenland ice cores (Dansgaard (1954)).
At this time no ice cores were available from Greenland for such investigations and the immense scientific scope of this proposal was hardly realized,

even 15 years later when the first results from the Camp Century core became available. Carl Benson at the U. S. Army Snow, Ice and Permafrost Research Establishment (SIPRE) was, however, already doing pit studies in NW and Central Greenland in the early and mid fifties (Benson (1962)). In cooperation with Epstein and Sharp he discovered the very strong annual isotopic cycle in the Greenland snow pack. This cycle became eventually most useful for measuring accumulation rates and for dating ice cores. When the Site 2 ice core (see Figure A.1), which was drilled by SIPRE in preparation for the International Geophysical Year's Antarctic activities in 1957, became available in 1955 Chester C. Langway, also from SIPRE, initiated the modern era of multi disciplinary ice core studies including detailed isotope profiles deep down in the core (Langway (1967)). The Site 2 isotope data (Epstein and Sharp (1959)) showed a clear annual cycle below the firn layers, but smoothed compared with the isotope data from Benson's pit studies (Langway (1967)). Thus Langway discovered the effect of the firn diffusion to be discussed below.

Willi Dansgaard continued his studies in Greenland and discovered the isotopic latitude effect for Greenland and the strong correlation between mean annual temperatures and isotopic values on the ice cap (Dansgaard (1961)). He also used the Rayleigh condensation model to better understand the physical basis for the climatic information contained in natural precipitation. Most of his earlier results are summarized in his classic Tellus paper (Dansgaard (1964)) where he also gives the first results from the IAEA precipitation network and introduced the deuterium excess.

The Camp Century deep ice core was recovered by Lyle Hansen and his co-workers from the U.S. Army Cold Region Research and Engineering Laboratories in 1966. Two years later Willi Dansgaard proposed to Chester C. Langway that he would do a comprehensive isotope study on the core, a proposal Langway accepted. This most fruitful cooperation was later extended with the group of Hans Oeschger from Bern, Switzerland, and became the basis for the Greenland Ice Sheet Program (GISP) that managed to recover a deep core from Dye-3 South Greenland with a new Danish deep drill in 1981. When the first Dye-3 isotopic results were published (Dansgaard et al. (1982)), the immense impact of the isotopic palaeostudies on Greenland deep ice cores was no more being challenged. In the early seventies the Danish group also built a unique inlet system for doing 512 mass-spectrometric oxygen isotope measurements each day. The original aim was to date the Dye-3 core by counting annual isotopic cycles through most of the Holocene by measuring a total of 80,000 samples. However, this system strengthened greatly the isotope work to be done on subsequent Greenland ice cores and soon one million samples will have been analyzed with this system.
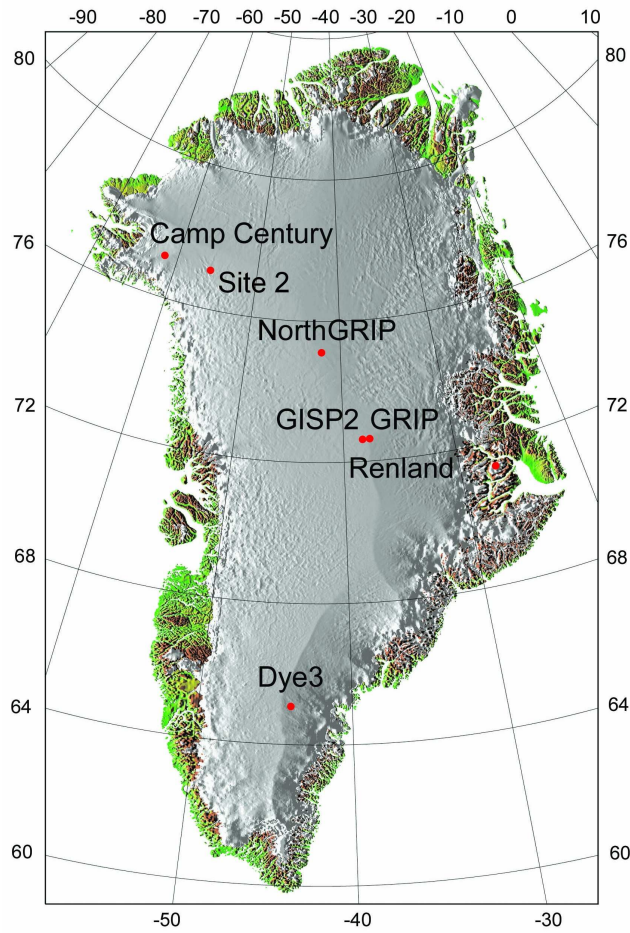
Figure A.1: Locations of selected Greenland ice cores. The Site 2 core was the first ice core drilled in Greenland. The Camp Century, Dye-3, GISP2, GRIP, NGRIP and Renland cores all contain ice from the Holocene, glacial and Eemian periods.

A.3   Shallow ice cores - the role of diffusion

A large number of ice cores reaching a depth of 100-200 m have been drilled at various locations on the Greenland ice sheet. Such cores offer a time span of a few hundreds to one thousand years, depending on core depth and local accumulation rates. As instrumental climatic observations are limited to the past two centuries for most of the northern hemisphere, the records of $\delta^{18}O$ from shallow ice cores are a valuable asset when investigating relations between climate and $\delta^{18}O$. Having multiple cores available, it is possible to stack the records and thereby reduce the glaciological noise in the $\delta^{18}O$ data. Using cores from various locations, it is also possible to resolve local climatic variations affecting only parts of the ice sheet. The investigation of $\delta^{18}O$ records from the upper part of the ice cores is complicated by water vapor diffusion in the pores of snow and firn in the top 60-70 m of the ice sheet. This diffusion will tend to smooth the high frequency oscillations of the $\delta^{18}O$. In Figure A.2 and A.3 the diffusion related decay of the annual $\delta^{18}O$ cycle can be seen for a central Greenland shallow core.
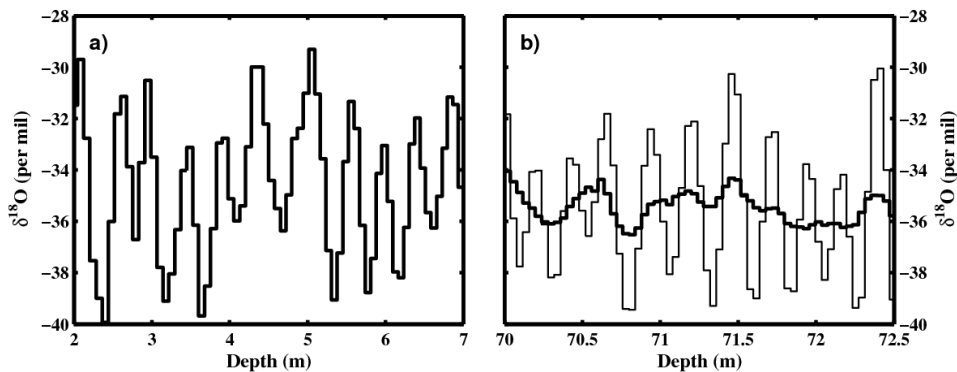
Figure A.2: Measurements of $\delta^{18}O$ from different depths in the Site E central Greenland ice core. Left: near the surface before firn diffusion dampens the annual cycle. Right: below the diffusion zone, the annual cycle is significantly dampened. The thin curve is diffusion corrected data. Annual accumulation at Site E amounts to 21 cm of ice equivalent

A.3.1   The climate signal in seasonal $\delta^{18}O$

The close relation between $\delta^{18}O$ and site temperature makes $\delta^{18}O$ a valuable proxy both for Greenland climate and northern hemisphere atmospheric circulation patterns. To fully exploit the potential of Greenland $\delta^{18}O$ records it has recently been shown by Vinther et al. (2003a) that it is essential to look into the seasonal oscillations in the $\delta^{18}O$ records.
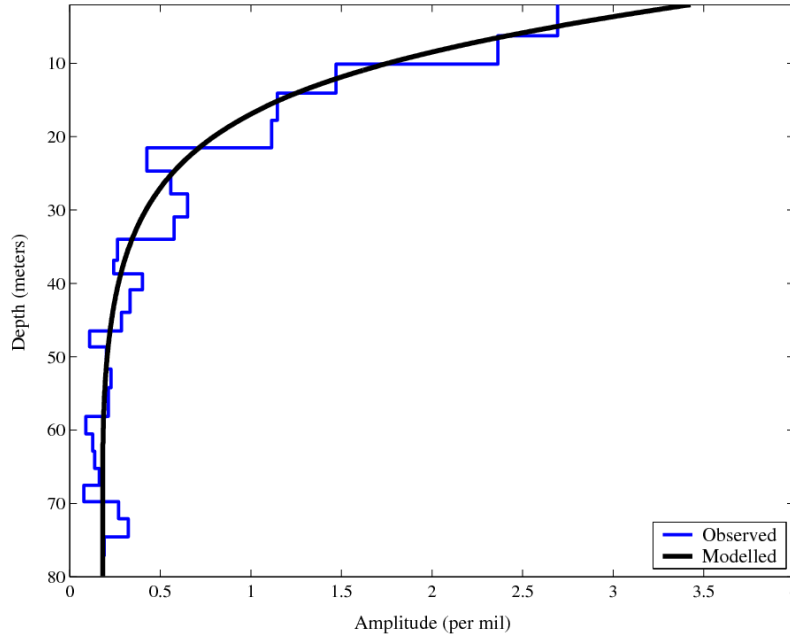
Figure A.3: Amplitude of the annual δ^{18}O cycle in the Site E central Greenland ice core and model estimate.

In the vast areas of the Greenland ice sheet where annual accumulation exceeds 20 cm of ice equivalent, seasonal oscillations of δ^{18}O can be retrieved through most of the Holocene. In areas of lower accumulation the seasonal δ^{18}O cycles will be obliterated by the diffusion in the upper snow and firn layers.

As can be seen in Figure A.2 and A.3, the seasonal cycle of δ^{18}O will be influenced by diffusion even in areas with accumulation rates larger than 20 of cm ice equivalent per year. In the top 60-70 m of the ice sheet, a marked decay in amplitude of the δ^{18}O cycle can be observed. If a climatic interpretation of seasonal δ^{18}O values is to be pursued, it is necessary to understand the diffusion process that masks the seasonal oscillations in the δ^{18}O signal.

In Johnsen (1977) the first step was taken in comprehending the physics behind the diffusion process. Later papers by Merlivat and Jouzel (1979), Herron and Langway (1980) and Schwander et al. (1988) led to the Johnsen et al. (2000) paper where a physical model covering both δ^{18}O and D diffusion was presented and validated. The Johnsen et al. (2000) model predictions of the diffusion driven dampening of the annual δ^{18}O cycle can be seen in Figure A.3.

Using the Johnsen et al. (2000) diffusion model and the mathematical formulation of the diffusion problem presented in Johnsen (1977), it is possible to correct δ^{18}O series for diffusion. An example of diffusion corrected δ^{18}O

Table A.1: Correlations (r) of winter δ^{18}O with Tasiilaq Dec-Mar temperatures (1895-1982).

Ice Core	Site A	Site B	Site E	Site G	Mean ABEG
Acc. (ice eq.)	29 cm	31 cm	21 cm	25 cm	-
r (before diff. cor.)	0.29	0.43	0.25	0.21	0.36
r (after diff. cor.)	0.33	0.50	0.41	0.37	0.52

data can be seen in Figure A.2b. Having diffusion corrected data, the underlying seasonally resolved climatic signal can be retrieved from ice core δ^{18}O records.

It is easy to verify the importance of correcting the seasonal δ^{18}O records for diffusion before any climatic interpretation is pursued. Four different central Greenland ice cores were drilled in 1984/85 about 500 km from the coastal Tasiilaq meteorological station. Table A.1 demonstrates that correlations between winter season δ^{18}O and Dec-Mar temperatures at the Tasiilaq station [Laursen, 2003] are greatly improved by diffusion correcting the records. Furthermore it can be seen that the ice core records from the areas of modest accumulation (Site E and G) benefits the most from the diffusion correction. Using the approach of diffusion correction on several Greenland ice cores, Vinther et al. (2003a) demonstrated that winter season δ^{18}O from Greenland ice cores contained both a distinct Greenland temperature signal and the signature of the North Atlantic Oscillation (NAO), a large scale atmospheric flow pattern. A linear regression between the multi-ice core winter δ^{18}O signal and northern hemisphere Dec-Mar sea level pressure (slp) is seen in Figure A.4.

The NAO pattern with opposite pressure trends over Iceland and the Azores is clearly seen in Figure A.4. The regression is carried out for the years 1872 to 1970 and the slp-data are from the HadSLP1 dataset (Basnett and Parker (1997)).

A.4 Deep ice cores - climate during 125 millennia

During the past 40 years a total of 5 deep ice cores have been drilled all the way through the Greenland ice sheet. All 5 records contain ice from the entire Holocene, the last glaciation and the Eemian. A sixth ice core drilled through the small east coast Renland ice cap also reaches into the Eemian (for drill site locations, see Figure A.1). Measurements of δ^{18}O have been carried out on the full length of all six ice core records. From Figure A.5 it is clearly seen that the six δ^{18}O records are very similar for the past 40,000 years. Below 40,000 years the Dye-3 record is disturbed by ice flow, as is the Renland core below 60,000 years. The GRIP and GISP2 records are affected
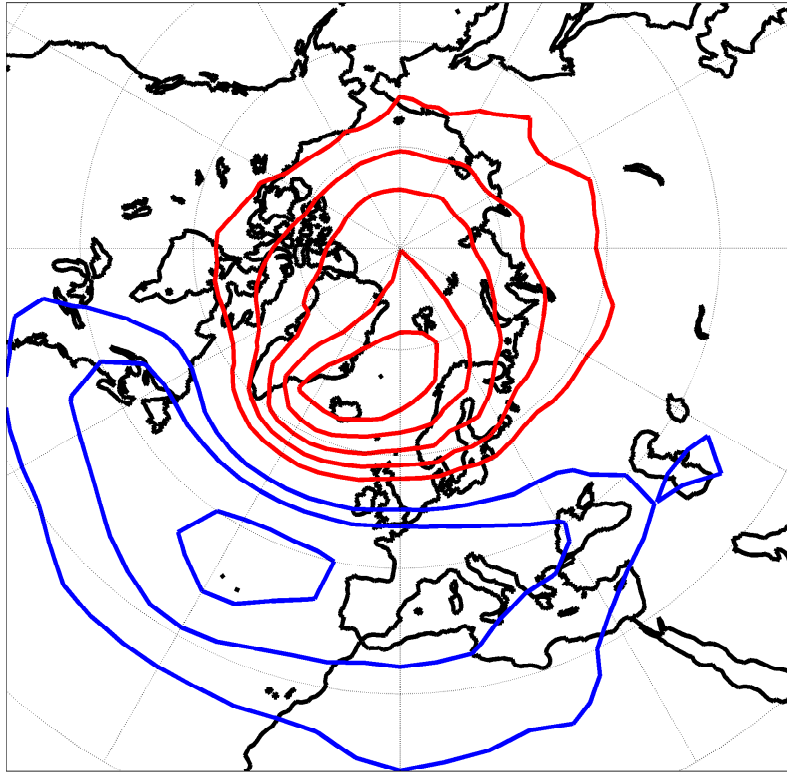
Figure A.4: Dec-Mar SLP-response to a one-sigma increase in winter δ^{18}O in a series based on multiple Greenland ice cores. Contour interval is 0.4hPa, red contours are positive while blue are negative.

by flow induced foldings below 105,000 years. The NGRIP core presents the only δ^{18}O record known to be stratigraphically continuous into the Eemian. However, Eemian ice is found in all six ice cores.

A.4.1 Timescales for deep ice cores

A pre-requisite for the climatic interpretation of the deep ice cores is to have a well established depth-age relation. For most of the Holocene, counting annual layers using the seasonal oscillations in δ^{18}O is a very robust way of obtaining a timescale for the Greenland ice cores. During the glacial, generally lower accumulation rates leads to diffusion caused obliteration of the annual δ^{18}O cycles rendering counting impossible.

The first approach to date the glacial part of the ice cores relied on analytical two-dimensional flow-model estimates of the progressing thinning of annual layers (Dansgaard and Johnsen, (1969)). The flow model presented by Dansgaard and Johnsen (1969) (the D-J model) proved to be very adaptive and in Johnsen and Dansgaard (1992), the analytical D-J model was
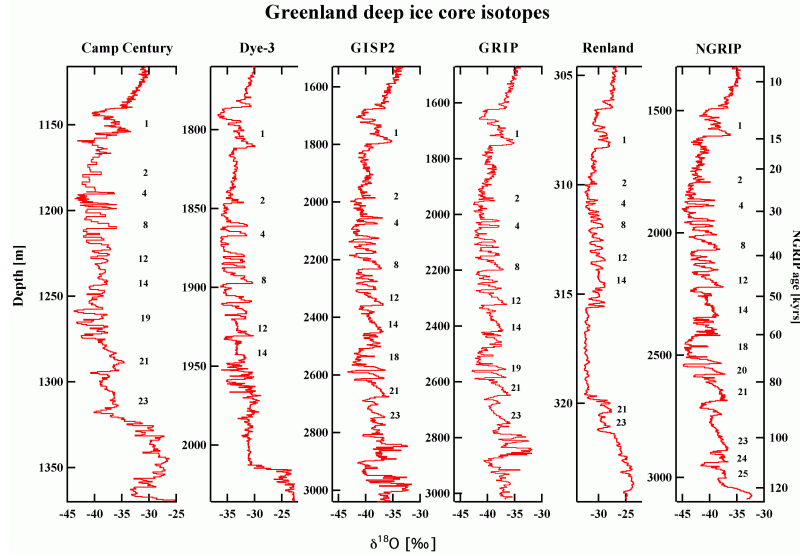
Figure A.5: Early Holocene, Glacial and Eemian δ^{18}O records from 6 Greenland ice cores. The cores are all on depth scales. The NGRIP timescale is shown to the right. Numbers are given for the most prominent interstadials

refined to account for both increased shear near the bottom of the ice sheet and sliding of the ice sheet over the bedrock. The D-J model can also be modified to include flow due to bottom melting affecting the ice sheet.

To include temporal variations of the accumulation rate a numerical version of the D-J model is required. The first effort to create such a model was made by Johnsen et al (1992a). Numerical D-J flow models have been used to provide timescales to both the GRIP and the NGRIP ice cores (NGRIP members (2004)). These models require past accumulation rates as an input parameter. A requirement which can be fulfilled by using relationships between δ^{18}O and accumulation rates at the drill sites. Figure A.6 shows the Dye-3, GRIP and NGRIP δ^{18}O profiles on timescales derived from numerical D-J flow models. As the bottommost part of the Dye-3 core is disturbed by ice flow, only the past 40,000 years of the Dye-3 profile is shown. The similarity of the three profiles is striking.

The first effort to count annual layers during the glacial was carried out on the GISP2 core (Meese et al. 1997). Seasonally changing features in the visual stratigraphy of the GISP2 core were used for the layer counting. Surprisingly the glacial GISP2 timescale derived using this methodology did not show a persistent relation between the δ^{18}O and the accumulation rate back in time. A relation underpinned both by modern observations and the following simple argument: A change in δ^{18}O is associated with a change in site air temperature, and as the air temperature determines the maximum water vapor content of the air, the amount of moisture reaching the site will

VIII
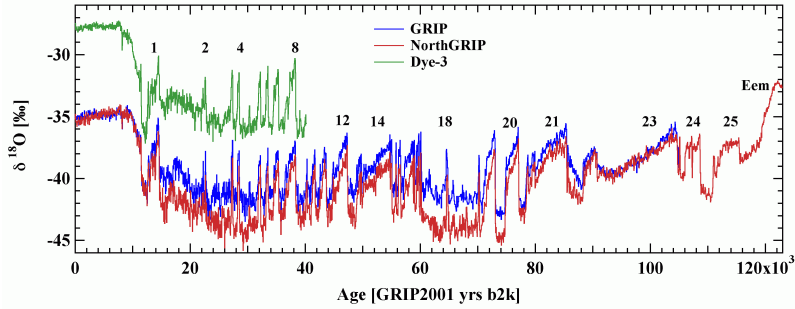
Figure A.6: Profiles of $\delta^{18}O$ from the Dye-3, GRIP and NGRIP cores, on the ss09sea flow-modeled timescale. Numbers are given for the most prominent interstadials. The expression b2k is a short for before 2000 A.D.

be related to observed $\delta^{18}O$ values. Based on a new effort to date the glacial part of the NGRIP core using both seasonal oscillations in chemical impurities and visual stratigraphy, it is now believed that the apparent breakdown of the $\delta^{18}O$/accumulation relationship observed in the GISP2 core is an artifact caused by erroneous interpretation of the GISP2 visible strata (K. K. Andersen, submitted, 2006; A. Svensson, in submitted, 2006).

A.4.2 The Holocene

The major part of the deep ice cores consists of Holocene ice. Looking at Figure A.7, it is obvious that the Holocene is in general a period of remarkable stable $\delta^{18}O$ values. This is surprising as Dahl-Jensen et al. (1998) has shown that borehole temperature measurements at GRIP and Dye-3 implies that temperatures on the ice sheet were $\sim3°C$ higher than present during the climatic optimum some 4000-8000 years ago. The reason for the apparent failure of the $\delta^{18}O$ to capture the temperature increase during the climatic optimum is not well understood. It is speculated that changes in the seasonality of the precipitation reaching the central Greenland ice sheet could be part of the explanation, as a slight increase in depleted winter precipitation could significantly lower average $\delta^{18}O$ values.

In the southern Dye-3 record, ice flow masks the climatic optimum, as this core is drilled on a slope. The ice from the climatic optimum precipitated 25-35 km upstream at 100-150 m higher altitudes and thereby lower temperatures. The Dye-3 $\delta^{18}O$ from the climatic optimum and back in time has therefore been artificially lowered by 0.5-1.0‰. If corrected for the effect of ice flow, the Dye-3 $\delta^{18}O$ record would therefore show a slight decrease in $\delta^{18}O$ from a peak value some 8000 years ago to a recent minimum. A weak but similar trend is present in the NGRIP $\delta^{18}O$ as well. It should be noted that neither trend is anywhere near what is expected, as a 3°C decrease in

IX
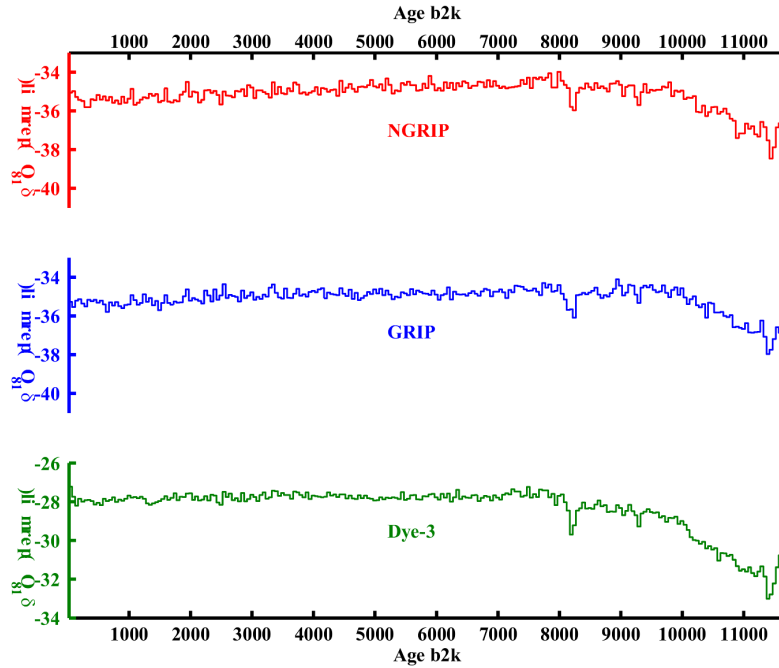
Figure A.7: Holocene profiles of δ^{18}O on the new GICC05 counted and synchronized timescale. The expression b2k is a short for before 2000 A.D.

temperature should be associated with a 2‰ decrease in δ^{18}O, following the δ^{18}O/temperature relationship for the Greenland ice sheet derived in Johnsen et al. (1989). However, it is still an open question, if the Johnsen et al. (1989) spatial relation (derived from pairs of δ^{18}O and temperature observations from different locations on the ice sheet) is valid for the temporal changes in temperature affecting Greenland δ^{18}O.

The δ^{18}O records shown in Figure A.7 are plotted on the Greenland Ice Core Chronology 2005 (GICC05). GICC05 is a new counted timescale that synchronizes the three ice cores using common volcanic reference horizons (Rasmussen et al. (2006a), Vinther et al. 2006b). Exploiting the synchronization of the δ^{18}O records, Rasmussen et al. (2006b) showed that the only significant common events in the early Holocene Dye-3, GRIP and NGRIP records are the decreases in δ^{18}O some 8200, 9300 and 11400 years ago.

These events are known as the 8.2k and 9.3k cold events and the preboreal oscillation, and they are observed in ocean sediment cores, tree ring data and stalagmite records all over the northern hemisphere. The events are believed to be associated with very large fresh water outbursts from the decaying Laurentide ice sheet. The large amount of fresh waters would temporarily weaken the North Atlantic overturning circulation thereby diminishing the oceanic heat transport towards the polar region.

Table A.2: Average values and differences of $\delta^{18}O$ during different climatic periods (all values are given in per mille).

Drill Site	Present (P)	Stadial (S)	Eemian (E)	P-S	E-P
Camp Century	-29.5	-41.9	-27.0	12.4	2.5
Dye-3	-27.6	-36.1	-22.9	8.5	4.7
GISP2	-35.0	-42.2	-32.3	7.2	2.7
GRIP	-35.1	-41.9	-31.6	6.8	3.5
NGRIP	-34.4	-44.5	-32.3	9.1	3.1
Renland	-27.3	-32.1	-23.8	5.0	3.5

A.4.3   The last glaciation

The abrupt shifts in $\delta^{18}O$ leading to the warm Greenland interstadials (Johnsen et al. (1992a), Dansgaard et al. (1993)) are often referred to as Dansgaard-Oeschger events. These events are the most prominent features observed in the glacial parts of all Greenland ice cores (see Figure A.5 and A.6). The shifts are most probably due to large scale reorganizations of the atmospheric and oceanic circulations during the glacial. Hence full glacial (stadial) conditions are probably related to a shutdown of the North Atlantic overturning circulation, while the interstadials are warmed by the return of the overturning circulation. Changes from stadial climatic conditions to the 10-15°C warmer interstadial climate are believed to have happened within a decade or two. The glacial climate is therefore characterized by a degree of instability that cannot be found during the Holocene.

Johnsen et al. (1992a) found that an intercomparison between glacial $\delta^{18}O$ values observed in different Greenland ice cores shows important differences in the size of the $\delta^{18}O$ increase associated with the shift from stadial to Holocene climatic conditions. The Camp Century core shows the largest $\delta^{18}O$ changes while the changes at Renland are the most modest (see Table A.2 and Figure A.5). It is speculated that the large change in Camp Century (and NGRIP) $\delta^{18}O$ are related to those sites having a strongly depleted north-westerly source of precipitation during the stadials. Such a source could be due to a split in the polar jet-stream, into branches north and south of the Laurentide ice sheet. Precipitation arriving from the north-west would not be able to reach the Renland ice cap as it is situated east of the main ice sheet and therefore is shielded from any such precipitation. Hence the relatively modest decrease in Renland $\delta^{18}O$ values during the stadials can be understood in terms of the Renland ice cap not receiving precipitation from the depleted northern branch of a split jetstream.

Recent atmospheric modeling efforts suggesting a split jetstream during the glacial (i.e. Bromwich et al. (2004)) do therefore enjoy significant support from observations of stadial $\delta^{18}O$ in Greenland ice cores.

A.4.4 The Eemian

Ice from the last interglacial, the Eemian, has been found near the bedrock in all deep ice cores retrieved from the Greenland ice sheet (see Figure A.5). It is therefore safe to conclude that most of Greenland was covered by ice during the Eemian. Using the δ^{18}O values observed in Eemian ice it is possible to further quantify the changes in size of the Greenland ice sheet during the Eemian.

Comparing present day δ^{18}O values to those observed in the Eemian ice, it is clear that the Eemian had 2.5-3.5‰ higher δ^{18}O values than presently observed all across Greenland (Table A.2 and Figure A.5) except for at the southern Dye-3 site. At Dye-3 Eemian δ^{18}O was 4.7‰ higher than recent values.

The observed δ^{18}O value at a site on the Greenland ice sheet is dependant on elevation (the gradient is approx. -0.6‰ per 100 m altitude according to Johnsen et al. (1989)). It can therefore be inferred from the rather uniform ($\sim$3‰) increase in Eemian δ^{18}O, that the differences in elevation between the Camp Century, GRIP, GISP2, NGRIP and Renland sites during the Eemian were almost equal to those presently observed. Furthermore the elevated Eemian δ^{18}O values at the DYE-3 site indicate that the southern part of the Greenland ice sheet was lowered by some 400 m relative to the rest of the ice sheet (the $\sim$1.5‰ extra change at Dye-3 added to a $\sim$1‰ change due to ice flow induced extra lowering of the Eemian δ^{18}O).

The question about the absolute elevation of the main ice sheet during the Eemian is not as straight forward to asses. The general $\sim$3‰ increase in δ^{18}O could be attributed both to changes in elevation and changes in temperature, as the Greenland climate during the Eemian was significantly warmer than the present climate.

The fact that the small Renland ice cap experienced almost the same increase in δ^{18}O as most of the Greenland ice sheet does however put constraints on the possible changes in elevation.

The Renland ice cap is only about 330 m thick, and due to its setting on a high elevation plateau, it cannot grow any thicker. Furthermore the fact that a more than 3 m thick layer of Eemian ice has been found close to bedrock at Renland (see Figure A.5) does suggest that the Renland ice cap was well preserved during the Eemian. The ice flow driven thinning rate in the Renland ice cap estimated by Johnsen and Dansgaard (1992), probably could not have allowed the preservation of a 3 m thick slab of Eemian ice, had the Renland ice cap been significantly thinner during the Eemian than today.

It is therefore reasonable to assume that the Eemian thickness of the Renland ice cap was not very far from the 330 m observed today, thus imposing narrow constraints on thickness changes at Camp Century, GISP2, GRIP and NGRIP as well.

Given this information, it is obvious that most (if not all) of the 2.5-3.5‰

Eemian increase in $\delta^{18}O$ should be attributed to temperature change; not to elevation change. Hence it is probably only the southern part of the Greenland ice sheet that experienced significant decreases in thickness during the Eemian. In fact it could be argued that a slight increase in the thickness of the northern part of the Greenland ice sheet is supported by the $\delta^{18}O$ data, as NGRIP and Camp Century Eemian $\delta^{18}O$ seems to have increased a bit less than the Renland $\delta^{18}O$. The contribution to the global Eemian sea level rise from a thinning of the Greenland ice sheet is therefore believed to be modest, most likely less than 1m.

Appendix B

Note on gaussian smoothing of data series

As gaussian smoothing is used extensively in this dissertation, the following section introduces the main terminology which has been used.
Data series can be smoothed with a gaussian (bell-formed) filter in order to suppress high frequency oscillations in the data set.
The level of smoothing which is imposed by the gaussian filter on the data is determined by the standard deviation (σ) of the gaussian function:

$$A(\sigma) = A_0 \cdot e^{-\frac{2\pi^2\sigma^2}{T^2}} \tag{B.1}$$

Were A_0 is the original amplitude for an oscillation with period T and $A(\sigma)$ is the amplitude after filtering.
It is nice to express the degree of smoothing in terms of the period of oscillation in the data that is reduced in amplitude by 50% ($T_{1/2}$):

$$\frac{A(\sigma)}{A_0} = 1/2 = e^{-\frac{2\pi^2\sigma^2}{T_{1/2}^2}} \Rightarrow \tag{B.2}$$

$$T_{1/2} = \sigma\pi \cdot \sqrt{2/log(2)} \tag{B.3}$$

Hence $T_{1/2}$ will be used to quantify the smoothing imposed by the filter and it should be noted that when smoothing is described as being of decadal, centennial or millennial scale then it will always refer to gaussian smothing with $T_{1/2}$ equalling 10 years, 100 years and 1000 years respectively.

Bibliography

[1] Allen, R. and T. Ansell, A new globally-complete monthly historical gridded mean sea level pressure data set (HadSLP2): 1850-2003, *J. Climate*, accepted 2006.

[2] Alley, R. B., C. A. Shuman, D. A. Meese, A. J. Gow, K. C. Taylor, K. M. Cuffey, J. J. Fitzpatrick, P. M. Grootes, G. A. Zielinski, M. Ram, G. Spinelli and B. Elder, Visual-stratigraphic dating of the GISP2 ice core: Basis, reproducibility and application, *J. Geophys. Res.*, *102*(C12), 26,367-26,381, 1997.

[3] Andersen, C., N. Koc, A. Jennings and T. J. Andrews, Nonuniform resonse of the major surface currents in the Nordic Seas to insolation forcing: Implications for the Holocene climatic variability, *Paleoceanography*, *19*, PA2003, doi:10.1029/2002PA000873, 2004.

[4] Bard E., Abrupt climate changes over millennial time scales: climate shock, *Physics Today*, *55*(12), 32–38, 2002.

[5] Barlow, L. K., J. W. C. White, R. G. Barry, J. C. Rogers and P. M. Grootes, The North Atlantic Oscillation signature in deuterium and deuterium excess signals in the Greenland Ice Sheet Project 2 ice core, 1840-1970, *Geophys. Res. Lett.*, *20*, 2901–2904, 1993.

[6] Barlow, L. K., R. G. Berry, J. C. Rogers and M. C. Serreze, Aspects of climate variability in the North Atlantic Sector: Discussion and relation to the Greenland Ice Sheet Project 2 high resolution isotopic signal, *J. Geophys. Res. C12*, 26,333–26,344, 1997.

[7] Basnett, T. and D. Parker, Development of the Global Mean Sea Level Pressure Data Set GMSLP2, Climate Research Technical Note, 79, Hadley Centre, Met Office, FitzRoy Rd, Exeter, Devon, EX1 3PB, UK, 1997.

[8] Benson, C. S., Stratigraphic Studies in the Snow and Firn of the Greenland Ice Sheet, SIPRE Research Report, No. 70, pp 63, 1962.

[9] Box, J. E., Survey of Greenland instrumental temperature records: 1873-2001, *Int. J. Climatol.*, *22*, 1829–1847, 2002.

[10] Bromwich, D. H., E. R. Toracinta, H. Wei, R. J. Oglesby, J. L. Fastook and T. J. Hughes, Polar MM5 simulations of the winter climate of the Laurentide Ice Sheet at the LGM, *J. Climate*, 17 (17), 3415-3433, 2004.

[11] Clausen, H. B., N. S. Gundestrup and S. J. Johnsen, Glaciological investigations in the Crête area, central Greenland: A search for a new deep-drilling site, *Ann. Glaciol.*, *10*, 10–15, 1988.

[12] Clausen, H. B., and C. U. Hammer, The Laki and Tambora eruptions as revealed in Greenland ice cores from 11 locations, *Ann. Glaciol.*, *10*, 16–22, 1988.

[13] Clausen, H. B., C. U. Hammer, C. S. Hvidberg, D. Dahl-Jensen, J. P. Steffensen, J. Kipfstuhl and M. Legrand, A comparison of the volcanic records over the past 4000 years from the Greenland Ice Core Project and Dye 3 Greenland ice cores, *J. Geophys. Res.*, *102*(C12), 26,707–26,723, 1997.

[14] Dahl-Jensen, D., K. Mosegaard, N. Gundestrup, G.D. Clow, S.J. Johnsen, A.W. Hansen, and N. Balling, Past temperatures directly from the Greenland ice sheet, *Science*, *282* (5387), 268–271, 1998.

[15] Dahl-Jensen D., N. S. Gundestrup, H. Miller, O. Watanabe, S. J. Johnsen, J. P. Steffensen, H. B. Clausen, A. M. Svensson and L. B. Larsen, The NorthGRIP deep drilling programme, *Ann. Glaciol.*, *35*, 1–4, 2002.

[16] Dahl-Jensen D., N. S. Gundestrup, P. Gogineni and H. Miller, Basal melt at NorthGRIP modeled from borehole, ice-core and radio-echo sounder observations , *Ann. Glaciol.*, *37*, 207–212, 2003.

[17] Dansgaard, W., The O^{18}-abundance in fresh water, *Geochimica et Cosmochimica Acta*, 6 (5/6), 241-260, 1954.

[18] Dansgaard, W., The isotopic composition of natural waters, *Meddelelser om Grønland*, 165 (2), 120, 1961.

[19] Dansgaard, W., Stable isotopes in precipitation, *Tellus*, 16 (4), 436-468, 1964.

[20] Dansgaard, W. and S. J. Johnsen, A flow model and a time scale for the ice core from Camp Century, Greenland, *J. Glaciol.*, *8*, 215–223, 1969.

[21] Dansgaard, W., H. B. Clausen, N. Gundestrup, C. U. Hammer, S. J. Johnsen, P. M. Kristinsdottir, and N. Reeh, A new Greenland deep ice core, *Science*, *218*, 1273–1277, 1982.

[22] Dansgaard, W., S. J. Johnsen, H. B. Clausen, D. Dahl-Jensen, N. Gundestrup, C. U. Hammer, C. S. Hvidberg, J. P. Steffensen, Á. E. Sveinbjörnsdóttir, J. Jouzel and G. Bond, Evidence for general instability of past climate from a 250-kyr ice-core record, *Nature, 364*, 218–220, 1993.

[23] Epstein, S., and R. P. Sharp, Oxygen isotope studies, Transactions, American Geophysical Union, 40, 81-84, 1959.

[24] Fisher, D. A., Comparison of 100,000 years of oxygen isotope and insoluble impurity profiles from the Devon Island and Camp Century ice cores, *Quaternary Research, 11*, 299–304, 1979.

[25] Fisher, D. A., N. Reeh and H. B. Clausen, Stratigraphic noise in time series derived from ice cores, *Ann. Glaciol., 14*, 76–86, 1985.

[26] Fisher, D. A., R. M. Koerner and N. Reeh, Holocene Climatic Records from Agassiz Ice Cap, Ellesmere Island, NWT, Canada, *The Holocene*, Vol. 5, No. 1, 19–24, 1995.

[27] Fisher, D. A., R. M. Koerner, K. Kuivinen, H. B. Clausen, S. J. Johnsen, J. P. Steffensen, N. Gundestrup and C. U. Hammmer, Intercomparison of Ice Core $\delta^{18}O$ and Precipitation Records from Sites in Canada and Greenland over the last 3500 years and over the last few Centuries in detail using EOF Techniques, *NATO ASI Series*, Vol. 141, 297–328, 1996.

[28] Fisher, D. A., R. M. Koerner, J. C. Bourgeois, G. Zielinski, C. Wake, C. U. Hammer, H. B. Clausen, N. Gundestrup, S. Johnsen, K. Goto-Azuma, T. Hondoh, E. Blake, and M. Gerasimoff, Penny ice cap cores, Baffin Island, Canada, and the Wisconsinan Foxe Dome connection: Two states of Hudson Bay ice cover. *Science*, 279, 692–695, 1998.

[29] Fisher, D. A., High-resolution multiproxy climatic records from ice cores, tree-rings, corals and documentary sources using eigenvector techniques and maps: assessment of recovered signal and errors, *The Holocene, 12*, 401–419, 2002.

[30] Funder, S., Holocene stratigraphy and vegetation history in the Scoresby Sund area, East Greenland, *Grønlands Geologiske Undersøgelse Bulletin*, 129, 1978.

[31] Fleming, K. and K. Lambeck, Constraints on the Greenland Ice Sheet since the Last Glacial Maximum from sea-level observations and glacial-rebound models. *Quart. Science Rev.*, 23, 1053–1077, 2004.

[32] Funder, S., Hansen, L., 1996. The Greenland ice sheeta model for its culmination and decay during and after the last glacial maximum, Bulletin of the *Geology Society of Denmark*, 42, 137152, 1996.

[33] Greve, R., Relation of measured basal temperatures and the spatial distribution of the geothermal heat flux for the Greenland ice sheet, *Annals of Glaciology*, 42, in press 2005.

[34] Hammer, C. U., H. B. Clausen, W. Dansgaard, N. Gundestrup, S. J. Johnsen and N. Reeh, Dating of Greenland ice cores by flow models, isotopes, volcanic debris, and continental dust, *J. Glaciol.*, *20*, 3–26, 1978.

[35] Hammer, C. U., H. B. Clausen and W. Dansgaard, Greenland ice sheet evidence of post-glacial volcanism and its climatic impact, *Nature*, *288*, 230–235, 1980.

[36] Hammer, C. U., H. B. Clausen, W. L. Friedric and H. Tauber, The Minoan eruption of Santorini in Greece dated to 1645BC?, *Nature*, *328*, 517–519, 1987.

[37] Hammer, C. U., G. Kurat, P. Hoppe, W. Grum and H. B. Clausen, Thera eruption date 1645BC confirmed by new ice core data?, The Synchronisation of Civilisations in the Eastern Mediterranean in the Second Millennium B.C., Proceedings of the SCIEM 2000 - EuroConference Haindorf, May 2001, M. Bietak. Vienna, Verlag der Österreichischen Akademie der Wissenschaften, Band XXIX: 87–93, 2003.

[38] Herron, M. M. and C. C. Langway Jr., Firn densification: An empirical model, *J. Glaciol.*, 25, 373-385, 1980.

[39] Hurrel, J. W., Decadal trends in the North Atlantic Oscillation regional temperatures and precipitation, *Science*, *269*, 676–679, 1995.

[40] Hurrel, J. W., Influence of variations of extratropical wintertime teleconnections on Northern Hemisphere temperatures, *Geophys. Res. Lett.*, *23*, 665–668, 1996.

[41] Hurrel, J. W. and H. van Loon, Decadal variations in climate associated with the North Atlantic Oscillation, *Climatic Change*, *36*, 301–326, 1997.

[42] Hurrel, J. W., Y. Kushnir, G. Ottersen and M. Visbeck, An Overview of the North Atlantic Oscillation, In North Atlantic Oscillation, Climatic Significance and Environmental Impact, *Geophysical Monograph.*, *134*, 1–35, 2003.

[43] Johnsen, S. J., Stable isotope homogenization of polar firn and ice, in *Proc. Symp. on Isotopes and Impurities in Snow and Ice, I.U.G.G. XVI, General Assembly, Grenoble, 1975*, 210–219, Washington D.C., 1977.

[44] Johnsen, S. J., Stable isotope profiles compared with temperature profiles in firn with historical temperature records, in *Proc. Symp. on Isotopes and Impurities in Snow and Ice, I.U.G.G. XVI, General Assembly, Genoble, 1975*, 388–392, Washington D.C., 1977b.

[45] Johnsen, S. J. and N. Andersen, On power estimation i maximum entropy spectral analysis, *Geophysics*, *4*, 681–690, 1978.

[46] Johnsen, S. J., W. Dansgaard and J. W. C. White, The origin of Arctic precipitation under present and glacial conditions, *Tellus*, *41B*, 452–468, 1989.

[47] Johnsen, S. J. and W. Dansgaard, On flow model dating of stable isotope records from Greenland ice cores, *NATO ASI Series*, Vol. I 2, 13–24, 1992.

[48] Johnsen, S. J., H. B. Clausen, W. Dansgaard, K. Fuhrer, N. Gundestrup, C. U. Hammer, P. Iversen, J. Jouzel, B. Stauffer and J. P. Steffensen, Irregular glacial interstadials recorded in a new Greenland ice core, *Nature*, *359*, 311–313, 1992a.

[49] Johnsen, S. J., H. B. Clausen, W. Dansgaard, N. S. Gundestrup, M. Hansson, P. Jonsson, J. P. Steffensen and Á. E. Sveinbjörnsdóttir, A deep ice core from east Greenland, *Meddelelser om Grønland*, 29, 3–29, 1992b.

[50] Johnsen, S., D. Dahl-Jensen, W. Dansgaard, and N. Gundestrup, Greenland palaeotemperatures derived from GRIP bore hole temperature and ice core isotope profiles, *Tellus B*, *47* (5), 624-629, 1995.

[51] Johnsen, S. J., H. B. Clausen, W. Dansgaard, N. S. Gundestrup, C. U. Hammer, U. Andersen, K. K. Andersen, C. S. Hvidberg, D. Dahl-Jensen, J. P. Steffensen, H. Shoji, Á. E. Sveinbjörnsdóttir, J. White, J. Jouzel and D. Fisher, The $\delta^{18}O$ record along the Greenland Ice Core Project deep ice core and the problem of possible Eemian climatic instability, *J. Geophys. Res.*, *C12*, 26,397–26,410, 1997.

[52] Johnsen, S. J., H. B. Clausen, K. M. Cuffey, G. Hoffmann, J. Schwander and T. Creyts, Diffusion of stable isotopes in polar firn and ice: the isotope effect in firn diffusion, in *Physics of Ice Core Records*, 121–140, Sapporo, 2000.

[53] Johnsen, S. J., D. Dahl-Jensen, W. Dansgaard, N. S. Gundestrup, J. P. Steffensen, H. B. Clausen ,H. Miller, V. Masson-Delmotte, Á. E. Sveinbjörnsdóttir and J. White, Oxygen isotope and palaeotemperature records from six Greenland ice-core stations: Camp Cebtury, Dye-3, GRI, GISP2, Renland and NorthGRIP, *J. Quart. Scien.*, 16(4), 299–307, 2001.

[54] Jones, P. D., T. Jonsson and D. Wheeler, Extension to the North Atlantic Oscillation using early instrumental pressure observations from Gibraltar and south-west Iceland, *Int. J. Climatol.*, *17*, 1433–1450, 1997.

[55] Jones, P. D., M. New, D. E. Parker, S. Martin and I. G. Rigor, Surface air temperature and its changes over the past 150 years, *Rev. Geophys.*, *37*, 173–199, 1999.

[56] Jones, P. D., T. J. Osborn and K. R. Briffa, The evolution of climate over the last millinium, *Science.*, *292*, 662–667, 2001.

[57] Jones, P. D., T. J. Osborn, K. R. Briffa, C. K. Folland, E. B. Horton, L. V. Alexander, D. E. Parker and N. A. Rayner, Adjusting for sampling density in grid box land and ocean surface temperature time series, *J. Geophys. Res.*, *106*, 3371–3380, 2001b.

[58] Jonsson, T., The observations of Jon Thorsteinsson in Nes and Reykjavik 1820-1854, *Icel. Met.Office Report*, 1989.

[59] Koerner, R. M. and D. A. Fisher, A record of Holocene summer climate from a Canadian high-Arctic ice core, *Nature 343*, 630–631, 1990.

[60] Langway Jr, C. C., Stratigraphic analysis of a deep ice core from Greenland, CRREL, Research Report 77, 130 pp, 1967.

[61] Langway Jr, C. C., H. Oeschger and W. Dansgaard, The Greenland ice sheet program in perspective, in: *Greenland Ice Cores: Geophysics, Geochemimistry and Environment.*, *AGU Monograph*, *33*, 1–8, 1985.

[62] Laursen, E. V., DMI monthly climate data, 1873-2002, contribution to Nordic Arctic Research Programme (NARP), Technical Report 03-25 from the Danish Meteorological Institute, 2003.

[63] Masson-Delmotte, V., et al., Holocene climatic changes in Greenland: Different deuterium excess signals at Greenland Ice Core Project (GRIP) and NorthGRIP, *J. Geophys. Res.*, 110, D14102, doi:10.1029/2004JD005575, 2005.

[64] Meese, D. A., A. J. Gow, P. M. Grootes, P. A. Mayewski, M. Ram, M. Stuvier, K. C. Taylor, E. D. Waddington and G. A. Zielinski, The accumulation record from the GISP2 core as an indicator of climate change throughout the Holocene, *Science*, *266*, 1680–1682, 1994.

[65] Meese, D. A., A. J. Gow, R. B. Alley, G. A. Zielinski, P. M. Grootes, M. Ram, K. C. Taylor, P. A. Mayewski and J. F. Bolzan, The Greenland Ice Sheet Project 2 deoth-age scale: Methods and results, *J. Geophys. Res.*, *102*(C12), 26,411-26,423, 1997.

[66] Merlivat, L. and J. Jouzel, Global Climatic Interpretation of the Deuterium-Oxygen 18 Relationship for Precipitation, *J. Geophys. Res.*, C8, 5029-5033, 1979.

[67] Morrison, J., T. Brockwell, T. Merren, F. Fourel and A. Phillips, On-line high-precision stable hydrogen isotopic analyses on nanolitre water samples, *Analytical Chemistry 73*(15), 3570–3575, 2001.

[68] Muscheler, R., J. Beer, G. Wagner and R. C. Finkel, Changes in deep-water formation during the Yonger Dryas event inferred from [10]Be and ^{14}C records, *Nature 408*, 567–570, 2000.

[69] North Greenland Ice Core Project members, High-resolution record of Northern Hemisphere climate extending into the last interglacial period, *Nature 431*, 147–151, 2004.

[70] Olsen, J., I. K. Seierstad, B. M. Vinther, S. J. Johnsen and J. Heine-meier, Memory effect in deuterium analysis by continuous flow isotope ratio measurements, *Int. J. Mass. Spec.*, In press 2006.

[71] Pearce, N. J. G., J. A. Weatgate, S. J. Preece, W. J. Eastwood, W. T. Perkins, Identification of Aniakchak (Alaska) tephra in Greenland ice core challenges the 1645 BC data of Minoan eruption of Santorini, *Goechem. Geophys. Geosyst.*, 5, Q03005, doi;10.1029/2003GC000672, 2004.

[72] Ramseier, R. O., Self-diffusion of tritium in natural and synthetic ice monocrystals, *J. Appl. Phys.*, 38, 2553–2556, 1967.

[73] Rasmussen, S. O, K. K. Andersen, A. M. Svensson, J. P. Steffensen, B. M. Vinther, H. B. Clausen, M.-L. Siggaard-Andersen, S. J. Johnsen, L. B. Larsen, M. Bigler, R. Röthlisberger, H. Fischer, K. Goto-Azuma, M. E. Hansson and U. Ruth, A new Greenland ice core chronology for the last glacial termination, *J. Geophys. Res.*, doi:10.1029/2005JD006079, 2006a.

[74] Rasmussen, S. O, B. M. Vinther H. B. Clausen and K. K. Andersen, Early Holocene oscillations recorded in three Greenland ice cores, *Q. Science Rev.*, in press 2006b.

[75] Reeh, N., H. B. Clausen, N. Cundestrup, S. J. Johnsen and B. Stauf-fer, $\delta^{18}O$ and accumulation rate distribution in the Dye-3 area, south Greenland, in *Proc. Symp. on Isotopes and Impurities in Snow and Ice, I.U.G.G. XVI, General Assembly, Genoble, 1975*, 177–181, Washington D.C., 1977.

[76] Reeh, N., S. J. Johnsen and D. Dahl-Jensen, Dating the Dye-3 ice core by flow model calculations, *AGU Geophysical Monograph*, 33, 57–65, 1985.

[77] Reeh, N., Dating by ice flow modelling: A useful tool or an exercise in applies mathematics?, in *Dahlem Konference: The Environmental Record in Glaciers and Ice Sheets*, edited by U. Oeschger and C. C. Langway Jr., John Wiley, New York, 1989.

[78] Rogers, J.C., J.F. Bolzan, and V.A. Pohjola, Atmospheric circulation variability associated with shallow-core seasonal isotopic extremes near Summit Greenland, *J. Geophys. Res.*, *103*(D10), 11,205-11,219, 1998.

[79] Schwander, J., B. Stauffer and A. Sigg, Air mixing in firn and the age of the air at pore close-off, *Ann. Glaciol.*, 10, 141–145, 1988.

[80] Shoji, H. and C. C. Langway Jr., Air hydrate inclusions in fresh ice core, *Nature*, *298*, 548–550, 1982.

[81] Tarasov L. and W. R. Peltier, Greenland glacial history, borehole constraints, and Eemian extent, *J. Geophys. Res.*, *108*B3, 2143, doi:10.1029/2001JB001731, 2003.

[82] Vinther, B. M., S. J. Johnsen, K. K. Andersen, H. B. Clausen and A. W. Hansen, NAO signal recorded in the stable isotopes of Greenland ice cores, *Geoph. Res. Lett. 30*(7), 1387, doi:10.1029/2002GL016193, 2003a.

[83] Vinther, B. M., K. K. Andersen, A. W. Hansen, T. Schmith and P. D. Jones, Improving the Gibraltar/Reykjavik NAO Index, *Geophys. Res. Lett.*, *30*, 2222, doi:10.1029/2003GL018220 , 2003b.

[84] Vinther, B. M., Seasonal $\delta^{18}O$ Signals in Greenland Ice Cores, *Master Thesis Univ. Copenhagen*, 2003.

[85] Vinther, B. M., K. K. Andersen, P. D. Jones, K. R. Briffa, and J. Cappelen, Extending Greenland temperature records into the late eighteenth century, *J. Geophys. Res.*, *111*, D11105, doi:10.1029/2005JD006810, 2006a.

[86] Vinther, B. M., H. B. Clausen, S. J. Johnsen, S. O. Rasmussen, J. P. Steffensen, K. K. Andersen, S. L. Buchardt, D. Dahl-Jensen, I. K. Seierstad, M-L. Siggaard-Andersen, A. M. Svensson, J. Olsen and J. Heinemeier, A synchronized dating of three Greenland ice cores throughout the Holocene, *J. Geophys. Res.*, *111*, D13102, doi:10.1029/2005JD006921, 2006b.

[87] Waelbroeck, C., L. Labeyrie, E. Michel, J. C. Duplessy, J. F. McManus, K. Lambeck, E. Balbon and M. Labracherie, Sea-level and deep water temperature changes derived from benthic foraminifera isotopic records. *Quat. Sci. Res.*, 21, 295-305, 2002.

[88] Weidick, A., Neoglacial changes of the ice cover and relatedresponse of the Earths crust in West Greenland, *Rep. Geol.Survey of Greebland*, 159, 121-126, 1993.